Cape Peninsula
University of Technology

AN EXPERIMENTAL INVESTIGATION OF THE EFFECT OF MICROSTRUCTURAL FEATURES ON MECHANICAL PROPERTIES OF EN8 STEEL

Cullen Mayuni Moleejane

BSc Mech Eng

A dissertation submitted to the Faculty of Engineering in partial fulfilment of the requirements for the degree of

Magister Technologiae

in

Mechanical Engineering

Department of Mechanical Engineering
Cape Peninsula University of Technology

Supervisor: Prof G.J. Oliver

I, Cullen Mayuni Moleejane, declare that the contents of this thesis represent my own unaided work, and that the thesis has not previously been submitted for academic examination towards any qualification. Furthermore, it represents my own opinions and not necessarily those of the Cape Peninsula University of Technology.

Signed.....August 2009.

ABSTRACT

Materials in almost all components are subjected to some kind of loading that must be correctly predicted to produce reliable designs. The understanding of a material's properties significantly impacts appropriate selection for a structure. This kind of material characterization is also important in the development of improved or new materials for high strength and novel applications. There are numerous metallurgical variables (composition and process parameters) that influence the physical and mechanical properties of materials.

The aim of this work has been to study the influence of microstructure on mechanical properties of steel, specifically the effect of grain sizes within solid phase mixtures. Parameters for simple models of the variation of material properties with grain size can be determined. These models can then be incorporated in the material data sets of Finite Element Analysis programs which will then allow for structural analysis with zones in a material having different grain sizes.

The deformation and damage behaviour of EN 8 steel have been studied with emphasis on the effects of grain size on the elastic-plastic response of the material. For that purpose, EN 8 specimens with a range of microstructures (grain size and phase) were prepared by heat treatment. The microstructural features were carefully characterized using two different experimental surface microscopy techniques; Light Optical Microscope and Scanning Electron Microscope. The deformation and hardness characteristics have been studied with the help of tensile and hardness tests. The mechanical properties were determined as a function of microstructure (grain size and phase). The yield stress followed the classical Hall-Petch relation. The results indicated that tensile strength and hardness increases with decrease in grain size while elongation decreases.

The main philosophy behind this research has been the study of the microstructure and information from the iron-carbon phase diagram together with numerical analysis of stress-strain data, in order, to understand the influence of grain size on mechanical behaviour of EN8 steel. This combination was then used to make general conclusions on mechanical behaviour of EN 8 based on heat treatment history.

ACKNOWLEDGEMENTS

I would like to express my sincere gratitude to Professor Graeme J. Oliver, Cape Peninsula University of technology for his patience, encouragement and great enthusiasm during this study. Without his guidance, none of this would have been possible.

Special thanks to Dr B. Julius of University of The Western Cape for letting me use their Scanning Electron Microscope and assisting me with specimen preparations and image acquisitions.

I would like to express my appreciation to several people at Cape Peninsula University of technology; Mr. Noel Mbonde and Professor Gryzagoridis for insightful comments and suggestions on various subjects.

I am also grateful to my MTech laboratory colleagues at CPUT, especially W. Maladzhi and A. Kayode who shared with me so much more than just the flat and who are not only my colleagues, but true friends.

I would like to thank Mr Z. Ngewana and Mr F. Hoffman for giving me the privilege to lecture in mechanical and mechatronics departments while pursuing my studies.

Finally, I express my thanks to my family and friends for their support and love during the whole period of this work. I would especially like to thank my grandmother Nyachimbirazowa who has been patiently waiting for my Mtech to finish. My brother Chrispine for taking care of me during this time and my friend, Neziwe who always kept me motivated to finish this thesis.

The project has been financially supported by the National Research Fund (NRF) and by Cape Peninsula University of Technology, which is greatly acknowledged.

DEDICATION

Dedicated to my parents and siblings, especially to my grandmother who has been patiently waiting for my MTech to finish.

TABLE OF CONTENTS Page

LIST OF FIGURES

LIST OF TABLES

1. CHAPTER ONE

1.0 Introduction

An understanding of the behaviour of materials and the ability to predict precisely their response when subjected to working environment is of ultimate importance to materials' engineer. Materials in almost all components are subjected to some kind of loading that must be supported and correctly predicted to produce reliable designs. Material characterization involves not only the stress-strain response, but also the influence of metallurgical aspects.

There are numerous metallurgical variables (composition and process parameters) that influence the physical and mechanical properties of materials and can be categorised as mechanical and physical metallurgy (Finel et al., 2002).

Mechanical metallurgy is concerned with using the microstructure ensuing from processing to understand macroscopic properties whereas physical metallurgy aims at predicting these microstructures from the process parameters. This thesis is concerned with mechanical metallurgy, in particular, the study of the influence of grain size on the mechanical properties of EN8 at room temperatures. Studies have shown that the properties of any material generally depend on the microstructure i.e., the arrangement of atoms, the size of the microstructural features, orientation and morphology of crystals and the chemical composition. Grain size, in general, has a marked influence on the mechanical properties of steel. With the knowledge of dynamical interplay between deformation and grain microstructures size, it is possible to predict the behaviour of steel when subjected to various working conditions. In fact, many of the important mechanical properties of steel, including yield strength and hardness, the ductile-brittle transition temperature and susceptibility to environmental embrittlement can be improved considerably by refining the grain size. Numerous aspects of microstructures and their effects on mechanical behaviour of metals have been studied, including grain size (Zhao et al., 2006; and Morris 2001), grain boundary (Ueji et al., 2002; Chen and Gan, 1986; and Muszka et al., 2006), crystal structure (Liu, 2006), crystal orientation (Liu et al., 2006 (a)).

a) SEM micrograph of EN8

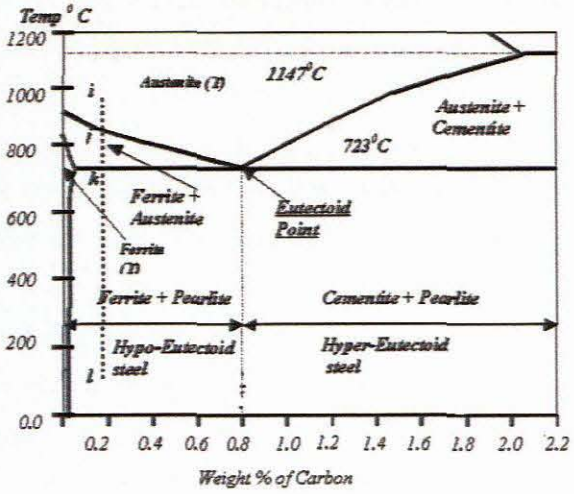

b) The iron-carbon phase diagram

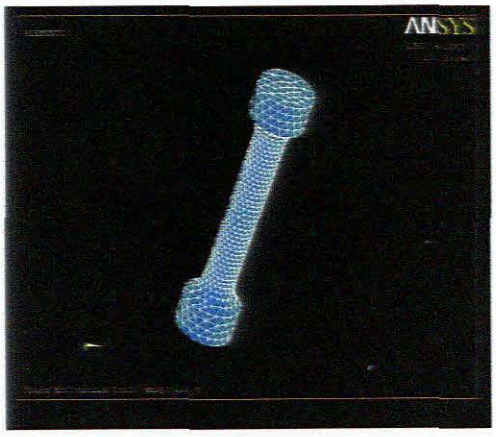

c) Numerical simulation of a tensile specimen

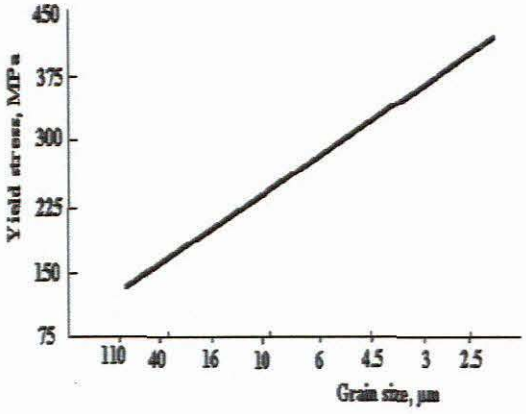

d) Variation of the yield stress with the inverse square root of grain size

Figure 1.1: Summary of the basic philosophy behind the current research

In mechanical metallurgy, it is well known, that amongst the various methods of improving mechanical properties of metals only strong grain refinement leads to an increase in strength of the material without any significant loss in its toughness and ductility. Furthermore, grain refining is attractive especially in that it doesn't require a usage of expensive alloy additions (Sen et al., 2007 and Muszka et al., 2006).

1.2 Scope of work

Figure 1.1 depicts the basic rationale behind this research. In this research work, a study of the microstructure is combined with information from the iron-carbon phase diagram together with numerical analysis of stress-strain data, in order, to

understand the influence of grain size on mechanical behaviour (deformation and damage) of EN8 steel.

1.3 Aims and Objective

The main aim of the research work is to study and analyse the influence of microstructure on mechanical behaviour of EN8. To achieve this main aim; the following objectives will be undertaken:

- Study and investigate the iron-carbon phase diagram
- Study and investigate phase and phase transformation in steel
- Study and analyze the mechanical behaviour from a fundamental point of view, which would enable us to draw general conclusions concerning the mechanisms behind the strengthening in metals due to grain size refinement.
- To understand the mechanical behaviour of EN8 particularly the yield strength, ductility and hardness with respect to grain size.
- Carry out numerical simulation of the influence of grain size on mechanical behaviour of EN8

The thesis surveys different aspects of microstructures contributing to the strengthening in metals. The survey is by no means complete and only one aspect, namely grain size effect, is discussed in detail. Other aspects like the grain boundary, crystal structure, crystal orientation and precipitates are only mentioned.

1.4 Structure of the thesis.

Chapter 2

Fundamentals of steel and Heat treatment

This chapter is divided into two parts. The first part is concerned with the fundamentals of steel and metallurgical transformations during heat treatment of steel components. We start with a brief look at metallurgy of steel. In this regard we briefly discuss iron, effects of alloying elements in particular carbon, microstructure and phases of steel. In the study of microstructure, we look at size, and morphologies of constituent phases and/or grains as observed under a microscope. The nature of the phases and their transformation from one phase to another is the subject of study under metallurgical transformations.

The second part is dedicated to consideration of heat treatment methods used in determining the mechanical properties through grain size control.

Chapter 3

Mechanical properties of steel

In chapter 3, we investigate the mechanical properties of steel and introduce the concepts of deformation and plasticity.

Chapter 4

Effects of grain size of mechanical properties of steel

In this chapter, the influence of grain size on the mechanical properties is discussed qualitatively.

Chapter 5

Experimental work

In order to characterise the material of interest, a number of experiments are carried out. The main focus of this chapter is the consideration and execution of relatively simple experiments to characterize the microstructure and determine the mechanical properties of the steel. To this end, four standard tests (tensile test, metallographic examination, dilatometry test and X-ray analysis (EDAX)) are undertaken.

Chapter 6

In chapter 6 we discuss the results obtained from experimental work carried out in chapter five.

Chapter 7

Numerical Simulation

Finite Element Method (FEM) is introduced and discussed in this chapter. No attempt is made to formulate the discrete and governing equations, however we merely list them. Next a review of numerical modelling is conducted and finally the commercial software used ANSYS is introduced.

Chapter 8

Conclusion and future work

Chapter 8 sums up the findings of this study and proposes areas of research for future work.

CHAPTER TWO

2.0 Fundamentals of steel and Heat treatment

2.1 Introduction

The industrial and scientific application of any metal or alloy is determined by its properties. These properties can be altered within limits by several methods, namely thermo-mechanical treatments, grain size control, alloying, and heat treatment. Heat treatment changes mechanical properties either by allotropic transformation or by changing relative solubility of elements in the parent metal. In this chapter, we discuss the fundamentals of steel and the heat treatment methods used to control the grain size.

Steel is basically an alloy of iron and carbon, but several other elements are added in various amounts that makes steel the most important and versatile engineering alloy. There are three phases involved in any steel—ferrite, cementite, and austenite, whereas there are a number of structures or mixtures of structures. In general, the strength of steel depends on the nature, distribution, and the size of phases and/or grains present.

Heat treatment of steel components is a fundamental metallurgical process and has numerous applications throughout the manufacturing industry. It involves careful selection of heating and cooling temperatures with or without external stresses. Properties of steel can be controlled and varied over a very wide range by heat treatment. Through different heat treatments and thermo-mechanical treatments (hardening, annealing, normalizing, tempering, etc) properties of steel components can be altered to suit particular applications. For instance, hardness is achieved by heating and cooling rapidly; on the other hand heating and cooling slowly may reduce hardness and relieve the steel components of internal residual stresses.

This ability comes from the variety of microstructures (which may or may not involve new phase formations) that result from heat treatments and other thermo-mechanical treatments. In part, the allotropic nature of iron and the size of carbon atoms in relation to those of iron, and the process parameters (cooling rate, temperature, deformation and deformation rate etc) are the underlying metallurgical phenomena that enable steel to be heat treated and give it wide range of applications (ASM International, 2006).

2.2 Scope and focus of this chapter

This chapter is divided into two parts. The first part is concerned with the fundamentals of steel and metallurgical transformations during heat treatment of steel components. We start with a brief look at metallurgy of steel. In this regard we briefly discuss iron (the base metal), effects of alloying elements in particular carbon, microstructure and phases of steel. In the study of microstructure, we look at size, and morphologies of constituent phases and/or grains as observed under a microscope. The nature of the phases and their transformation from one phase to another is the subject of study under metallurgical transformations.

The second part is dedicated to consideration of heat treatment methods used in determining the mechanical properties through grain size control are discussed.

2.3 Metallurgy of steel

2.3.1 Steel and alloying elements

Iron, in its pure form, has limited engineering application. However steel, an alloy of iron and carbon plus smaller quantities of other several elements, is by far the most widely used and versatile metal alloy (ASM International, 2006).

Pure iron exists in two distinct crystalline structures depending on temperature (see Figure 2.1). At temperatures from absolute zero to 912 °C, pure iron has a Body Centered Lattice (bcc), called alpha iron or ferrite; and changes to Face Centered Lattice (fcc) as temperatures increase past 920 °C. This structure is called gamma iron or austenite; and reverts to Body Centered Lattice (bcc) when it is heated to above 1395 °C and melts at 1538 °C (see Figures 2.1 and 2.2). This structure is called delta iron. There are three phases involved in any steel—ferrite, cementite (Iron carbide, Fe3C), and austenite, whereas there are a number of structures or mixtures of structures (ASM International, 2006).

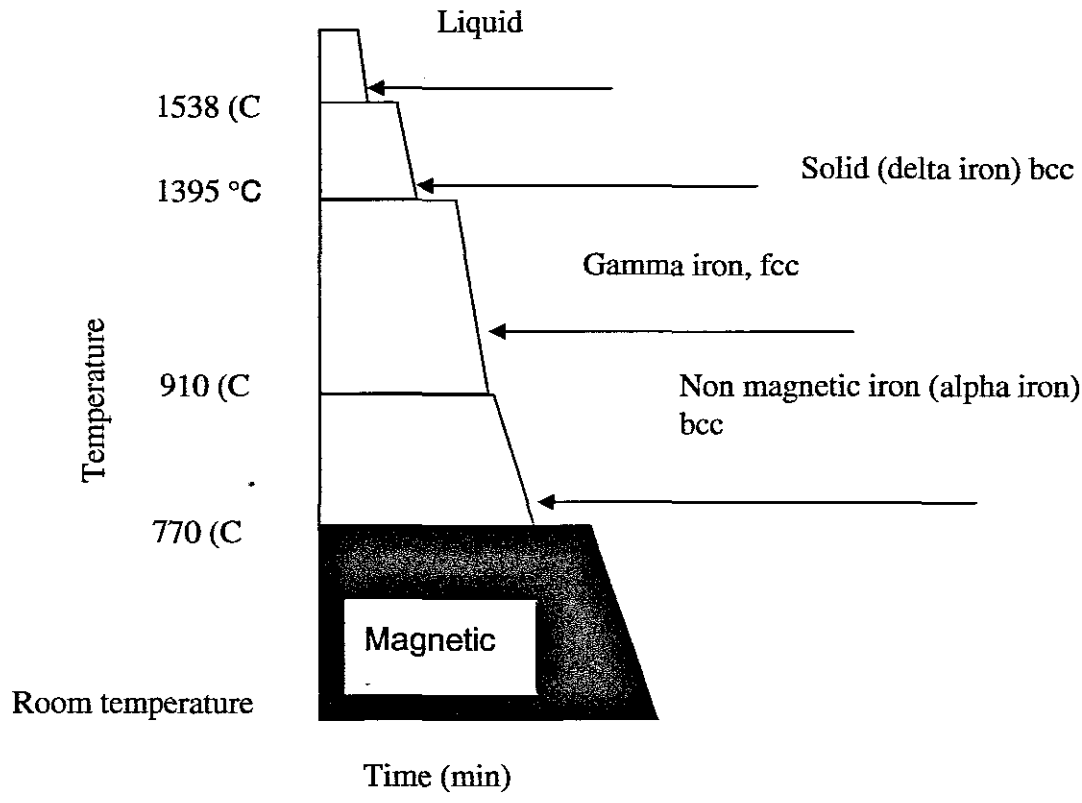

Figure 2.1: Changes in pure iron as it cools from the molten state to room temperature. Source: ASM International, 2006.

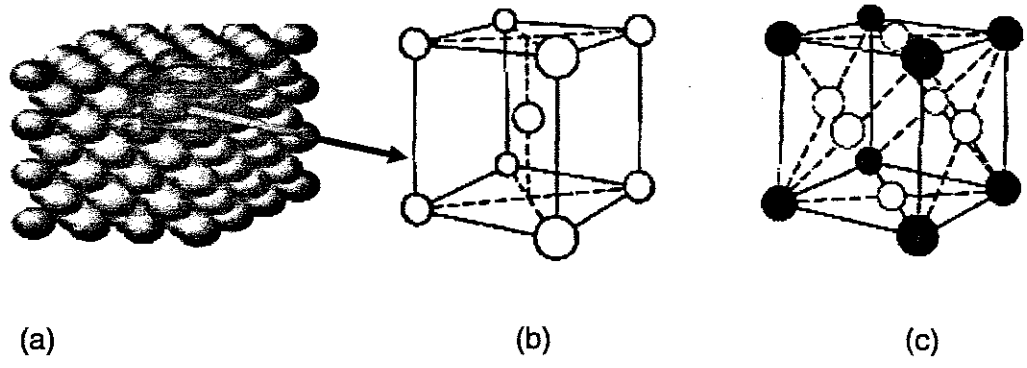

Figure 2.2: Arrangement of atoms in crystalline structures of pure iron.
(a) Crystal structure with many unit cells, (b) Body-cantered cubic lattice, (c) Face-centred cubic lattice. Source: ASM International, 2006.

2.3.2 Effects of carbon on the constitution of iron

Carbon is almost insoluble in iron, which is in the alpha or ferritic phase (i.e. in the bcc lattice at lower temperatures). However it is quite soluble in gamma iron (i.e. in the fcc and bcc at higher temperatures). The solubility of carbon in iron depends on temperature. The atomic diameter of carbon is less than interstices between iron atoms and the carbon atoms go into solid solution of iron. As carbon dissolves in the iron, it distorts the original crystal lattice of iron. Carbon when present in excess of 0.025% has two main effects on the properties of iron:

- It lowers the transformation temperatures, and
- Broadens the temperature range of transformation.

These effects of carbon on certain characteristics of pure iron are shown in Figure 2.3. In Figure 2.3(b), it can be seen that carbon lowers the melting point of pure iron and that it widens the temperature range of austenite. It elevates the temperature A4 at which ferrite changes to austenite and lowers the temperature A3 at which the austenite turns back to ferrite. Hence carbon is said be an austenitising element.

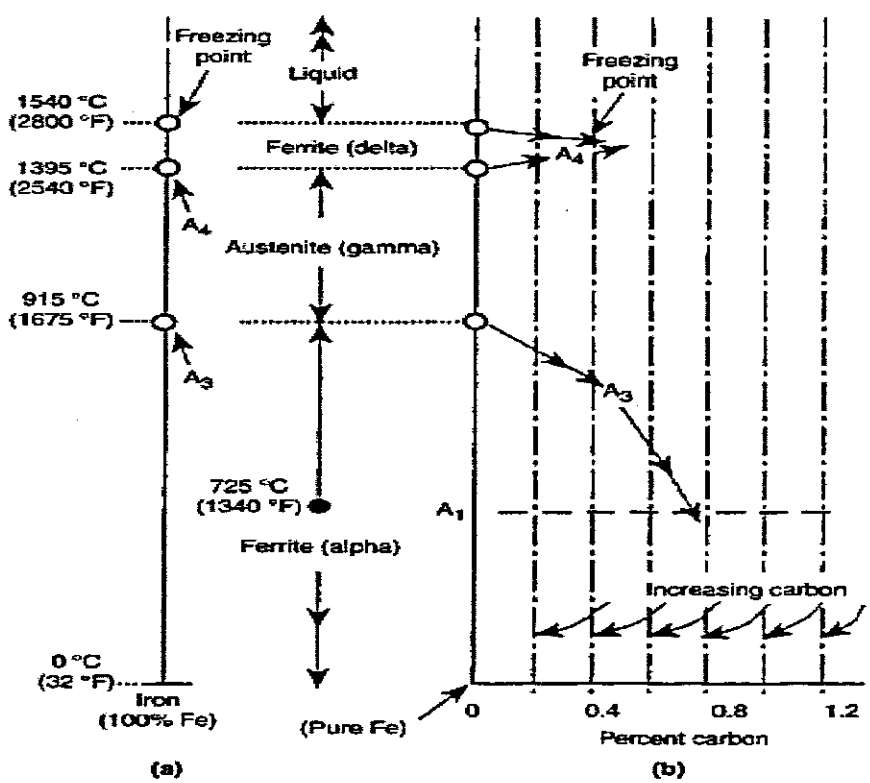

Figure 2.3: Effects of carbon on the characteristics of commercially pure iron.
Source: ASM International, 2006.

2.3.3 The iron carbon phase diagram

The iron-carbon phase diagram (shown in Figure 2.3) is a plot of transformation of iron with respect to carbon content and temperature.

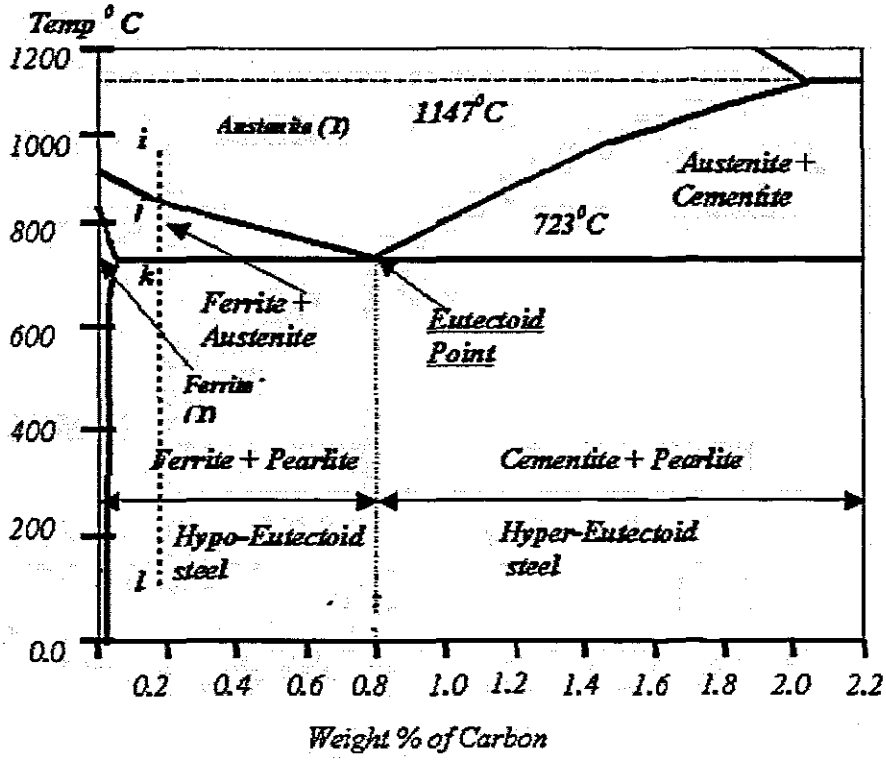

Figure 2.4: The iron-carbon phase diagram. Source: Tkalcec, 2004

Considering Figure 2.4, we can categorize steel into three classes:

- Hypoeutectoid steels (steels with carbon content to the left of the eutectoid point).
- Hypereutectoid steels (steels with carbon content to the right of the eutectoid point).
- Eutectoid steels (steels with 0.8 % carbon content)

2.4 Microstructure of steel

The term microstructure, as used in this thesis, refers in general to grains of steel: shapes and sizes of micro-constituents and their arrangement/morphology and distribution in the structure. Research has shown that the properties of steel are related to its structural make-up, i.e. its microstructure (Morris, 2001; Muszka et al., 2006; Chen and Gan, 1986 and Rack, 1978). Thus altering the size, shape and

distribution of its various micro-constituents can change mechanical properties of steel. For example, increased yield strengths can be achieved for a fixed composition by reducing the grain size (Fromm, 2008; Sen et al., 2007 and Qu et al., 2005).

2.4.1 The Crystal Structure of Metals

In most solid metals, the large metallic bond between atoms typically results in a crystalline structure. This means that atoms within materials are situated in a repeating array over long range. To describe crystalline structure, atoms are imaged as solid hard balls sitting next to each other with different patterns and the minimum repeating pattern is defined as a unit cell (see Figure 2.2).

Crystalline structure with atoms positioned at each corner of the unit cell and centres of all surfaces is called a face-centred cubic crystalline structure as shown in Figure 2.2 (b). Similarly, crystalline structure with atoms sitting on each corner and one located at the centre of the unit cell is call body-centred cubic crystalline structure bcc.

According to Seifert, 2003 crystal structure of metals formation from a melt starts with small regions (called seeds) as a result of atoms rearrangement in the lattice structure (see Figure 2.5). From these seeds, the crystallites (grains) grow in all directions. The number of seeds and also the rate of crystallization determine the size of grains.

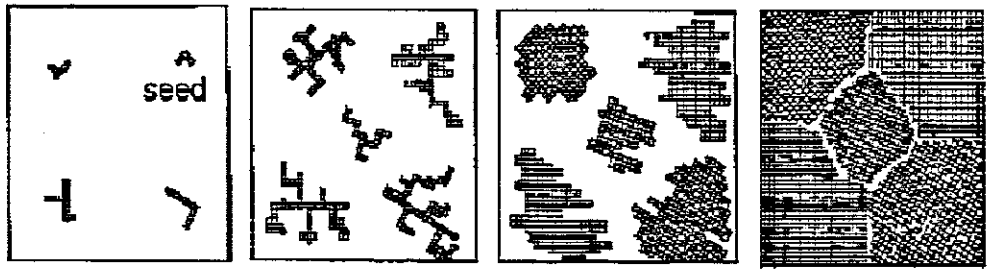

Figure 2.5: Solidification of a metal: a) formation of seeds, b) and c) growth of crystals, d) polycrystalline. Source: Seifert, 2003.

2.4.2 Grain size and morphology

Crystalline metals, except for single crystals, contain internal boundaries known as grain boundaries (Muszka et al., 2006 and Chen and Gan, 1986). When a new grain is nucleated during processes such as heat treatment, the atoms within each growing grain are arranged in a specific pattern that depends upon the crystal structure of the metal or alloy (Seifert, 2003). With growth, each grain will eventually impinge on others and form an interface where the atomic orientations are different (Liu, 2006; Muszka et al., 2006; ASM International, 2006; Ueji et al., 2002 and Chen and Gan, 1986). The major factors controlling grain structure are the requirement of space filling and the tendency toward minimum interfacial energy (ASM International, 2006).

In polycrystalline materials, different regions can be identified that are characterised by specific microstructures and associated morphological features. Despite the wide variety of microstructures, the present classification will focus only on three types: pearlite, austenite and martensite. In many experimental studies (Lei, 2007; Han et al., 2007; Clarke and Van Tyne, 2005 and Shulkosky et al., 2003), a number of microstructures and associated morphological features have been identified and characterised that are not mentioned herein. In most of these studies, the morphological shapes of the microstructure and grain-size distribution are assumed to be unique and specific to each microstructure (Ju et al, 2006).

2.4.3 Phase and Phase Transformation

A phase is a portion of an alloy physically, chemically or crystallo-graphically homogeneous throughout, which is differentiated from the rest of the alloy by clear-cut bounding surfaces (ASM International, 2006 and Liu et al., 2003 (b)). In steel, Phase Transformation is the process by which steel changes from one atomic arrangement to another when heated and this is a temperature characteristic of a particular alloy composition (see Figure 2.4). The transformation can be categorized into two groups: diffusion and diffusionless transformation (Ju et al., 2006 and Singh et al., 2004).

2.4.4 Diffusion-Type Transformation.

In order to determine the kinetics of diffusion transformation with regard to the JMAK equation, the decomposition of austenite ξ_A to ferrite and pearlite can be expressed by the following equation (Ju et al., 2006):

$$\xi_A = 1 - \exp\left\{ - \int_0^t f_t(T) f_s(\sigma_{ij}) f_c(C) (t - \tau^3 d\tau) \right\} \quad (2.1)$$

where $f_t(T)$, $f_s(\sigma_{ij})$ and $f_c(C)$ are the functions of temperature T and stress σ_{ij} and carbon content C, respectively.

2.4.5 Diffusionless Transformation

The martensite transformation is time independent. The volume fraction of the martensite ξ_M is just a function of temperature, carbon content and stress, but not time (Ju et al, 2006; and ASM International, 2006). According to Ju et al 2006 Martensite transformation can be determined using the Modified Magee's rule given as:

$$\xi_M = 1 - \exp\left\{ \psi_1 T + \psi_2 (C - C_o) + \psi_{31} \sigma_{ij} + \psi_{32} J_2^{1/2} + \psi_4 \right\} \quad (2.2)$$

where $J_2 = \frac{1}{2} S_{ij} S_{ij}$ is the second invariant of deviatory stress, S_{ij} is the deviatoric stress, σ_{ij} is the stress, and ψ_1, ψ_2, ψ_3 and ψ_4 are all coefficients obtained from experiments.

The presence of stresses during phase transformation has two major effects (Sleboda et al., 2004; Ueji et al., 2002; and Park et al., 2000):

- It modifies the kinetics of the transformation and
- It causes an irreversible strain even in the presence of stresses lower than the yield stress, termed transformation induced plasticity

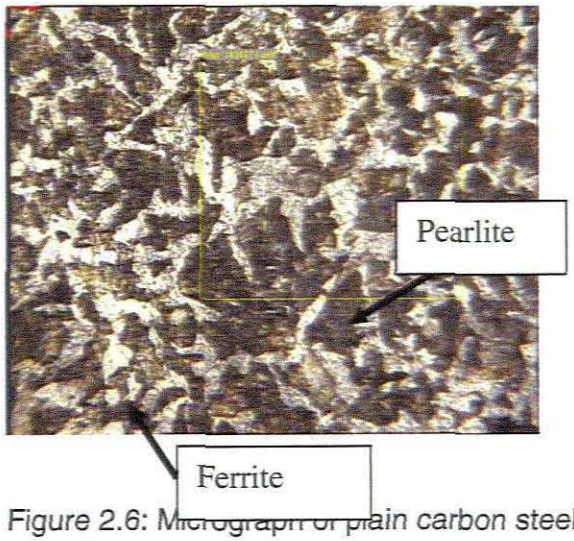

Figure 2.6: Micrograph of plain carbon steel showing pearlite and ferrite

In the study of phase transformation and the relation between temperature, time and transformations, a number of tools and diagrams are used. Isothermal Transformation (IT) Diagrams (see Figure 2.7) show the time dependence transformation while Continuous Cooling Transformation (CCT) Diagrams depict continuous cooling over time transformation. As shown in Figure 2.9, dilatometry data is used to characterize both diffusive and diffusionless transformation phase transformations (Ferguson et al., 2005)

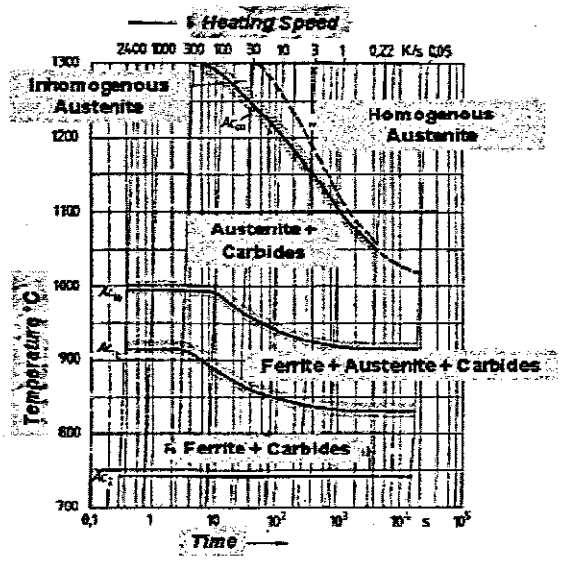

Figure 2.7: Time and Temperature diagram for continuous heating.
Source: ESI Group, 2004.

2.4.6 Metallo-Thermo-Mechanics

Materials that consist of more than one phase often behave in a complicated way during processes that involve phase transformation such as heat treatment, welding and casting. Materials characteristics such as atomic arrangement, microstructure and chemical constituents play a major role on the physical, chemical and mechanical properties on a macro scale (Rocha and Hirsch 2005).

2.4.7 Kinetics of Phase transformation

When a component that consists of a multi-phase structure is subjected to thermal or mechanical loads that cause structural changes due to phase transformation, an assumption is made that the mechanical and physical properties χ of the material are

a linear combination of the properties χ_I of the phases and can be described by the mixture law (Coret and Combescure, 2002):

$$\chi \equiv \sum_{I=1}^{N} \chi_I \xi_I \tag{2.3}$$

where $\sum_{I=1}^{N} \xi_I = 1$ and ξ_I is the volume fraction of the I th phase. (2.4)

During phase transformation, three types of parameters are dominant: temperature fields, phases of metallic structures, and elastic or inelastic—stress strain relationship (ASM International, 2006 and Coret and Cumbscure, 2002). The interaction of these parameters is referred to as metallo-thermal-mechanical coupling see Figure 2.8. ASM International, 2006 gives a brief description of the coupling whereas ESI Group, 2005 gives an excellent and detailed overview of the coupling mechanics—the background on the interaction of the three parameters and kinetics of phase transformation, as well as background on the relationship between microstructure and thermal stress are discussed. They also give the mathematical formulation of the stress—strain and phase evolution.

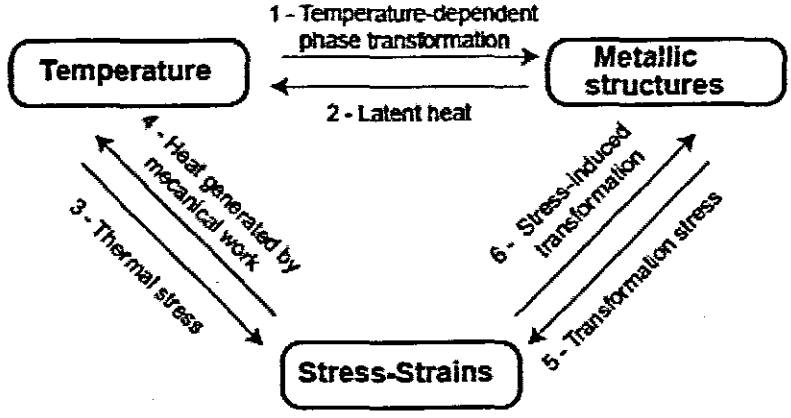

Figure 2.8: A graphic representation of coupling mechanisms.
Source: Coret and Combescure, 2004.

In order to predict the microstructural evolution during hot rolling, the subsequent phase transformation and finally the mechanical properties of micro alloyed steel,

Singh et al., 2004 conducted a series of experiments for plane strain hot compressive. They observed that the initial austenite grain size and the accumulated strain play a major role, besides the cooling rate, in determining the final ferrite grain size.

Serajzadeh (a), (2004) studied austenite phase transformation by means of Avrami's model under non isothermal conditions, and combining this with finite element method, developed a model to predict austenite transformation in carbon steel. The modified Euler's method was used so that the Avrami-type equation could handle the kinetics of phase change under non-isothermal conditions. They observed that: 1) the growth rate of the new phase is affected significantly by the initial grain size both for pearlitic and ferritic phase changes, and 2) at the surface where cooling is rapid, the austenite grain size has a stronger effect in comparison with the inner regions, with slower rate of transformation.

In another attempt to simulate the phase transformations Serajzadeh (b), (2004) proposed a model for predicting temperature history and microstructural changes during cooling of steel. He took cognisance of the effects of a number of factors including initial austenite grain size and its role on the kinetics of pearlite and ferrite transformation, the amount of residual strain within the cooling material and heat of transformation. The phase transformations were studied using the TTT-diagram (see Figure 4) and the Johnson-Mehl-Avrami-Kolmogorov (JMAK) equation for both the ferrite and the pearlite Transformation. It was observed that non-uniform cooling can cause inhomogeneous distribution of ferrite grain size in the final product.

Choi, (2003) carried out dilatomeric studies to quantitatively relate the dilatation curve to the proeutectoid ferrite and pearlite transformation kinetics during continuous cooling of the hypoeutectoid steels. He used the linear thermal contraction coefficients, the lattice parameters and the composition of the phases under paraequilibrium condition to measure the fraction of transformation during phase transformation.

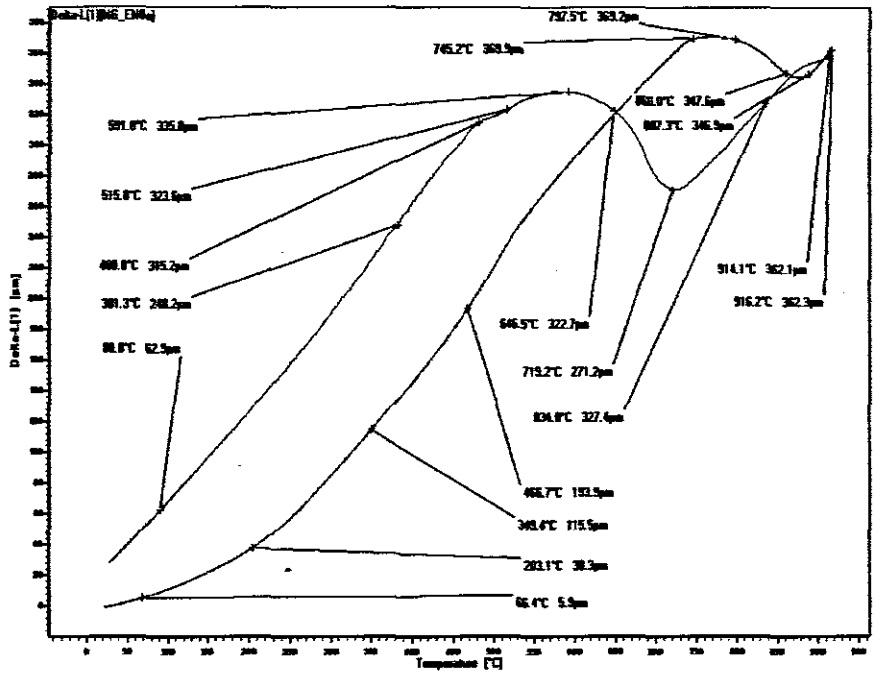

Figure 2.9: Dilatation curve for EN8 plotted as change in length (Delta) versus temperature.

2.5 Heat Treatment Process

Heat treatment of steel is a general term that depicts a number of processes involving controlled heating and cooling of steel components aimed at altering and improving the properties of the steel. The basic principles involved in all the different processes consist of the following three stages:

- Heating of the steel component to a critical temperature,
- Holding the component at that temperature for some time, and
- Cooling.

The temperature and time for the three processes are dependent on the metallurgical mechanism controlling the desired effect (ASM international, 2006). The heating and cooling processes create temperature gradients between the exterior and interior of the component. The geometry and size of the component determine the magnitude of the temperature gradients (Liu et al., 2003 and Phillips and Armstrong, 1969).

2.5.1 Heating and cooling

The temperature to which the material is heated before cooling has begun determines the phases that are present at the beginning and the end of the cooling process (Miokovic et al., 2006).

2.5.1.1 Heating

Heating of steel to austenitising temperature is the first step of almost all heat treatment processes. Nuclei of austenite are formed on heating an aggregate of ferrite and pearlite, ferrite and cementite or martensite and pearlite to eutectoid temperature, depending on whether the steel is of hypoeutectoid, eutectoid or hypereutectoid type respectively. These nuclei simultaneously nucleate and grow into primary austenitic grains until all the steel has transformed to austenite (See Figure2.13). The size of these austenitic grains is referred to as original grain size. Figure 2.10 shows the microstructure of lamellar pearlite that consists of alternate layers of ferrite and cementite.

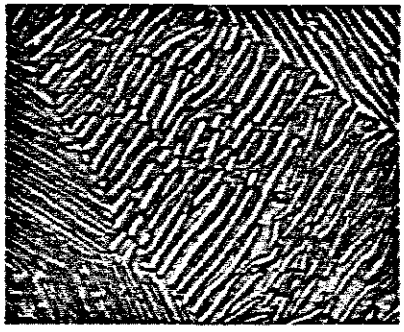

Figure 2.10: The structure of pearlite. Source: ASM International, 2006.

The intermetallic compound cementite has 6.67-weight percent carbon, whereas ferrite is almost pure iron, free from carbon. Maximum content of carbon in ferrite is about 0.025 percent at eutectoid temperature. Below this temperature, the carbon content is less and decreases to a value of about 0.008 percent at room temperature. As the temperature increase, carbon of cementite gradually dissolves into gamma iron, and primary austenite grains are formed. These primary austenite grains dissolve the surrounding ferrite and austenite grains grow at the expense of ferrite (See Figure 2.13).

2.5.1.2 Transformation temperature and holding time

Austenitisation starts soon as the eutectoid temperature is reached, and proceeds by nucleation and growth reaction till all ferrite and cementite dissolve to from austenite (Tkalcec, 2004). The growth rate of austenite is higher than the rate of dissolution of the cementite into austenite because of the transformation of alpha iron to gamma

iron and diffusion of carbon atoms from austenite to ferrite. The austenite thus formed at eutectoid temperature is not homogeneous. The carbon concentration is higher in these regions which are adjacent to the original cementite lamella than those which are adjacent to the ferrite mass. Chemically homogeneous austenite grains can be attained by holding steel above the eutectoid temperature (Liu et al 2006 (a)). The holding time should be sufficient so that carbon atoms may diffuse and result in uniform distribution of carbon atoms but at the same time short enough to prevent excessive austenite grain growth (Ju et al., 2006 and Keehan, 2004). In practice, because of the existence of thermal gradient in a component, it is not possible to heat steel with equilibrium rate of heating (ASM International, 2006). It has been experimentally observed that on heating, austenite formation always occurs at a temperature higher than predicted by the Fe-C equilibrium diagram (Keehan, 2004). For higher heating rates, the transformation will start at higher temperature, whereas for slower heating rate, transformation will start at lower temperatures. Hence, for any given practical rate of heating, the formation of austenite will occur over a range of temperatures, and does not take place at a constant temperature.

2.5.1.3 Cooling

In the next section we shall consider the decomposition of austenite upon cooling (See Figure 2.12). Slow cooling of steel to below the eutectoid temperature results in the formation of ferrite and cementite (Fe3C). This might appear as proeutectoid ferrite and a lamellar ferrite/cementite structure called pearlite, depending on the carbon content of the steel and the cooling rate. Slower cooling rates produce coarser microstructures. On the other hand, faster cooling rates will inhibit the transformation of austenite containing carbon into ferrite and cementite (pearlite), which would happen with slow cooling. The carbon atoms "dissolved" in austenite remain trapped, causing the tetragonal distortion of the bcc lattice and the formation of a very hard metastable phase: martensite. The martensitic transformation in steel (See Figure 2.11) is just one example of a more general phenomenon of martensitic transformations described as shear-dominant, lattice-distortive, diffusionless transformations occurring by nucleation and growth (Ju et al., 2006). Bainite, a fine, feathery microstructure consisting of ferrite and cementite, is formed by cooling rates in between the two regimes and holding at a relatively low temperature

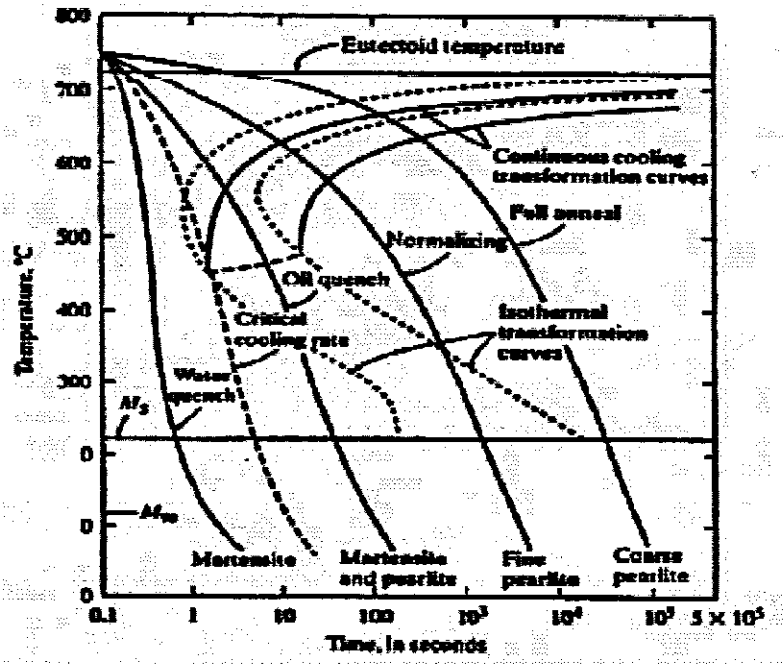

Figure 2.11: Effects of temperature and time on phase transformation in steel.
Source: ATSM International, 2006.

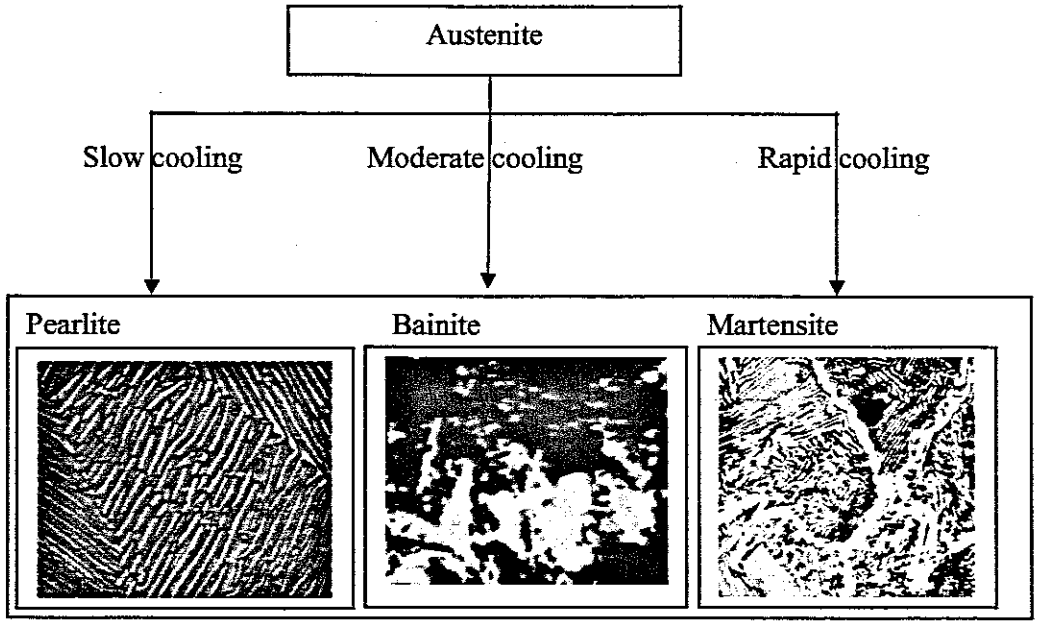

Figure 2.12: Austenite decomposition upon cooling from austenizing

The decomposition of austenite upon cooling is a complex process (Han et al., 2007) in the sense that it involves compositional as well as configurational changes (Phase transformation and crystal structure changes). Carbon present in the austenite adjusts itself in such a way that at one end it leaves behind an almost carbon-free phase (ferrite) and on the other it combines with iron to form cementite (Fe3C). Similarly, large-scale redistribution of alloying elements takes place when the solubility of the element is restricted in alpha iron, and/or there is a strong tendency for the element to form carbides (Gupta et al., 2005).

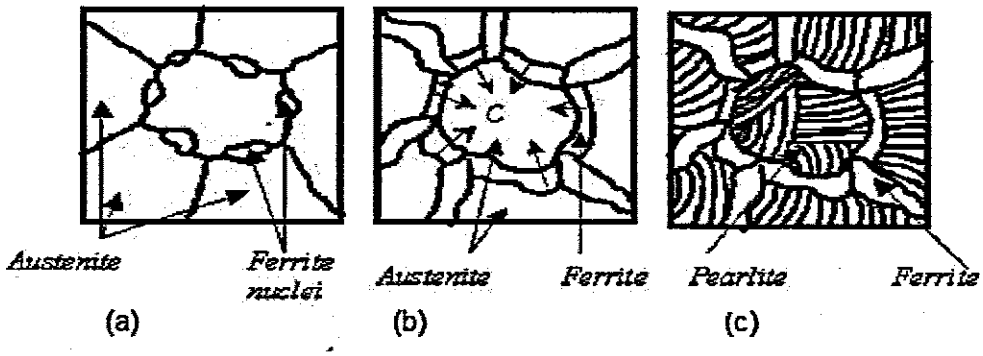

Figure 2.13: Austenite decomposition upon cooling. Source: Kumar and Kumar, 10 July 2008

2.6 Heat treatment methods used to control grain size of steel

Grain refinement is one of the most effective strengthening mechanisms for improving mechanical properties of steel without loss in ductility (Fromm, 2008; Lim et al., 2007 and Qu et al., 2005). There are several methods for grain refinement in steels and these include the following (Greger et al., 2006; Park et al., 2004; and Storojeva et al., 2004):

- Phase transformation
- Recrystallization
- Controlled rolling
- Severe plastic deformations (SPD),
- Cyclic thermo-mechanical treatment
- Forming of duplex alloys and distribution of phases in duplex alloys

Micro-alloying elements are also used to retard grain growth and therefore enhance grain refining by formation of fine nitrides and carbides in steels. The typical alloying additions used include: Ti, V, Nb and Al (Sen et al., 2007).

In the present study, we shall consider the possibilities of refining grain size by means of phase transformation and recrystallization only: annealing and normalising. According to Greger et al., 2006 the mechanism in phase transformation and re-crystallisation processes is based on formation of nuclei of new grains inside the grains of initial structure.

2.6.1 Annealing

Heat treatment for annealing involves heating the steel to a predetermined temperature, holding at this temperature, and finally cooling at a very slow rate. The temperature, to which steel is heated, and the holding time are determined by various factors such as the chemical composition of steel, size and shape of steel component and the final properties desired (Phillips and Armstrong, 1969 and Manesh and Taheri 2003). Annealing treatment can be classified into four groups, based on temperature of treatment, phase transformation that takes place during treatment, and the purpose of the treatment:

- *Diffusion annealing*
- Softening
- Phase-recrystallization annealing or full annealing (normalization, high temperature or coarse grain annealing, pearlitization)
- Stress relief annealing and crystallization annealing.

2.6.2 Normalizing

Normalizing consists of heating the steel to about 40-50 °C above the critical temperature (A3 or Acm), holding for proper time, and then cooling in still air or slightly agitated air to room temperature (See Figure 2.14). After normalizing, the resultant microstructure should be pearlitic. Since the temperature involved in this process is more than that for annealing, the homogeneity of austenite increases and it results in better dispersion of ferrite and cementite in the final structure. The grain size is finer in normalized structure than in annealed structure. Grain size of normalised steel is governed by section thickness. As cooling rates differ considerably from case to core, there is variation in grain size of normalized steel over its cross-section.

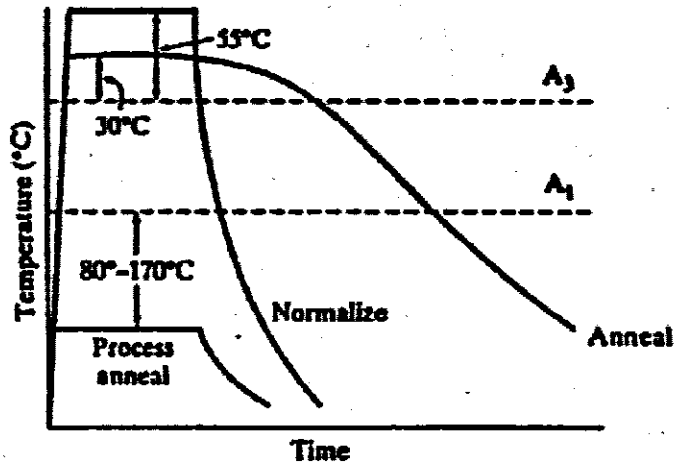

Figure 2.14: Annealing and Normalizing heat treatment temperatures and time. ASM Handbook Vol. 4

CHAPTER THREE

3.0 Mechanical properties of steel

3.1 Deformation

When a metal or any other structural material is subjected a large enough external load, it deforms (i.e. change shape and or dimensions). The deformation can be time dependent or independent and it is often defined in terms of stress and strain (see Figure 3.1)

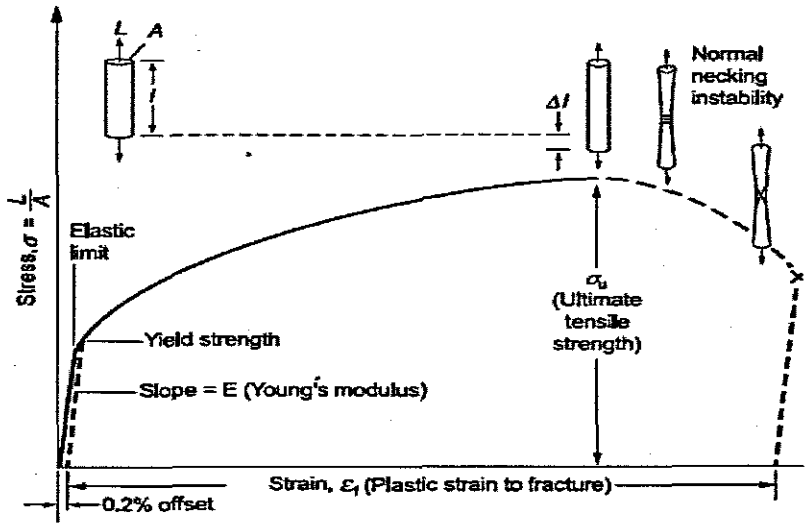

Figure 3.1: Stress-strain curve for ductile material.

3.1.1 Elastic deformation

A temporary change in shape that is self-reversing after the load is removed, so that the solid body reverts to its original shape or size, is called elastic deformation. This type of deformation involves stretching of the atomic bonds, but the atoms do not slip past each other. Most solids when subjected to stress, upon removal of load, return to their original shape and dimensions provided the applied stress is below a characteristic threshold (elastic limit or yield point) for the material of which they are made. Beyond this yield point the non-reversible deformation occurs. In general an elastic solid is characterised by the following responses to deformation:

- The rate of load application does not have an effect.
- Upon removal of the loading, the deformations disappear completely.
- The deformations are very small.

3.1.2 Plastic Deformation

A deformation of a solid body caused by an applied stress, which remains after the stress removed, is called plastic deformation. When the applied stress is large enough it causes the breaking of a limited number of atomic bonds by the movement of dislocations leaving residual deformation in the solid body. The movement of dislocations allows atoms in crystal planes to slip past one another at a much lower stress levels. Since the energy required to move dislocation is lowest along the densest planes of atoms, dislocations have a preferred direction of travel within grains of the material. This results in slip that occurs along parallel planes within the grain. These parallel slip planes group together to form slip bands, which can be seen with an optical microscope (Belytschko et al., 2003 and Maugin, 1992).

3.2 Motions and Deformation

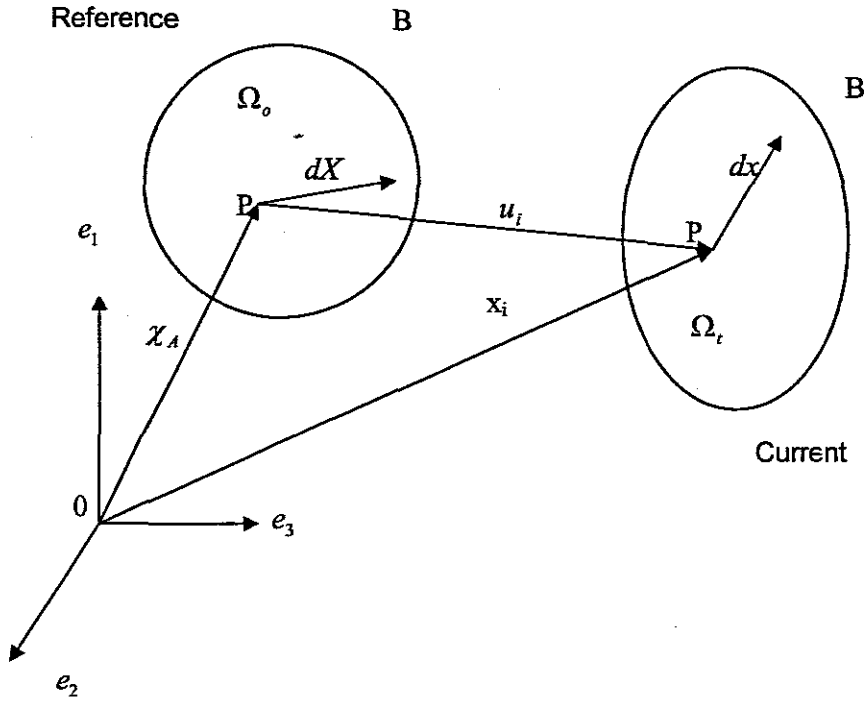

Figure 3.2: Deformation and motion in space

Consideration is given here to an idealised material particle representing a micro region, which is part of the continuum body B initially in the un-deformed state (initial configuration) Ω_o at time t_o as shown in Figure 3.2 above. After undergoing deformation due to transformations taking place inside the material the particle is

displaced through $u(X,t)$ and is in the deformed state (current configuration) Ω_t at time t > t_0. The internal deformation (damage) of the generalised particle is delimited in terms of the local coordinate system whereas displacements at non-characteristic point of the material element are defined relative to the characteristic point.

The general motion of a continuum from the initial position to the current position and its response to deformation can be described in two ways: the Lagrangian description where the independent variables are material coordinate and time, and the Eulerian description where the independent variables are the spatial coordinates and time (Belytschko et al, 2003). However, in this thesis we considered only the former.

3.2.1 Lagrangian Description of Motion

The motion of the body from its initial position to its current position is described by:

$$x = \phi(X,t) \qquad \text{or} \qquad x_i = \phi_i(X,t) \tag{3.1}$$

where x is the spatial position at time t of a material particle with a material coordinate X. The material coordinate X and time t are regarded as independent variables. The function $\phi(X,t)$ is a map between the initial and current domains. The materials coordinates are in the current configuration, so that

$$X = x(X,0) \equiv \phi(X,0) \tag{3.2}$$

3.2.2 Displacement

Displacement is defined as the difference between its current position and its initial position, and is given as:

$$u_i = \phi_i(X_{j,t}) - X_i \tag{3.3}$$

During deformation an initial infinitesimal material line element dX at the initial configuration is transformed, through displacement, into a current infinitesimal material line element dx at time $t > t_o$. The relation between dX and dx is called deformation gradient. The deformation gradient is in an important variable in characterising deformation and it is defined by:

$$F_{ij} = \frac{\partial \phi_i}{\partial X_j} \equiv \frac{\partial x_i}{\partial X_j} \tag{3.4}$$

where F_{ij} is the deformation gradient at X, $dX = \phi(X,0)$ and $dx = \phi(X+dX,t) - \phi(X,0)$.

Assuming that mapping in equation (3.1) is one-to-one and continuously differentiable, the Jacobian of the transformation is given as:

$J = \det\left(\frac{\partial X_i}{\partial X_j}\right)$ and it is finite and positive. (3.5)

3.2.3 Rate of deformation

The second kinematic measure to be considered here is the rate of deformation D. It is the also known as velocity strain and is defined by:

$$L_{ij} = D_{ij} + W_{ij} \tag{3.6}$$

where $D_{ij} = \frac{1}{2}(L_{ij} + L_{ji})$ and $W_{ij} = \frac{1}{2}(L_{ij} - L_{ji})$

3.2.4 Strain and Stress Relationship

3.2.4.1 Strain Measure

In nonlinear transformation different types of measures of strains are used (Belytschko et al, 2003), but in this thesis we considered only the Green (Green-Lagrange) Strain, E defined by:

$$E_{ij} = \frac{1}{2}(F_{ij}^T F_{kj} - \delta_{ij}) \tag{3.7}$$

or in terms of displacement gradients, the Green (Green-Lagrange) Strain, E given as:

$$E_{ij} = \frac{1}{2}\left(\frac{\partial u_i}{\partial X_j} + \frac{\partial u_j}{\partial X_i} + \frac{\partial u_k \partial u_k}{\partial X_i \partial X_j}\right) \tag{3.8}$$

The Green strain can be also expressed in terms of the rate of deformation as:

$$E_{ij} = F_{ik} D_{kl} F_{ij} \tag{3.9}$$

where $D_{kl} = \frac{1}{2}\left(\frac{\partial u_k}{\partial X_l} + \frac{\partial u_l}{\partial X_k}\right)$ is the rate of deformation

3.2.4.2 Stress Measure

Cauchy stress tensor is obtained by (Maugin, 1992):

$$\sigma_{ij} = \frac{\partial W}{\partial \varepsilon_{ij}}, \; W = W(\varepsilon) \tag{3.10}$$

where $W(\varepsilon)$ is the energy density per unit volume and is given by:

$$W = \frac{1}{2}\varepsilon_{ij} C_{ijkl} \varepsilon_{kl} \tag{3.11}$$

where C_{ijkl} is the fourth order tensor of elasticity coefficients, ε_{ij} infinitesimal finite

3.3 Balance Laws

In addition to the motion considered above, we list the balance equations to describe the behaviour of deforming elastic materials. It is assumed that the motion is smooth and the quantities involved in the equations of balance are defined throughout the material and over the time interval $t \geq t_o$ (Makowski et al., 2006 and Davison et al., 1977):

3.3.1 Mass conservation

The conservation of mass is assumed to be trivially satisfied, assuming small displacements, it is defined as:

$$m(\Omega) = \int_{\Omega} \rho(X,t) d\Omega \tag{3.12}$$

where ρ_0 is the mass density. This law requires that the mass of any material domain be constant.

3.3.2 Conservation of Angular Momentum

The conservation of angular momentum is satisfied by the assumption that there are no body moments when the stress tensor is symmetric and it is given as:

$$\frac{D}{D}\int_{\Omega} x \times \rho v d\Omega = \int_{\Omega} x \times b d\Omega + \int_{\Gamma} x \times t d\Gamma \tag{3.13}$$

where $\times$ denotes the cross product, b is the body force and Γ is the material boundary. Finally, the following satisfies the conservation of linear momentum

3.3.3 Conservation of Linear Momentum

The conversation of linear momentum is defined as:

$$p(t) = \int_{\Omega} \rho v(x,t) d\Omega \tag{3.14}$$

where ρv is the linear momentum per unit volume. Using the Newton's second law of motion for a continuum and invoking the Cauchy's relation (neglecting inertial forces), equation leads to the equilibrium equation:

$$\frac{\partial \sigma_{ij}}{dx_j} + \rho b_i = 0 \tag{3.15}$$

And assuming that body forces and inertial effects are negligible equation (3.15) leads to:

$$\frac{\partial \sigma_{ij}}{\partial x_j} = 0 \tag{3.16}$$

3.4 Plasticity and Plastic Flow

In this section we begin by considering elastic deformation, i.e. recoverable time independent stress, σ and strain, ε. Thus, for a Hookean solid, the stress-strain relationship is generally given as:

$$\sigma_{ij} = C_{ijkl}\varepsilon_{kl} \tag{3.17}$$

or

$\sigma = E\varepsilon$ for isotropic uniaxial deformation. (3.18)

Where E is the Young's Modulus.

If the strain is increased beyond the elastic limit, it has been experimentally observed that deformation is not wholly recoverable. The material behaviour is said to be

elastic-plastic. For most ductile metals we get a stress-strain curve like the one given in Figure 3.3.

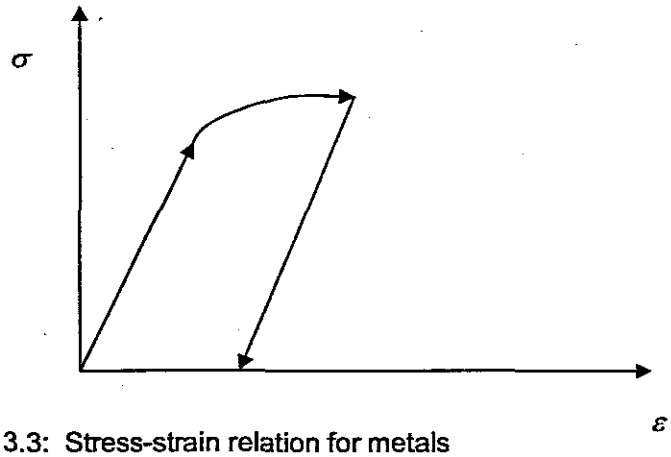

Figure 3.3: Stress-strain relation for metals

3.4.1 Approaches to plastic deformation analysis

There are two main approaches to analyse plastic deformation in materials (Yeh and Lin, 2006; Barlat et al., 2005 and Lubarda, 1999):

- microscopic
- macroscopic

3.4.1.1 Microscopic approach

Microscopic approach considers the mechanism of plastic flow in an individual crystal, e.g., in a metal, this relates to the slipping of the material on glide planes by the passage of dislocations.

3.4.1.2 Macroscopic approach

Here the material is treated, in the first approximation, as an isotropic continuum and its constitutive equations are defined as for the case of elasticity. This approach is valid for polycrystalline materials, but the assumption of isotropy is not valid for single crystals or textured materials.

In this study, we focus mainly on the macroscopic continuum mechanics approach developed with the framework of internal variables thermodynamics (Pirond et al., 2006; Zhu and Cescotto, 1995; Jiang 1995 and Tai and Yang, 1987;).

Numerous models have been proposed and discussed in the literature to approximate material response to deformation within the macroscopic approach (See Figure 3.4). Mathematical models describing the relationship between the stresses, strains, their derivatives, temperature and microstructure are referred to as the constitutive law or relationship. It has been observed that for a number of materials, different mechanisms influence their response to deformation (Shin et al., 2002) and formulating a model that completely describe the materials behaviour can be extremely complex. In general the total strain experienced by the material during deformation at a particular temperature, T, is given as the resultant of metallurgical phenomenon occurring in the material when subjected to mechanical loading σ. Mathematically it can be represented as (Muszka, et al., 2006; Panov, 2006; Tkalcec, 2004 and Cailletaud et al., 2003):

$$\varepsilon = f\{\sigma, \dot{\sigma}, T, \xi\} \tag{3.19}$$

Where ξ represents microstructural features such as grain size, phase, crystal orientation etc and $\dot{\sigma}$ is the stress rate. According to ASM International, 2006 and Han et al., 2007, the total strain in a solid at a given stress level and temperature can be decomposed additively into two parts: a small recoverable elastic part, ε_{ij}^{e} and a large irrecoverable plastic strain ε_{ij}^{p}, and it can be written as:

$$\varepsilon_{ij} = \varepsilon_{ij}^{e} + \varepsilon_{ij}^{p} \tag{3.20}$$

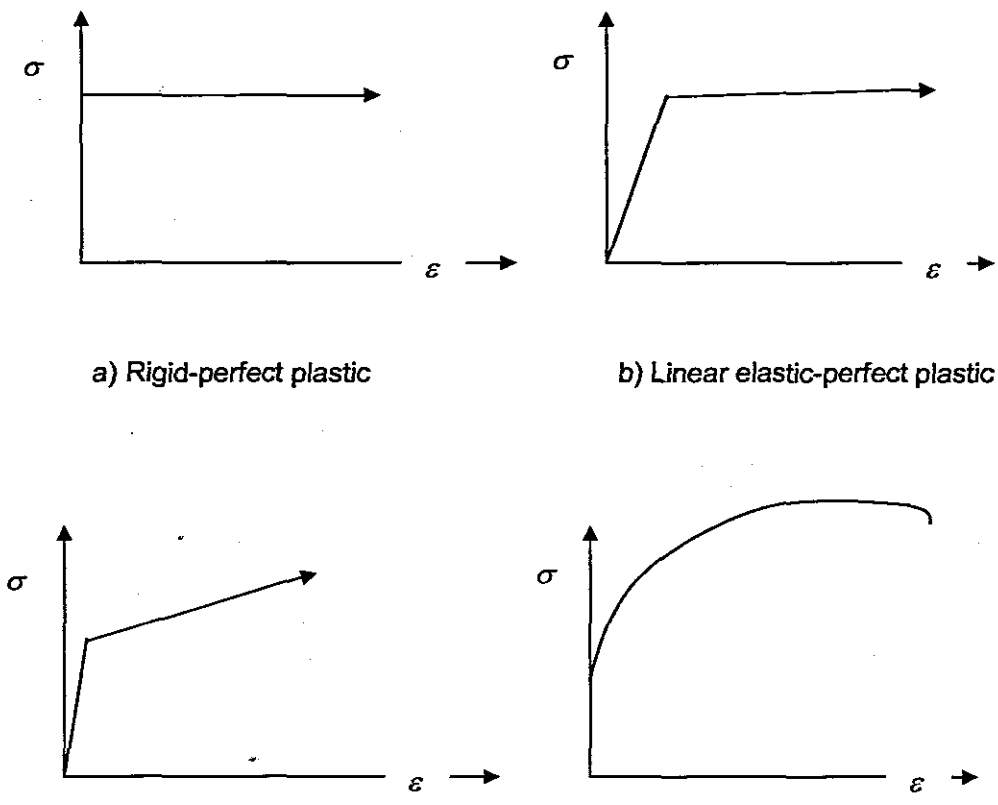

a) Rigid-perfect plastic

b) Linear elastic-perfect plastic

c) Linear elastic-linear work hardening

d) Power law: $\sigma = K\varepsilon^n$

Figure 3.4: Elastic-plastic models for polycrystalline materials

3.4.2 Key concepts in modelling plasticity in metals

In order to predict the internal stress distributions (stress flow); temperature, physical properties and mechanical properties have to be known at any time and point within the material. Thus, the following properties are generally used to characterize the material behaviour during deformation (Yeh and Lin 2006 and Barlat et al., 2005):

- Yield Surface—which predicts whether the material will deforms elastically or plastically.
- Plastic Flow Rule—which states the relationship between stress and plastic strain under multi-axial loading.
- Strain Hardening Rules—which states the way in which resistance to plastic flow increases with straining.

- Loading surfaces that define the limits of elastic and plastic behaviour beyond initial yielding exists

3.4.2.1 Yield Criterion

As shown in Figure 3.1, during tensile test of ductile materials, at point, σ_Y the stress-strain curve deviates from the straight-line relationship and beyond this stress level, permanent deformation occurs and the material is said to be yielding. The yield criterion therefore determines the stress level at which yielding is initiated. In the classical theory of plasticity, two assumptions are made to characterise yielding:

- Yielding depends on the deviatoric stress only.
- The solid is isotropic—onset of yielding depends on the magnitude of the principal stresses $(\sigma_1, \sigma_2, \sigma_3)$.

For multi-component stresses, yield criterion is represented as a function of the individual components, $F(\{\sigma\})$ which can be interpreted as an equivalent stress, σ_e. where $\{\sigma\}$ is the stress vector.

3.4.2.2 Von-Mises Yield Criterion

$$(\sigma_1 - \sigma_2)^2 + (\sigma_2 - \sigma_3)^2 + (\sigma_1 - \sigma_3)^2 = 2\sigma_y^2 \tag{3.21}$$

or

$$\sigma_e = \sqrt{\frac{2}{3} S_{ij} S_{ij}} \tag{3.22}$$

where $S_{ij} = \sigma_{ij} - \frac{1}{3}\sigma_{kk}$ is the deviatoric stress.

3.4.2.3 Flow Rule

The flow rule determines the direction of plastic straining and is generally expressed through use of plastic potential ϕ, which is a function of stress and hardening variables (Yeh and Lin, 2006 and Barlat et al., 2005). For an isotropic material, the evolution of the plastic strains $d\varepsilon_i^p$ is assumed proportional to the gradient of ϕ with respect to the principal stresses σ_1, σ_2 and σ_3:

$$d\varepsilon_i^{\ p} = \lambda \frac{\partial \phi}{\partial \sigma_i} \tag{3.23}$$

where λ is the plastic multiplier.

A special case of this potential is the normality flow rule, also known as the associated flow rule where, plastic potential is the same as the yield function, or $\phi = F$

Equation (3.23) can then be rewritten as:

$$d\varepsilon_i^{\ p} = \lambda \frac{\partial F}{\partial \sigma_i} \tag{3.24}$$

Where $\lambda = \sqrt{\frac{2}{3} d\varepsilon_{ij}^{p} d\dot{\varepsilon}_{ij}^{p}}$ is the plastic multiplier (which determines the amount of plastic straining).

3.4.3 Strain Hardening Laws

Experiments have shown that if the solid is plastically deformed, when unloaded it will show an increased resistance to further plastic flow upon reloading (As the amount of deformations increases, the resistance to further deformation also increases). This behaviour is known as hardening and it affects development of the subsequent yield surface (Voyiadjis and Abed, 2006). There are many ways to describe hardening (Voyiadjis and Abed, 2006 and Shen et al., 2005). Here we describe only the two basic approaches:

- Isotropic.
- Kinematic hardening.

3.4.3.1 Isotropic hardening

The material subjected to plastic deformation is said to be hardening isotropically when its yield-surface increases in size, but remains the same shape. It is also referred to as work hardening.

3.4.3.2 Kinematic hardening

On the other hand, when the yield-surface translates without changing its shape, it is called kinematic hardening. The stress-strain curves for isotropic and kinematic hardening are given in Figure 3.5 below.

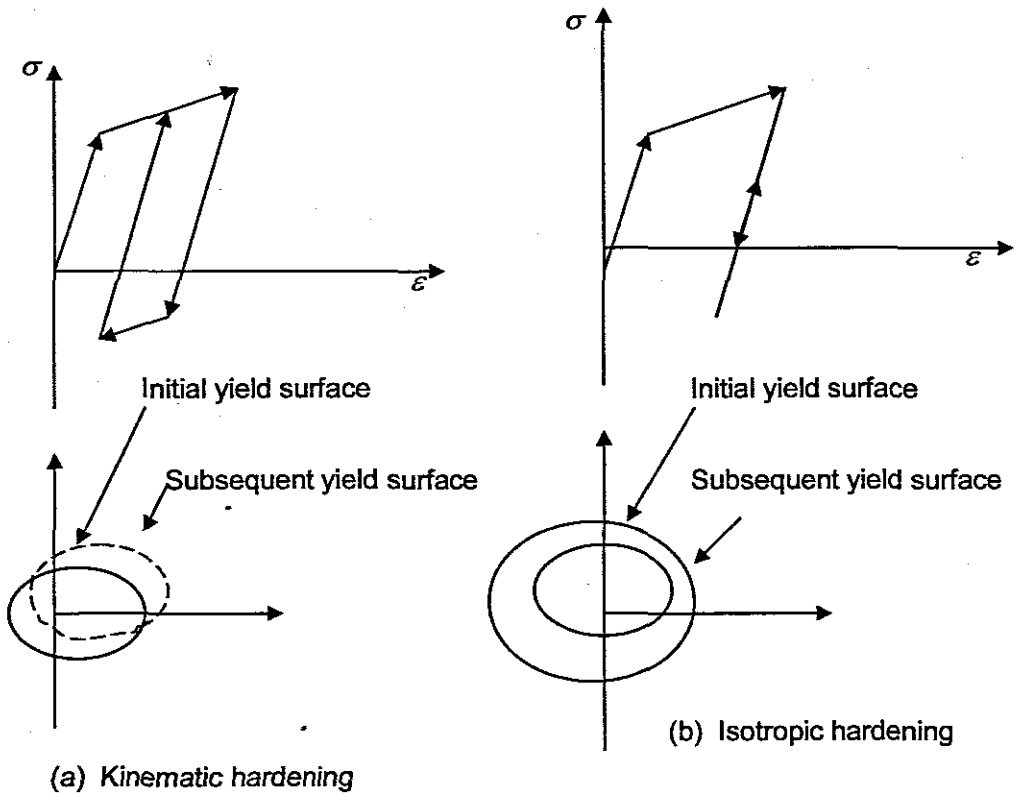

Figure 3.5: Hardening behavior

There are many functions that describe the hardening behaviour of materials, however, in this study, we use the Power—Law hardening material behaviour given as:

$$\sigma_{ij} = K\left(\varepsilon_{ij}\right)^{n} \tag{3.25}$$

or

$$\sigma_{ij} = K\left(\varepsilon_{o} + \varepsilon_{ij}^{p}\right)^{n} \tag{3.26}$$

where K is the flow stress constant, ε_o is the initial strain offset and n is the strain hardening exponent are material constants. These constants are determined by fitting a curve expressed by Equation (3.26) between experimental points obtained from the tensile test. To achieve this; elastic properties are assumed negligible, the material behaviour is considered as rigid-plastic material model and stress-strain

curve for deformation starts at the initial yield stress $\sigma_y\left(\varepsilon^p = 0\right)$as shown in Figure 3.6 below

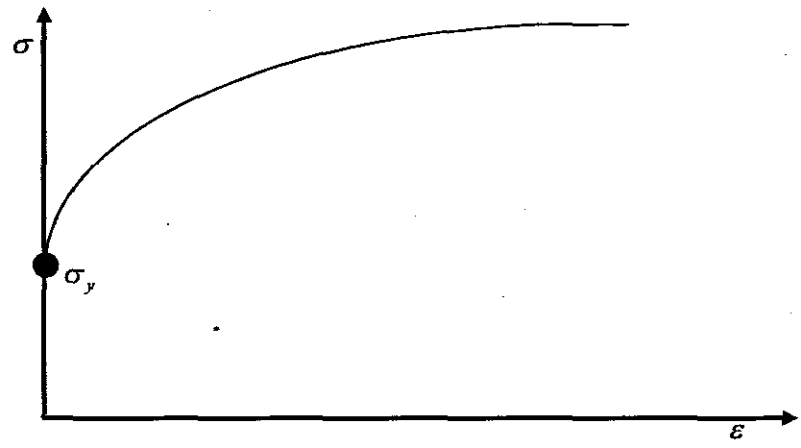

Figure 3.6: Stress-strain curve, rigid plastic material model

The constant, K , represents the stress level for $\varepsilon_0 + \varepsilon^p = 1.0$ and its value indicates the overall stress level at which the material is deformed plastically. The constant indicates the rate of material strain hardening. On a logarithmic scale graph, Figure 3.6 represented by Equation (3.26) becomes a straight line with the slope n,

$$\log(\sigma) = n\log\left(\varepsilon_o + \varepsilon^p\right) + \log(K) \qquad (3.27)$$

3.5 Yield Function incorporating material hardening behavior and microstructural effects

ASM International, 2006 proposed a yield function, F, for materials with plastic strain that incorporated hardening parameter κ at temperature T under multi-axial stresses and volume fraction of phases as:

$$F = \left(\sigma_{ij}, \kappa, \varepsilon_{ij}^p, T, \xi_1\right)\begin{cases} F < 0 \\ F \equiv 0 \end{cases} \qquad (3.28)$$

The yield function F is defined such that a stress state inside the yield surface ($F<0$) corresponds to an elastic deformation process and a stress state on the yield surface ($F\equiv 0$) corresponds to the plastic deformation process.

Equation can be differentiated so that the consistency condition is:

$$dF=\frac{\partial F}{\partial \sigma_{ij}}d\sigma+\frac{\partial F}{\partial \varepsilon_{ij}^{p}}d\varepsilon_{ij}^{p}+\frac{\partial F}{\partial T}dT+\frac{\partial F}{\partial \kappa}d\kappa+\sum_{I=1}^{N}\frac{\partial F}{\partial \xi_I}d\xi_I=0 \qquad (3.29)$$

If the various interactions between temperature and internal state variables can be neglected equation (3.29) can be written as:

$$dF=\frac{\partial F}{\partial \sigma_{ij}}d\sigma+\frac{\partial F}{\partial \varepsilon_{ij}^{p}}d\varepsilon_{ij}^{p}+\frac{\partial F}{\partial \kappa}d\kappa+\sum_{I=1}^{N}\frac{\partial F}{\partial \xi_I}d\xi_I=0 \qquad (3.30)$$

The hardening parameter κ depends on the loading history and its evolution is expressed by plastic work as (Ansys-Rate Independent Plasticity)

$$\kappa=\int\{\sigma\}^{T}[M]\{\dot{\varepsilon}^{p}\} \qquad (3.31)$$

Where

$$[M]=\begin{bmatrix}1&0&0&0&0&0\\0&1&0&0&0&0\\0&0&1&0&0&0\\0&0&0&2&0&0\\0&0&0&0&2&0\\0&0&0&0&0&2\end{bmatrix} \qquad (3.32)$$

and $\dot{\varepsilon}^{p}$ is the plastic strain rate.

CHAPTER FOUR

4.0 Relationship between Grain Size and Mechanical Properties of Steel

The properties of any material generally depend on the microstructure i.e., the arrangement of atoms, the size of the microstructural feature in one, two or three dimensions, orientation and morphology of crystals as well as chemical composition and thermal-mechanical loading history (Lim et al., 2007 and Muszka et al., 2006). *Grain size, in general, has a marked influence on the mechanical properties of steel.* With the knowledge of grain size, it is possible to predict the behaviour of steel when subjected to various working conditions. In fact, many properties of steel are dependent on grain size of steel. Tensile strength, yield strength, toughness, hardenability and machinability can be altered considerably by varying the grain size of steel (Sen et al., 2007; Storojeva et al., 2004 and Morris, 2001). However, according to Muszka et al., (2006) reliable prediction of mechanical properties of materials is more complicated because of different mechanisms that come in play (such chemical composition, the evolution of deformation microstructure, amount of deformation, heat treatment profile, average grain size distribution etc)

Production of different Materials with the controlled manipulation of their microstructure in order to improve properties is an active field of study in materials science. Starting with the pioneering works of Hall, 1951 and Petch, 1953 various studies have been undertaken (Sen et al., 2007; Morris, 2001; and Rack, 1978) and have shown the dependence of polycrystalline metals' mechanical properties on grain size.

4.1 Influence of grain size on deformation

Yield strength is the amount of stress at which plastic deformation becomes noticeable and significant (see Figure 4.1). Besides grain size, yield strength is also influenced by other factors such as chemical composition (see Figure 4.2), forming process, heat treatment process, etc (Lei, 2007; Muszka et al., 2006 and Chen and Gan, 1986).

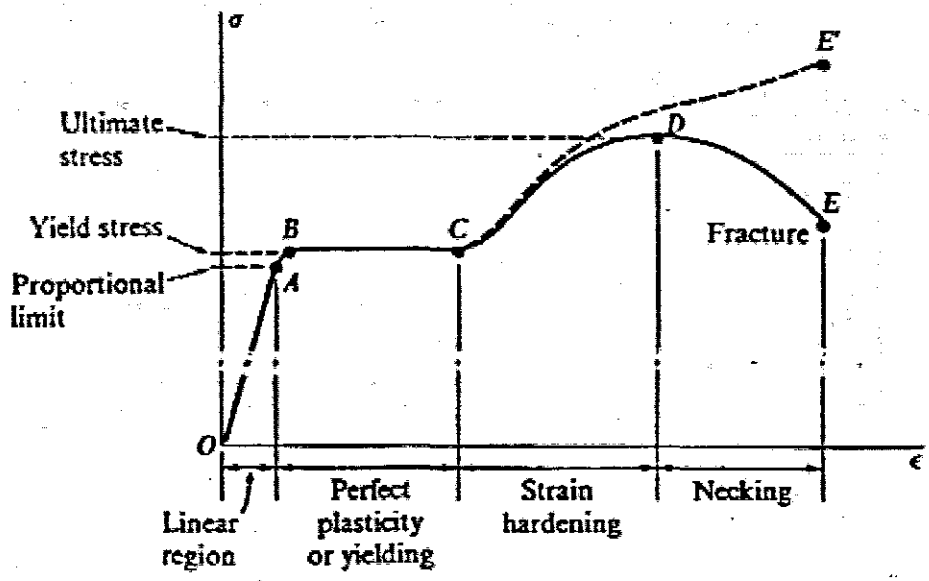

Figure 4.1: Deformation behaviour of a ductile material under tensile load. Source: TPPInfo.com

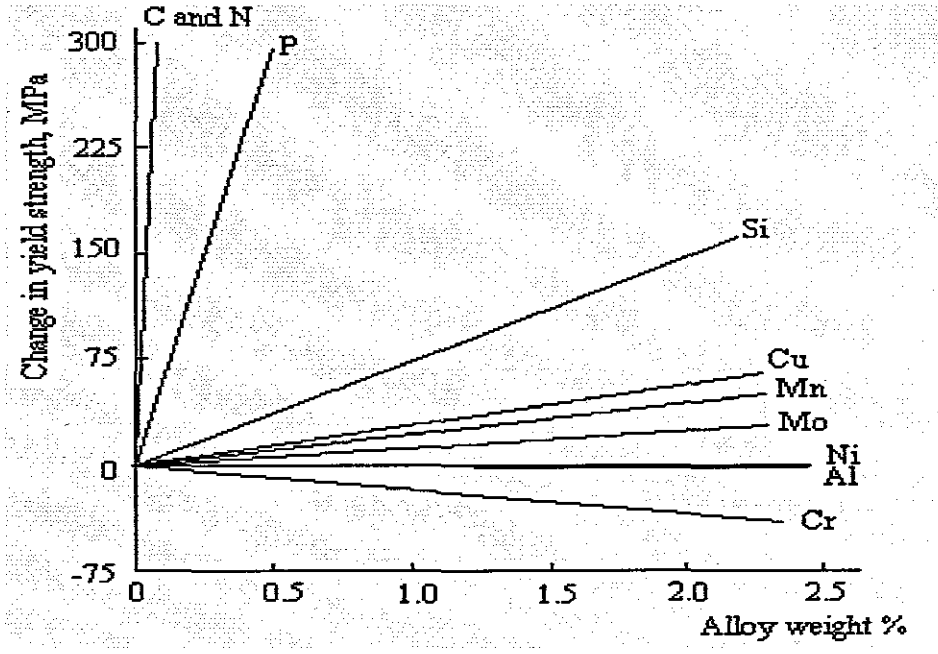

Figure 4.2: effect of alloying elements on yield strength of steel. Source: MET205

The relation between the grain size and the yield strength known as the Hall-Petch (see Figure 4.3) and is given as:

$$\sigma_o = \sigma_i + K_y d^{1/2} \qquad (4.1)$$

Where σ_o is the yield strength, σ_i is the frictional stress opposing motion of a dislocation, K_y is the extent to which dislocations are piled up at barriers, and *d* is the average grain diameter.

In general, as the average grain size decreases, the metal becomes more resistant to plastic flow (yield strength increase) and as the grain size increases, the opposite effect on strength occurs (yield strength decrease). However, many researchers report that the yield strength initially increases following the Hall-Petch equation, but as the grain size reduces to the nano-range (below 1 micron) it deviates (see Figure 4.4) and decreases (Sen et al., 2007; Guduru, 2006; Morris, 2001; Chen and Gan, 1986 and Rack, 1978).

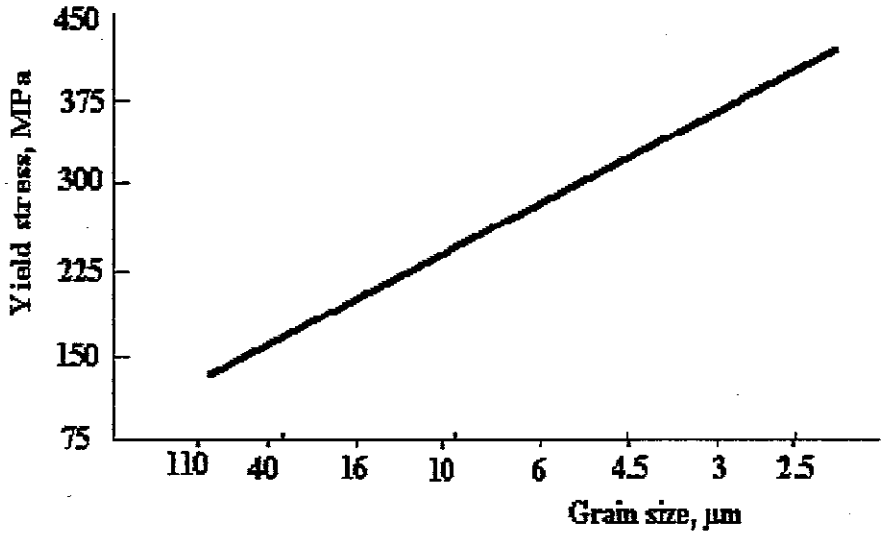

Figure 4.3:Variation of the yield stress with the inverse square root of grain size.
Source: TPPInfo.com

Several different types of mechanisms have been proposed in literature to explain the experimental observations of the Hall-Petch relationship (Morris, 2001). Of these mechanisms, three fundamentally different models can be identified:

- Pile-up models.
- Dislocation density models and.
- Composite models.

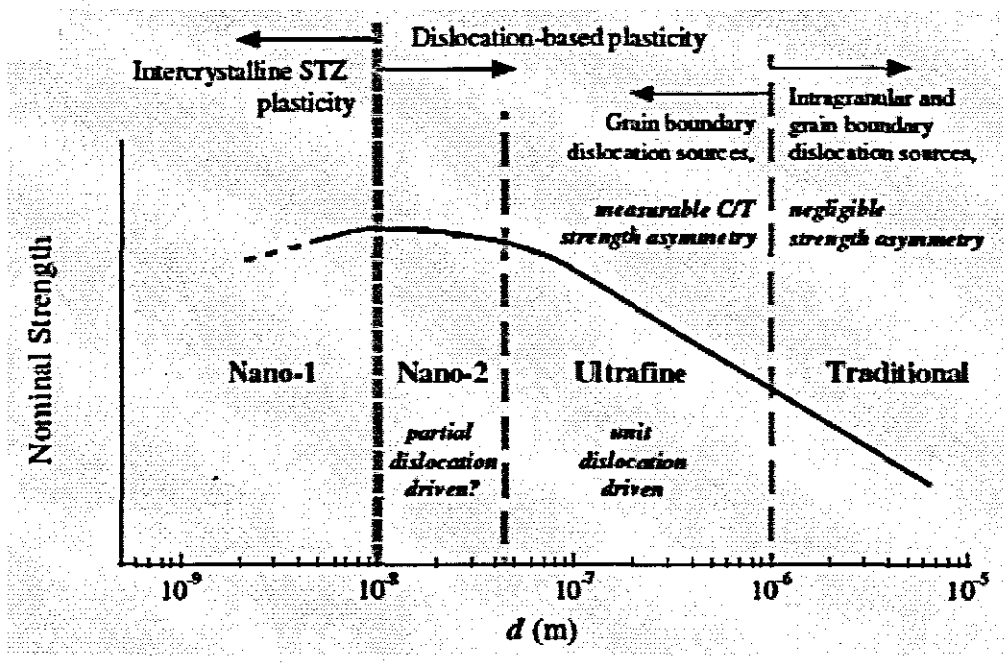

Figure 4.4: Deformation mechanism map with changing grain size (d) (STZ – shear transformation zone, C – compression, T – tensile). Source: Guduru, 2006.

4.1.1 Pile-up models

The Hall-Petch relationship was first discovered by Hall and Petch (Morris, 2001 and Zhang et al., 1995). In this model, it is assumed that dislocations pile up at a grain boundary thereby causing a repulsive force between dislocations (Schiotz, J., 2001). As the grain size decreases, the surface area to volume ratio of the grain increases, resulting in more build-up of dislocations at the grain edge. Since it requires a lot of energy to move dislocations to another grain, these dislocations build up along the boundary increase the yield stress of the material. This model involves two major assumptions (Zhang et al., 1995):

- The stress to move a dislocation through a boundary must be greater than the stress required to move a dislocation in an infinite, homogeneous medium.
- The slip must be mostly planar, so that once a dislocation is emitted from a source, the dislocation remains on the original slip plane or at least on a nearby parallel plane

4.1.2 Dislocation Density Models

Another approach to explain the Hall-Petch relationship is based on the Ashby's model (Ashby 1970). Ashby's model is based on the assumption that the strengthening mechanism due to dislocations can be decomposed into two contributions:

- Contribution from statistically stored dislocations and independent of grain size
- Contribution from geometrically necessary dislocations and dependent on grain size

4.1.3 Composite models

Composite models are based on the idea that the flow stress is a result of contributions from grain boundaries and grain interiors. Models in this category are a combination of the former two models and a number of different variants have been postulated in the literature (Hirth 1972)

4.2 Effects of Grain Size on Ductility, Elongation and Toughness

The dependence of uniform elongation and toughness on microstructure (grain size, morphology and phase) in steel has been investigated by numerous researchers (Muszka et al., 2006; Zmika et al., 2003 and Chen and Gan, 1986). Toughness is defined as the product of yield strength and uniform elongation. The dependence of yield strength on grain size is well described by the Hall-Petch relation; however, uniform elongation versus grain size is not well reported in the literature.

Qu et al., (2005) systematically studied the effects of microstructure on static and dynamic mechanical property of dual phase steel and showed that under uniform displacement conditions, both static and dynamic maximum forces increase with the increase of the martensite fraction. They also observed that for the same martensite fraction, high-temperature-annealed specimen generally exhibited higher maximum force than low-temperature-annealed one. The effects of annealing temperature and time on the mechanical properties on steel subjected to tensile deformation at constant strain was also studied systematically by Manesh and Taheri (2003) using the stress-strain curves of steel annealed at constant temperature and different time. In particular, Manesh and Taheri (2003) showed that the annealing temperature and time have remarkable effects on yield strength, elongation and the ultimate tensile strength of Al clad steel. The reason lies in the grain growth that occurs after

recrystallisation that is a function of temperature and time as expected according to the Larsen–Miller parameter (Zhao et al., 2006).

4.3 Effects of Grain Size on Ultimate Strength and Hardness

Hardness can be roughly defined as a measure of metal's resistance to plastic deformation usually by penetration. However, the term hardness may also refer to resistance to bending, scratching, abrasion or cutting. Hardness can also be used as an indicator of a metal's strength. Consequently, they are roughly proportional. Commonly a correlation between hardness and tensile strength is given in many textbooks for approximately estimating the tensile strength of steel from its hardness value. The correlation of hardness with tensile strength is generally good (difference usually less than ± 10 %). Sleboda et al., (2004) report that Polycrystalline materials often show an increase in hardness and strength with decreasing grain size according to the Hall–Petch relationship. In another study Schiotz, (2001) showed that hardness of steel increases sharply for decreasing grain size, reaches a peak at a critical grain size and decreases as shown in Figure 4.4.

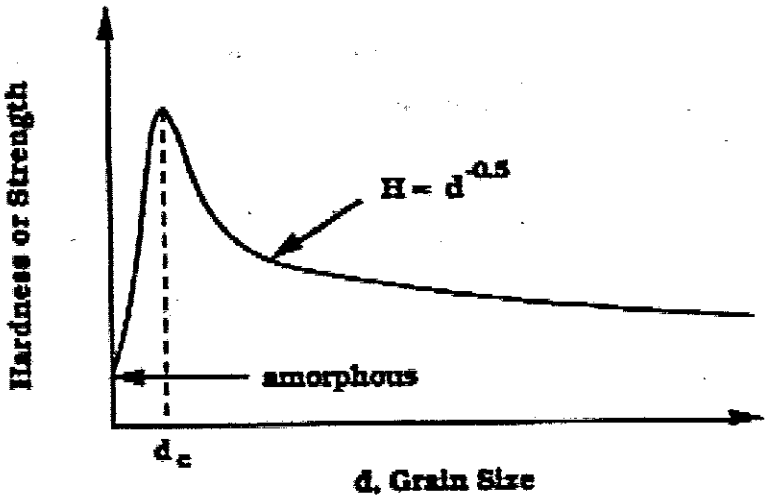

Figure 4.4: Schematic diagram showing hardness or strength as a function of grain size. Source: (Schiotz, 2001).

CHAPTER FIVE

5.0 EXPERIMENTAL TECHNIQUES FOR MECHANICAL PROPERTIES CHARACTERISATION

5.1 Introduction

The main focus of this chapter is the consideration of relatively simple experimental methods to determine material properties of steel with different grain size. To this end, four standard experimental tests were undertaken with the aim of finding the mechanical properties (yield strength, elongation, ductility, ultimate strength and hardness), chemical composition and grain size for the chosen material. The material chosen for this research project is EN8 (BS 970 080M40, black steel) having nominal chemical composition as shown in Table 5.3 below. EN8 is a commercial plain carbon steel commonly used for manufacturing machine components requiring medium tensile strength.

5.2 Heat treatment

The test specimens were prepared using heat treatment experiments. Ten tensile samples (two per category) with dimensions as given in Table 5.2 were machined using CNC machines. Initially 8 specimens were annealed in order to reduce the effects of machining. They were divided into four sets of tensile tests. These sets were heated at 914 °C, held at this temperature for 3 minutes and quenched in cold water (25°C). After that each specimen set received a specific heat treatment regime, as described in Table 5.1 below.

Table 5.1: Heat treatment regime employed to produce various microstructural features.

Specimen	Heat treatment
A	"As received" specimen
B	Austenised at 950°C, held for 180 min and cooled in furnace
C	Austenised at 914°C, held for 10 min, cooled in furnace to 680 °C and cooled in water.
D	Austenised at 914°C, held for 3 min, cooled in furnace to 715 °C and quenched in oil.

5.3 Standard tensile test and the principle of operation

The tensile test is one of the most commonly used tests for evaluating material properties. In its simplest form a specimen is fixed on one end while the other end is pulled in tension by a machine see Figures 5.1 and 5.2. During the test, the force applied to the specimen and the resulting elongation of the specimen are measured and recorded simultaneously at regular intervals. The force-elongation data is then used to quantify a number of important mechanical properties some of which are listed below:

- Yield and ultimate tensile strength.
- Strain and damage hardening characteristics.
- Ductility properties, such as elongation and reduction in area.
- Elastic deformation properties, such as the Young's modulus and Poisson's ratio.

In this study, specimens were incrementally loaded uniaxially along their axes until fracture occurred (see Figures 5.2 and 5.3). The tests were carried out in accordance with ASTM E 28 at room temperature and constant strain rate of 5mm per minute.

Figure 5.1: Tensile test machine.

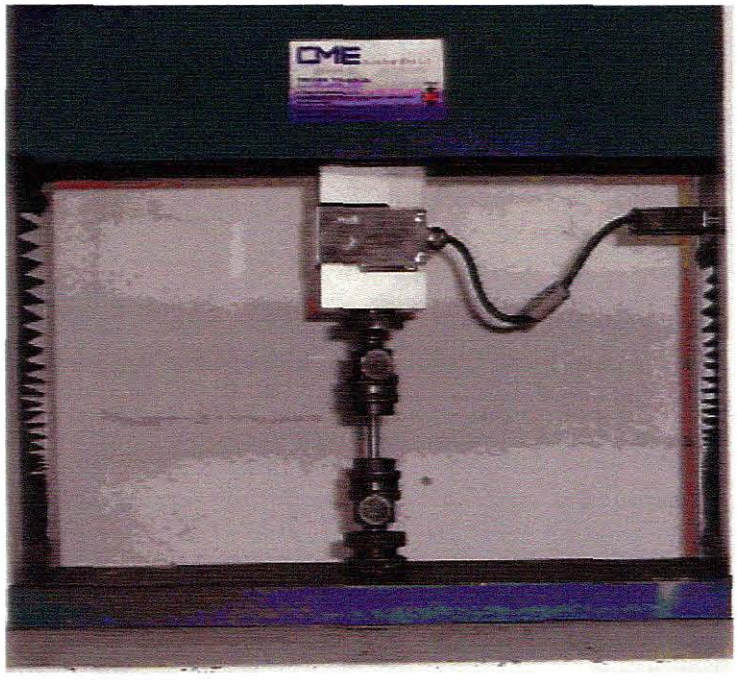

Figure 5.2: Tensile test piece mounted on the machine

5.3.1 Definition and terminology

The basic results of a tensile test are quantities of stress and strain that are measured. These basic terms as defined by ASTM E 28 are listed below.

5.3.1.1 Engineering variables

5.3.1.2 Stress

Stress is defined as the amount of force that acts over a given cross sectional area. Stress can be classed into engineering and true stress.

Engineering stress, σ: The force at any time during the test divided by the initial area of the specimen;

$$s = \frac{F}{A_o} \tag{5.1}$$

here F and A_o are the force and initial cross sectional area of the specimen respectively.

True stress, s; The force at any time divided by the instantaneous cross sectional area of the specimen;:

$$\sigma = \frac{F}{A_{int}} \tag{5.2}$$

where F is the force and A_{int} is the instantaneous cross sectional area of the specimen.

5.3.1.3 Strain and elongation

Strain and elongation are similar terms that define the amount of deformation from a given amount of applied stress. Strain is a general term that can be expressed mathematically, either as engineering strain or true strain.

5.3.1.4 Engineering strain

Nominal or engineering strain denoted by the letter e is defined as:

$$e = \frac{\Delta L}{L_o} = \frac{(L - L_o)}{L_o} \tag{5.3}$$

here ΔL and L_o are nominal change in length and original length respectively.

5.3.1.5 True strain

The equation for true strain ε is based on the instantaneous change in length, dl given as:

$$\varepsilon = \int_{L_o}^{L} \frac{dl}{l} = \ln\left(\frac{L}{L_o}\right) \tag{5.4}$$

5.3.1.6 Relationship between the two strain measures

$$\varepsilon = \ln(1 + e) \tag{5.5}$$

5.4 Effects of strain rate and temperature on deformation

It has been observed experimentally that material fracture characteristics are generally affected by internal and external variables (strain, strain-rate, temperature, loading history etc.). Temperature and strain rate are two very important external ones (Wang, 1993). The mechanism of plastic deformation and fracture of materials may change at different temperatures and strain rates. According to Kanasaki et al., (1997) and Kallerova and Wald, (2007) the mechanical properties of most metals and alloys vary considerably as the strain rate and temperature changes. Wang

conducted uniaxial tensile tests on a high strength low alloy steel and found out that temperature plays an important role on mechanical behaviour of material. His findings are presented graphically in the Figure 5.5 below. Temperature also affects the Hall-Petch relationship. It has been shown experimentally that in low carbon steels, the Petch slope has strong temperature dependence for quenched and aged specimens while in slowly cooled specimens it is relatively insensitive to temperature (Dingley and McLean 1967).

5.5 Strain rate

The rate at which strain is applied to the tensile specimen has an important influence on the stress-strain curve see Figure 5.4. However, for most metallic materials at room temperature, the strain rate is often ignored since it has only a small effect on the flow curve. But as the temperature increases its effect on the flow curve becomes more pronounced and at a fixed strain and temperature it can be accounted for by the expression (ASM International, 2006):

$$\sigma = C\dot{\varepsilon}^m \tag{5.6}$$

The exponent, m, is called the strain rate sensitivity and $\dot{\varepsilon}$ is the strain rate.

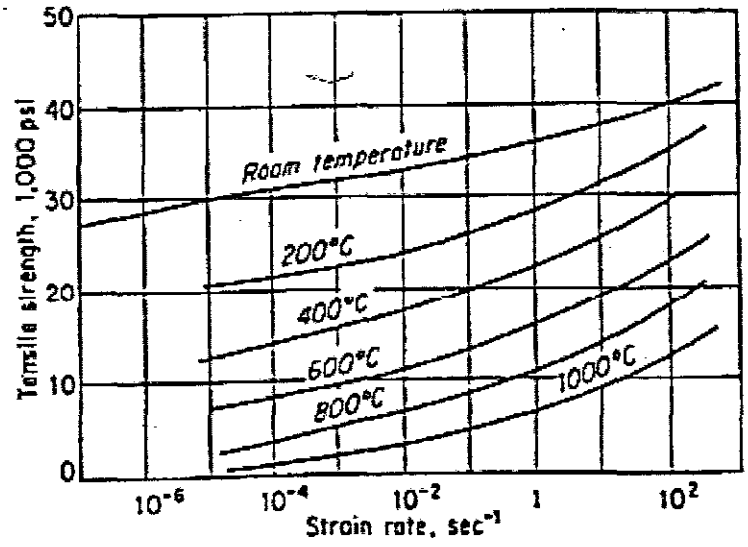

Figure 5.4: Effects of temperature and strain rate on the strength of copper.
Source: ASM International, 2006

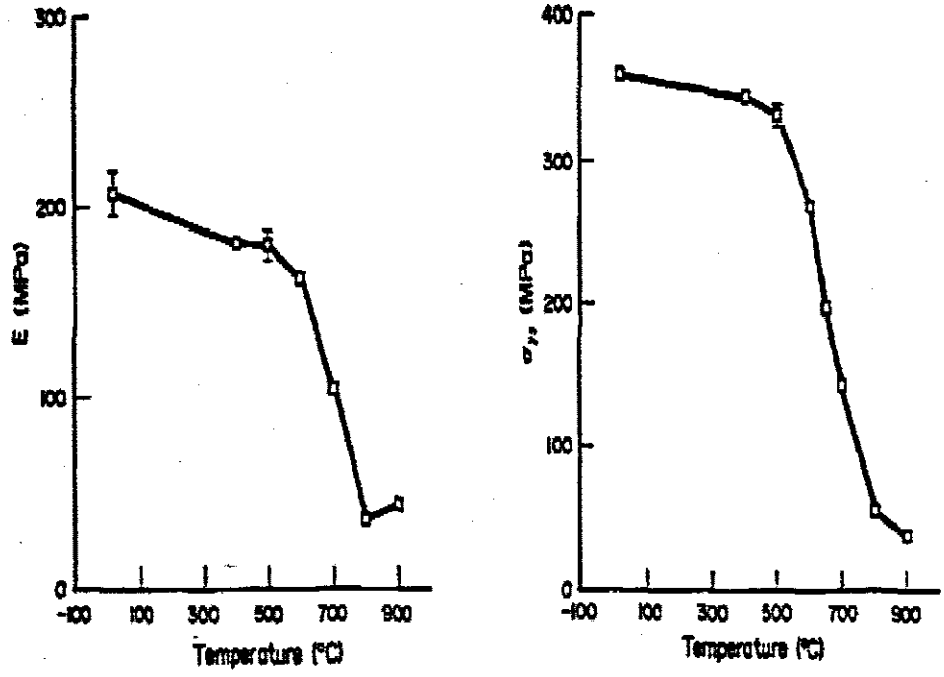

Figure 5.5: Relationship between temperature and mechanical properties of a low alloy steel: a) Relationship between temperature and Young's modulus, b) Relationship between temperature and 0.2% offset yield strength, c) Relationship between temperature and ultimate tensile strength and d) Relationship between temperature and percent elongation.
Source: Wang, 1993.

5.6 Test specimen geometry

The measurement of tensile properties was performed using standard round bar test specimens (see Figure 5.6) according to ASTM E 28.

Table 5.2 Standard specimen size in mm

Parameter	Standard specimen	Small size specimen proportional to standard
D, Nominal diameter	12.699	6.35
G, Gauge length	57.1499	25.53
R, Radius of the fillet	9.5249	4.76
A, Length of the reduced length	50.799	31.75

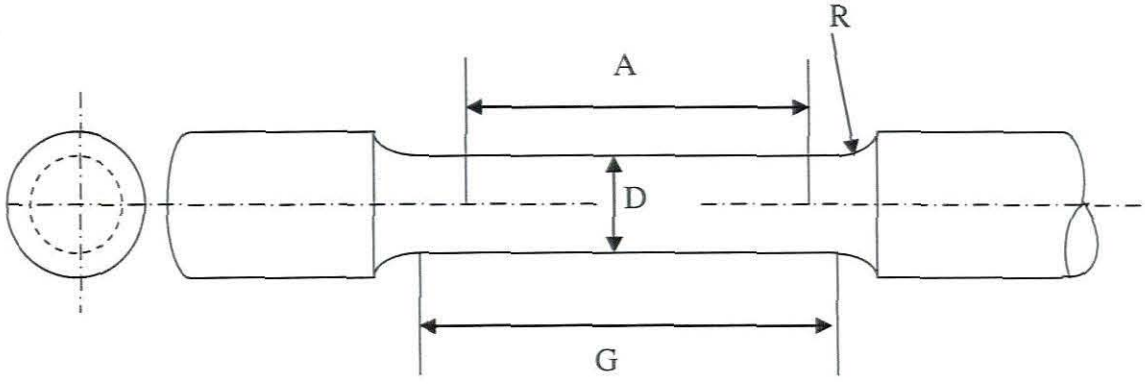

Figure 5.6 Round bar specimen

5.7 Hardness testing

In this study, indentation hardness testing methods were used. The three most common hardness testing methods in this category are:

- *Brinell hardness testing (HB)*
- Rockwell hardness test (HR)
- Vickers hardness test

5.7.1 Brinell hardness testing (HB)

The typical test uses a 10 mm diameter ball indenter with a 29 kN force (see Figure5.7). For softer materials a steel ball and smaller force is used whereas for harder materials a tungsten carbide ball is substituted for the steel ball. The indentation is measure and hardness is calculated as:

$$BHN = \frac{2P}{\pi D\left(D - \sqrt{D^2 - d^2}\right)}$$

Where

P = applied force (kN)

D = diameter of indenter (mm)

d = diameter of indentation (mm)

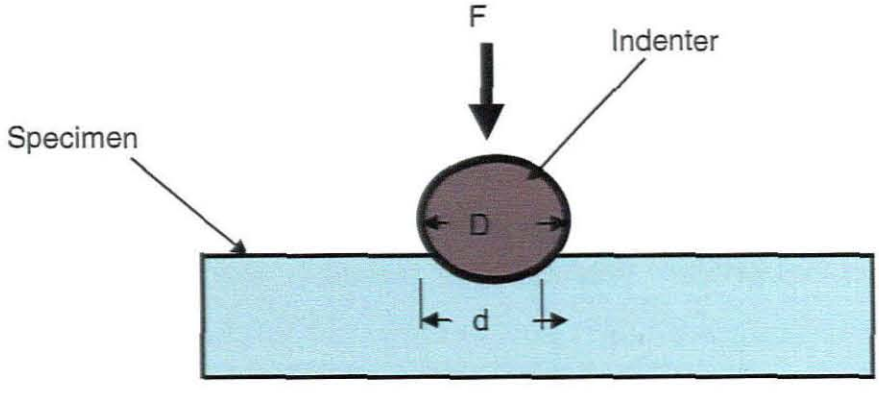

Figure 5.7: Schematic of Brinell hardness testing

5.7.2 Vickers hardness testing (HV)

The Vickers test is an alternative and often easier to measure hardness of material (since the required calculations are independent of the size of the indenter, and the indenter can be used for all materials irrespective of hardness). The Vickers test can be used for all metals and has one of the widest scales among hardness tests. The unit of hardness given by the test is known as the **Vickers Pyramid Number (HV)**.

The Vickers hardness test uses a diamond, with the shape of square-based pyramid with an angle of 136° between opposite faces as an indenter (22° between the indenter face and surface). It is based on the principle that impressions made by this indenter are geometrically similar regardless of load. Accordingly, loads of various

magnitudes are applied to a flat surface, depending on the hardness of the material to be measured. The Vickers Pyramid Number (HV) is then determined by the ratio:

$$HV = \frac{F}{A} \approx \frac{1.854P}{d^2} \qquad (5.7)$$

Where **F** is the force applied to the diamond and **A** is the surface area of the resulting indentation.

5.7.3 Rockwell hardness test (HR)

The Rockwell hardness test method consists of characterising materials hardness through the depth of penetration of an indenter, loaded on a specimen. Its hardness values are noted by HR* where * is the letter for the scale used. There are several alternative scales, the most commonly used being the "B", and "C" scales. Both scales express hardness as an arbitrary dimensionless number. n all the scales, the determination of the Rockwell hardness of a material involves the application of a minor load followed by a major load, and then reading the hardness value directly from a dial or display (which is the main advantage of Rockwell hardness test as compared other hardness measurement techniques that involve tedious calculations).

Figure 5.8: Rockwell hardness test machine

5.8 Microstructural Investigation

In this study, Scanning Electron Microscope (SEM) and Light Optical Microscope (LOM) were used for phase identification and microstructure characterization of EN8. These techniques are briefly discussed in the following sections.

5.8.1 Scanning Electron Microscopy (SEM)

Scanning electron microscopy was carried out on the Hitachi X-650 SEM at the University of Western Cape which is a 40 kV machine offering resolution of up to 6 nm (see Figure 5.9). The machine is equipped with a secondary electron detector and a backscattered electron detector for normal imaging, and a solid state detector for elemental analysis as well as electron beam induced current imaging. The machine utilizes a 3-stage electromagnetic lens system and the only movable aperture is the objective aperture which was normally set at 400 µm. A working distance of 5mm was generally used to further boost the resolving power of the machine except in cases where a backscattered electron image was collected in which case the working distance was adjusted to 15 mm due to a positioning constraint. Accelerating voltage of 10 kV and 30 kV were used interchangeably to bring out certain features on the specimen surface or from slightly below the surface. Filament current between 70 and 80 µA was generally used. X-ray analysis (EDAX) was used as a qualitative tool to identify elements within the sample and the results are given in Table 5.3 below.

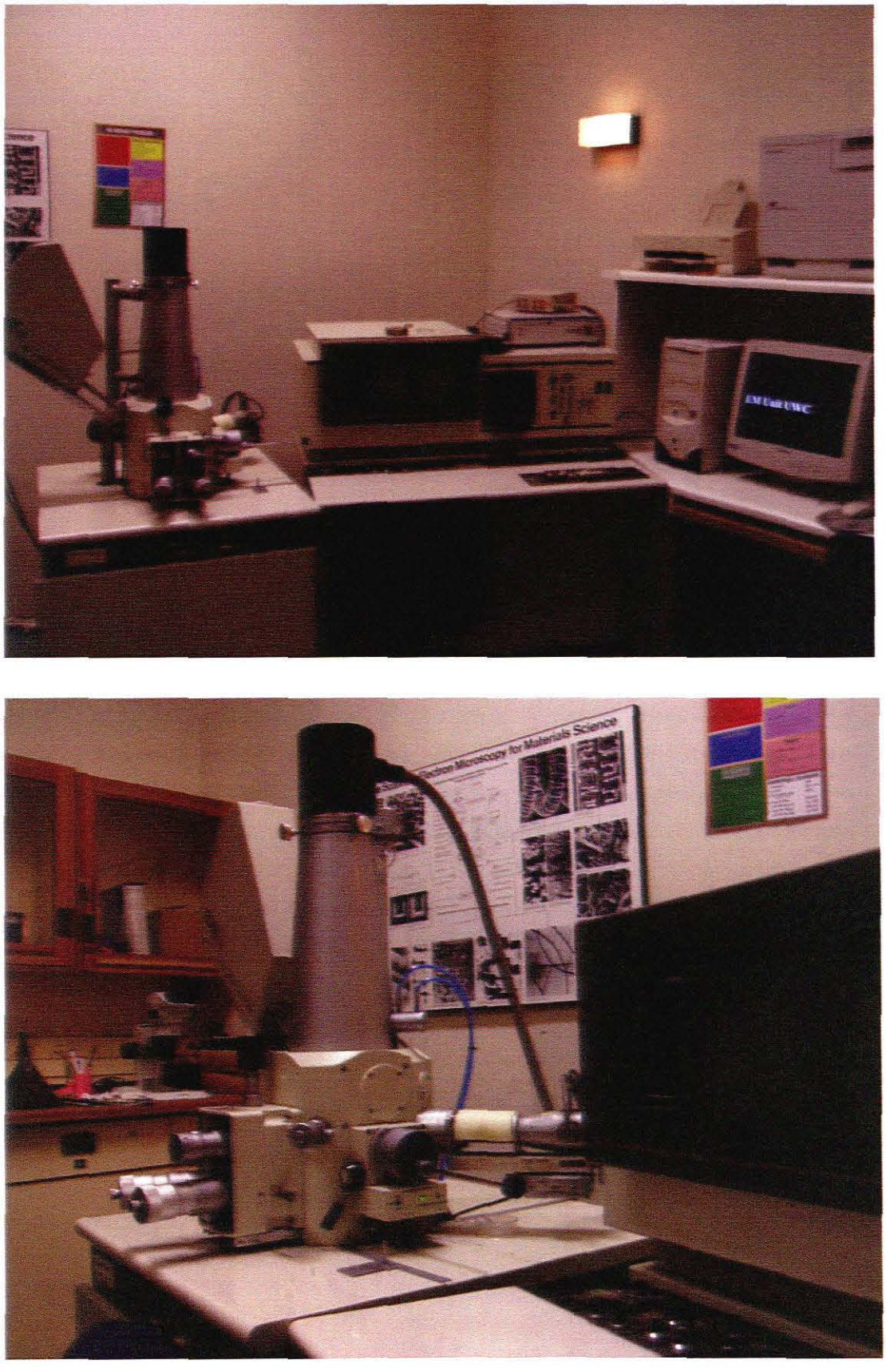

Figure 5.9: Scanning Electron Microscope (SEM)

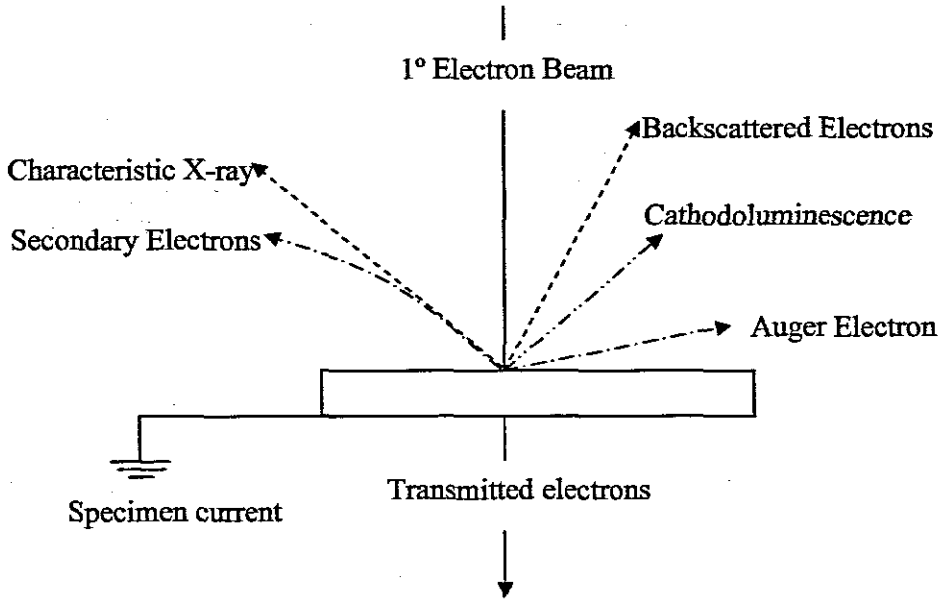

Figure 5.10: Schematic illustration of the possible signals generated by the primary electron beam-specimen interaction in the scanning electron microscope

5.8.2 Light Optical Microscope (LOM)

Light Optical Microscopy is one of the most commonly used techniques for microstructure characterisation in steels. Steels are opaque to visible light and as a result only the surface of the metal sample is subject to investigation with this technique. The image contrast is a result of variations in reflectivity in the different regions of the microstructure. Limitations of this technique are its spatial resolution at approximately 0.5 μm and its depth of field. Investigations in this work were carried out at Cape Peninsula University of Technology using Nikon Eclipse L150 light optical microscope (see Figure 5.11) equipped with analySIS docu software for image analysis.

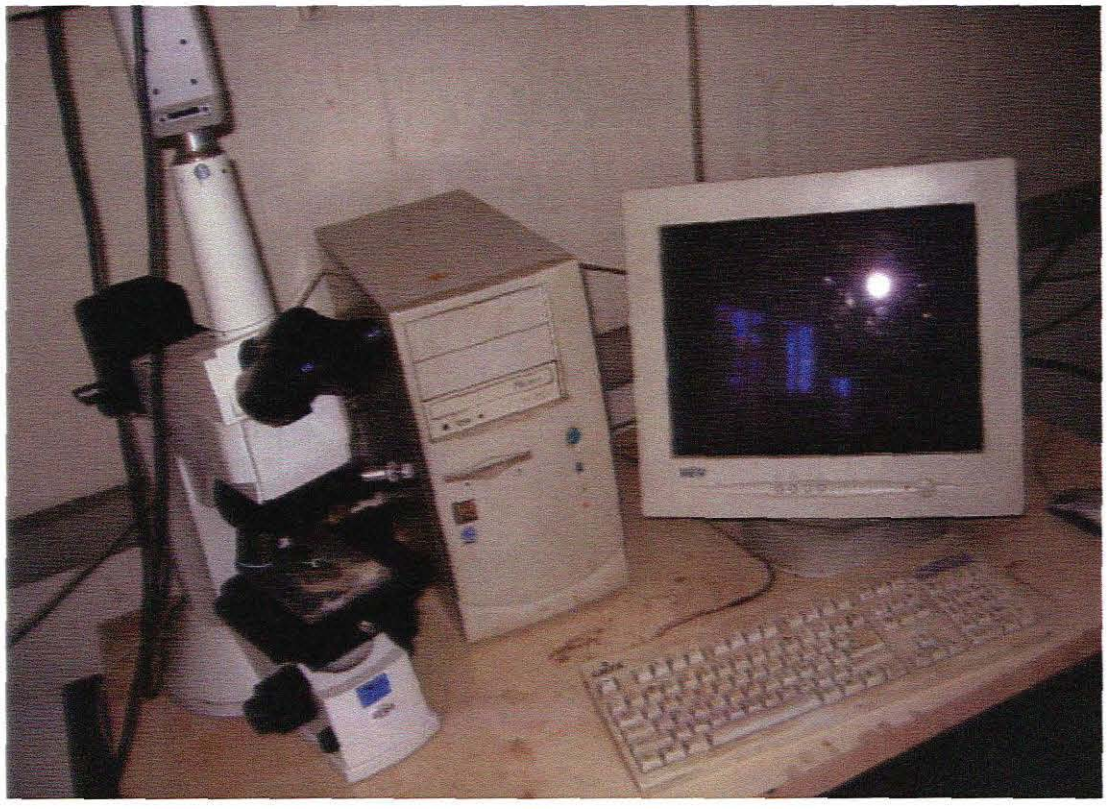

Figure 5.11: Light Optical Microscope

5.8.3 Specimen preparation for SEM and LOM

Samples were prepared as described below following the ASTM A-395 standard. In this study 10 test specimens measuring 5 mm long were cut using the metallurgical saw (see Figure 5.12).

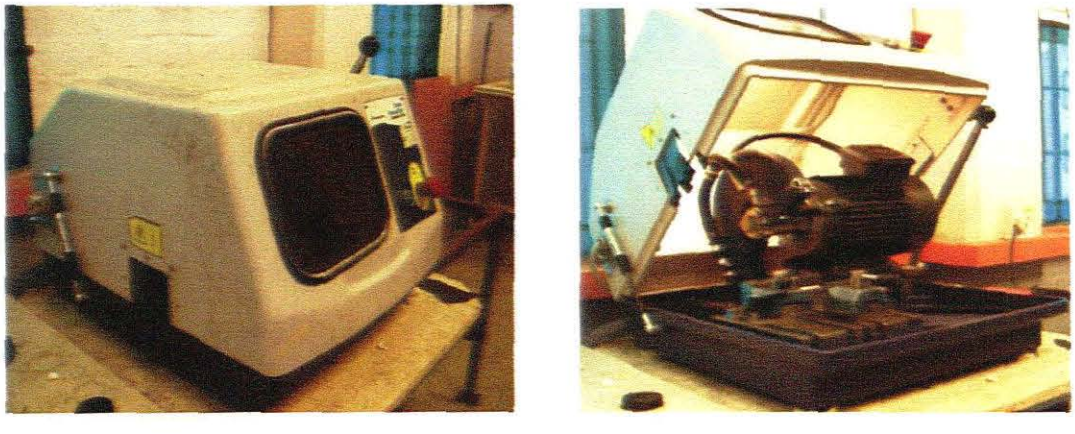

Figure 5.12: Metallurgical cut-off saw.

The test specimens were then embedded in acrylic hot mounting resin using a thermal-compression mounting machine, see Figure 5.13.

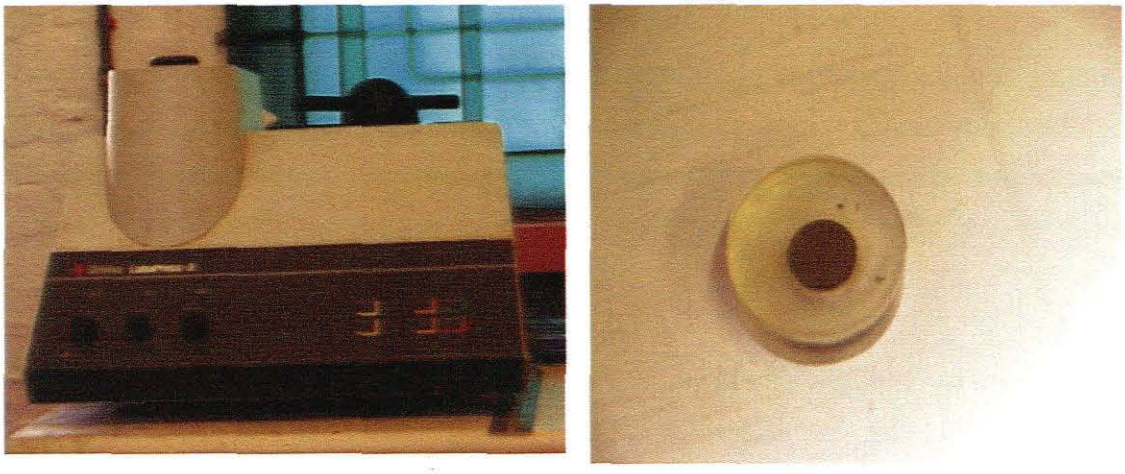

a) b)

Figure 5.13: a) Thermal compression moulding machine, b) Specimen in the mould

The specimens, one at a time, were placed flat on a steel piston (rubbed with anti sticking compound) within the machine cylinder. Acrylic hot mounting resin was poured on and around the test specimen. A steel cap dubbed with anti sticking compound was placed and screwed onto the cylinder. A temperature of 180°C and a constant force of 30 kN were applied for a period not more than 30 minutes sequentially. After curing, the machine was allowed to cool down, and the test specimen was removed from the machine.

Figure 5.14: Rotary Grinding-Polishing machine

5.8.4 Test specimen grinding and polishing

Three specimens at a time were mounted on a rotary polishing-grinding machine for grinding and polishing see Figure 5.14 above.

The process was carried out in two stages. The first stage involved the use of a piano disk with water as the lubricant. The wheel was set to rotate at 200 rpm and the pressure of about 6N on the test specimen was roughly maintained by periodically adjusting the spring load on the machine. The essence of this 15 minute-process was to grind the test specimen flat.

This rough grinding process was followed by a 30-minute three-step-polishing procedure to achieve a scratch free-mirror finish surface. A largo disk in conjunction with 9 micron diamond suspension (no water) was used as above to remove the larger scratches. The second step involved the use of MD plus disk with 3 micron diamond suspension for finer polishing. The process ended with the use of MD nap with 1 micron diamond suspension. This process took 30 minutes—10 minutes per stage.

5.8.5 Etching solution

Etching followed final polishing. The test specimens were taken off the machine and thoroughly cleaned in running water to remove polishing debris. After cleaning, the test specimens were swabbed in alcohol ready for etching.

An appropriate attack etching solution was prepared as follows: 98 millilitres of ethyl alcohol was mixed with 2 millilitres of concentrated nitric acid, forming a solution called 2% Nital. The solution was chosen because the material to be investigated was a plain carbon steel. The effects of Nital 2% on plain carbon steel are listed in Table 5.3 below.

Table 5.3: The effects of Nital 2% solution on low carbon alloy steels

Nital 2% solution (2mL Nitric acid + 98 mL ethyl alcohol	
1	Darkens pearlite and give contrast between pearlite colonies
2	Reveals ferrite boundaries
3	Differentiates ferrite from Martensite

5.8.6 Imaging

5.8.6.1 Electron beam-specimen interaction

Solid specimens subjected to electron beam excitation in SEM exhibit complex interactions with primary beam electrons. These interactions result in a variety of signals that may be detected in the SEM (see Figure 5.10)

In order to study surface morphology in the SEM, the surface of the sample must be electrically conductive for effective viewing. In view of this our samples, which were imbedded in non-conductive materials, were stripped with thin copper film and silver paste as shown in Figure 5.13 (c). The test specimen was carefully placed on the SEM and viewed at three different resolutions.

5.8.7 Image analysis

The test specimen was examined for the following features:

The size, shape and type of grain present.

The chemical composition of EN 8 was determined using the EDAX, and is given in the Table 5.3 below.

Table 5.3: Chemical composition of EN8

Element	C	Fe	P	Mn	S
Composition wt %	0.76	97.8	0.05	1.44	0.11

5.8.8 Determination of Grain Size

In this study we used the mean lineal intercept method (Heyn procedure) as described in ASTM E 112-88. This technique is one of the numerous procedures within the field of stereology that have been developed to estimate average grain size, grain shape, grain distribution, grain orientation etc. Metallographic measurements are usually made in a 2-D planar section of a volume and in this specific case, the average grain size calculations were based on measurements made on LOM micrographs.

The mean lineal intercept length is the average length of a line segment that crosses a sufficiently large number of grains. The mean lineal intercept length is determined by laying a number of randomly placed test lines on the image and counting the

number of times that grain boundaries are intercepted. Mathematically, it is defined as:

$$\bar{L}_L = \frac{1}{N_L} = \frac{L_T}{PM} \tag{5.8}$$

Where N_L is the number of intercepts per total length of the test lines L_T, P is the total number of grain boundary intersections and M is the magnification.

The ASTM grain size number is based on the number of grains per square inch at a magnification of 100X. The basic equation defining the ASTM E 112 grain size number is given as:

$$n = 2^{G-1} \tag{5.9}$$

Where upon taking logs on both sides it follows that:

$$G = \frac{\log n}{\log 2} + 1 \tag{5.10}$$

Or from the mean intercept length

$$G = -3.2877 - 6.6439 \log \bar{L}_L \tag{5.11}$$

Where **n** is the number of grains per square inch at 100x and **G** is the ASTM (Timken) the equivalent grain size number.

CHAPTER SIX

6.0 Experimental Results

6.1 Microstructural results

As described above, EN8 steel, with five different microstructures was characterised by two different experimental surface microscopy techniques; Light Optical Microscope and Scanning Electron Microscope. Results obtained are presented below.

6.1.2 Scanning Electron Microscope

Figures 6.1-6.4 show micrographs (SEM images) of the specimens A, B, C and D of EN8 prepared according the heat treatment regime described in chapter five. The polished samples were made conductive using silver paste and observed in a field emission high-resolution scanning electron microscope in the backscattered electron-imaging mode.

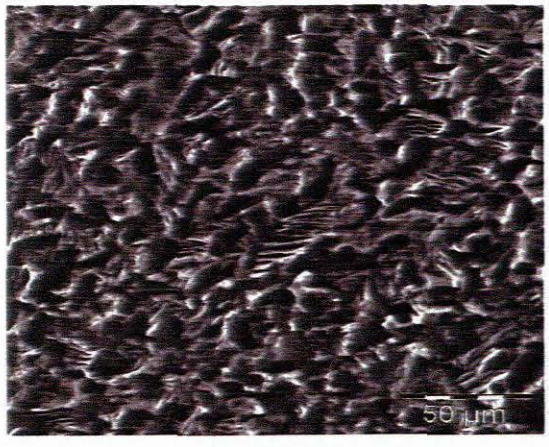

Figure 6.1: Micrograph A

Figure 6.2: Micrograph B

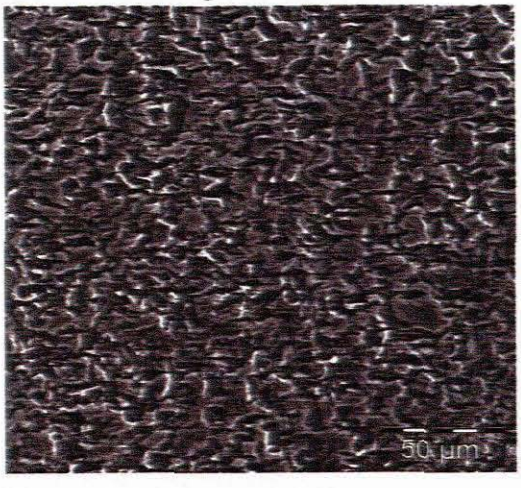

Figure 6.3: Micrograph C

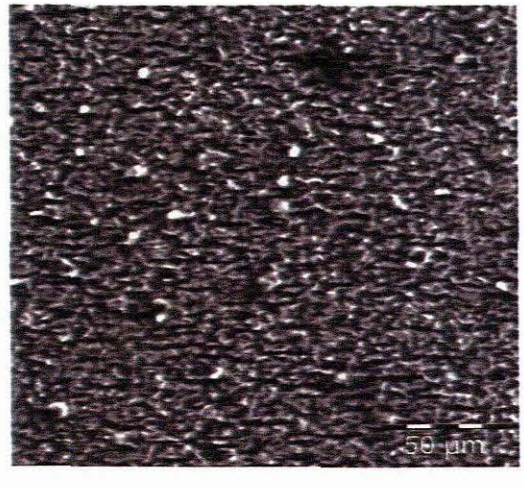

Figure 6.4: Micrograph D

6.1.3 Light Optical Microscope

Figures 6.5-6.8 show micrographs (LOM images) of the specimens A, B, C and D of EN8 prepared according the heat treatment regime described in chapter five.

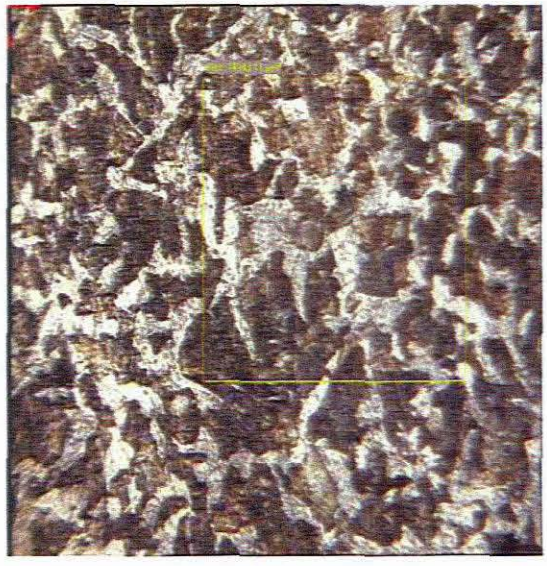

Figure 6.5: Micrograph A

Figure 6.6: Micrograph B

Figure 6.7: Micrograph C

Figure 6.8: Micrograph D

From Figures 6.1-6.8, it can be observed that the heat treatment regime employed produced five different microstructures. The micrographs show, both grains and phase present in the specimens. Another interesting feature that can be observed with SEM and LOM is the individual grain boundaries, which can be distinguished quite easily at higher magnifications (see Figures 6.9 and 6.10).

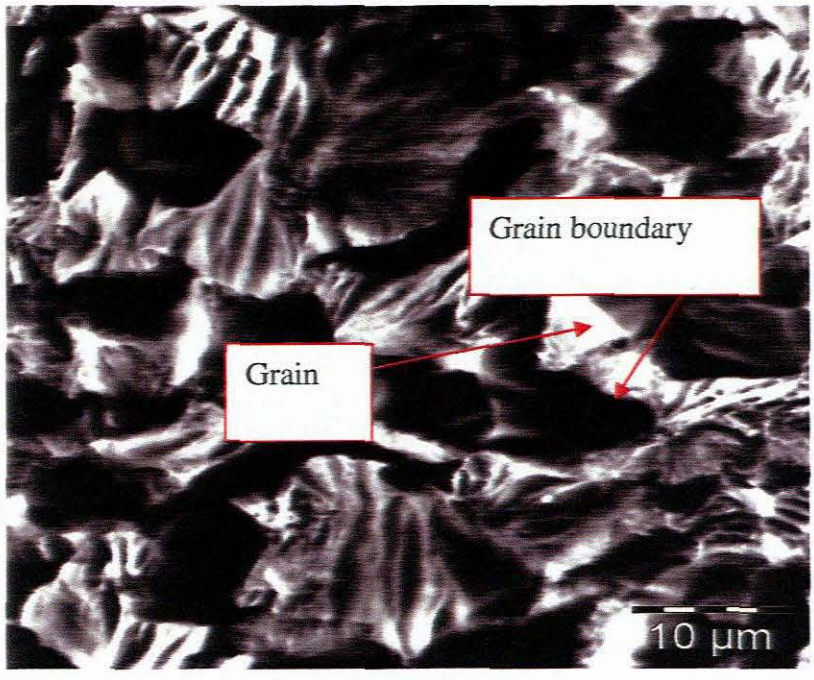

Figure 6.9: SEM micrograph showing individual grains and grain boundaries

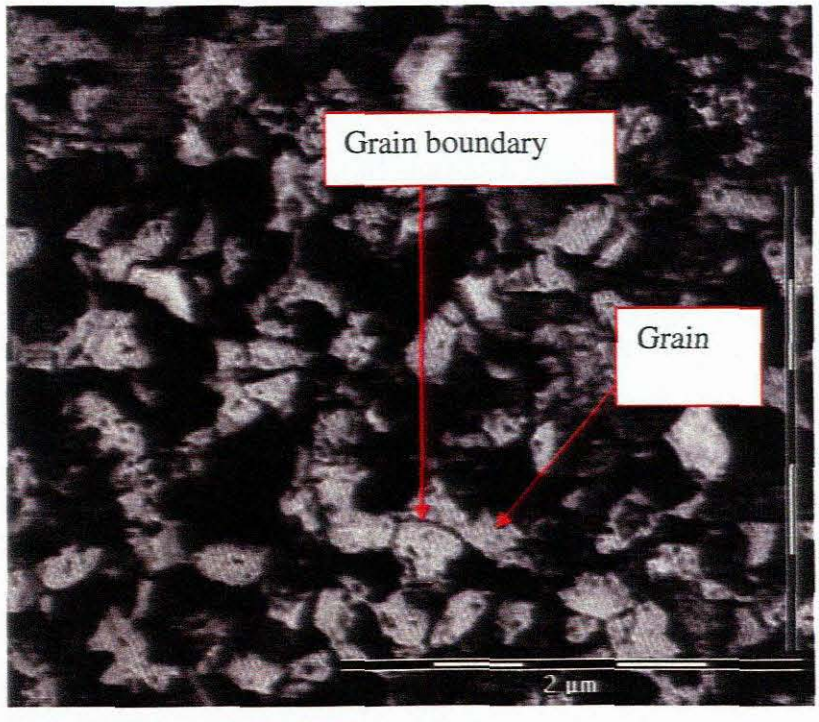

Figure 6.10: LOM micrograph showing individual grains and grain boundaries obtained in the heat treatment B. Ferrite (clear), martensite and bainite (dark).

As shown in Figures 6.1 - 6.10 micrographs of the specimens studied are populated by different phases. The heat treatment regime employed produced multiphase microstructure with different morphologies.

The microstructure of specimens A and B (see Figures 6.5 and 6.6) were mainly composed of ferrite and pearlite. However, a slight change in morphology and marked coarsening of microstructure was observed in specimen B.

Micrograph C, presented in Figure 6.7, formed a similar microstructure to micrograph D, basically a ferritic matrix with second phase islands. However, the heat treatment temperature and soaking/holding time provided two interesting effects: heating steel at 914 °C and reducing holding time at this resulted in formation of small grains in micrograph D (See Figure 6.8). On the other hand, increasing holding time at this temperature produced relatively large grains in micrograph C.

Table 6.1 shows the volume fraction of the steel phases obtained from statistical analysis of LOM for all the microstructures obtained by the heat treatments A, B, C and D studied in this thesis.

Table 6.1: Phase volume analysis obtained from LOM analysis

Specimen	Phase 1	Phase 2	Phase 3	Phase 4
	%Volume	%Volume	%Volume	%Volume
A	21.05	74.94	3.91	0.13
B	17.18	75.95	6.71	0.16
C	16.09	73.56	7.00	3.35
D	23.04	61.62	8.38	6.96

The fast cooling rates in heat treatments C and D favoured the formation of the phases of martensite and bainite, in comparison with heat treatment B. Whereas heat treatment B did not favour the formation of bainite and martensite. The microstructure obtained in heat treatment C presented a similar fourth phase volume fraction in comparison to the microstructure obtained in treatment D. This was

suspected to be martensite. Brinell hardness test was carried out. The increase in austenising temperature soaking time and slow cooling rate in heat treatment B induced a marked decrease in hardness in specimen B (see Table 6.2). This reduction in hardness may be attributed to two microstructural aspects: grain coarsening and reduction in fourth phase observed in specimen B. The maximum hardness values were obtained in heat treatments C and D. This confirmed the suspicion of the presence of harder phases (martensite and bainite) in specimens C and D as alluded to above. No test was conducted to ascertain the phases present, nevertheless, the heat treatment regime employed was appropriate for the production of microstructure with multiphases; pearlite, martensite and bainite (Ju et al., 2006). However, from the analysis of the phase volume fractions, grain size and hardness values of specimens A, B, C and D; it was observed that grain size had a major influence on variation in the hardness values observed.

Table 6.2: Grain size and Brinell hardness values of EN8 steel studied.

Specimen	Average grain diameter (μm)	Hardness (Brinell)
A	123.46	164
B	156.25	147
C	46.3	194
D	39.6	206

Table 6.2 shows the average grain size. It was observed that increase in time at an intercritical temperature increased the grain size. Heat treatment D produced microstructure with small grains, while treatment B promoted grain growth. From micrograph C results, it was observed the soaking time above critical temperature had a major influence on the microstructure. Heat treating at or above the critical temperature caused metallurgical changes (see Figure 9.2) and soaking time favoured the growth of grains. The distribution of the phases and grains also showed a continuous change of the microstructure with increasing temperature and soaking time. As reported by Tamehiro and Nakasugi, (1985) grains generally grow, coalesce and coarsen with increasing temperature and soaking time.

6.2 Tensile and hardness test results

Figures 6.11 - 6.14 show the typical force–elongation response and micrograph of virgin EN8 steel examined. The specimen exhibited the elastic–plastic behavior and the tensile results are summarized in Table 6. 3.

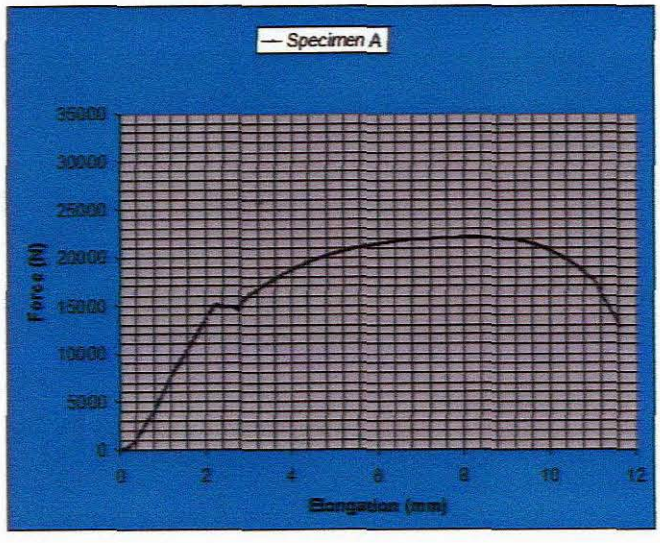

Figure 6.11: Force – extension curve of EN8 steel

Figure 6.12: SEM Micrograph of virgin EN8 steel

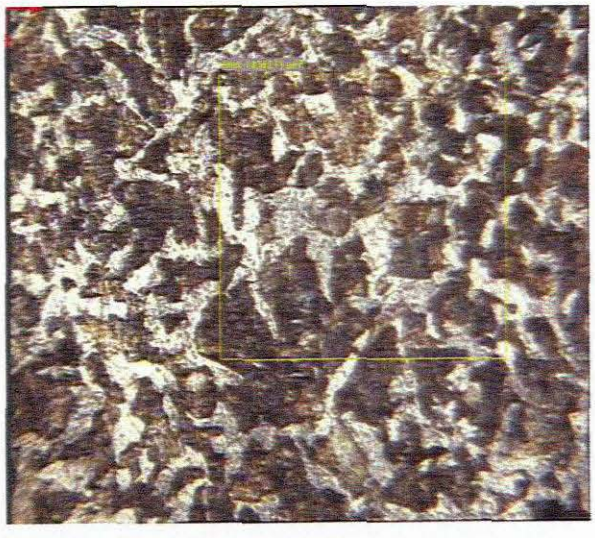

Figure 6.13: LOM micrograph of Virgin EN8 steel

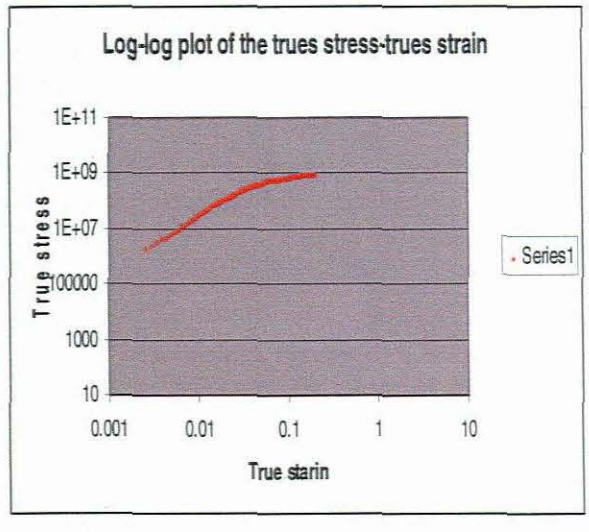

Figure 6.14: True stress-strain curve

Observation of force-extension curve in Figure 6.11 reveals that the deformation of specimen A is mixed mode, comprising elastic and plastic regions. The fractured specimen shows a combination of a cone and cup shapes (Figure 6.15). High magnification observations of the tensile fracture surfaces revealed that the final fracture resulted from the fine microscopic features (Wei and Batra, 2006 and Lassance et al., 2006). Microvoid nucleation at the areas of large strains (at the necked area) was distinctly evident (Figure 6.16).

Figure 6.15: Fractured specimen showing a cone and cup fracture mode

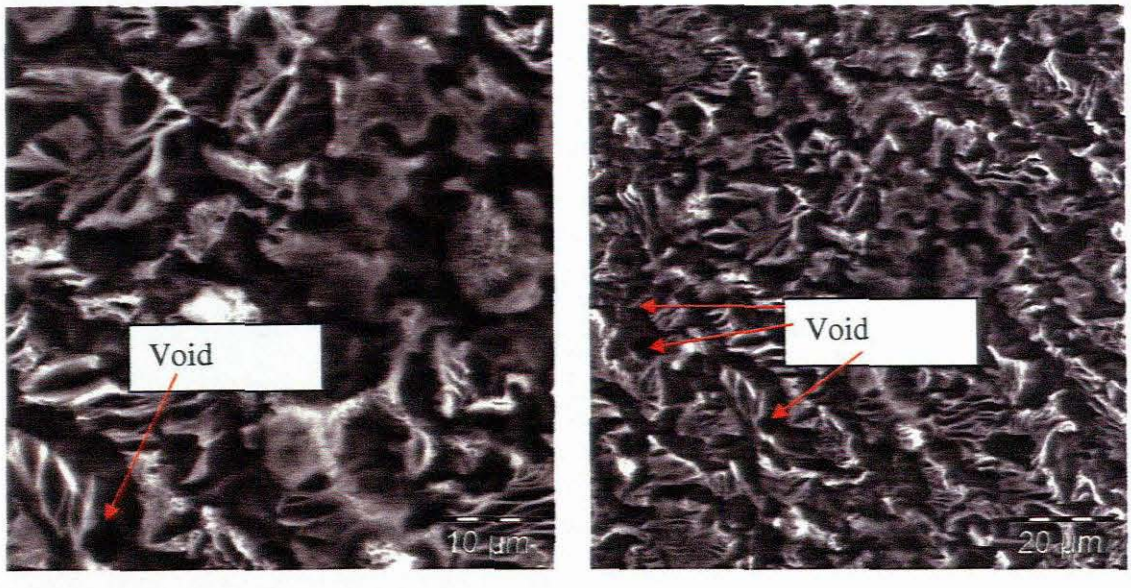

(a) (b)

Figure 6.16: Microvoid nucleation. (a) SEM micrograph at X2000 magnification
(b) SEM micrograph at X1000 magnification

Brunig, 2003 reports that nucleation of micro-void in ductile material is generally governed by large strains of the material. They initiate at discontinuities soon after the onset of plastic yielding and grow due to plastic deformation (Wei and Batra, 2006 and Lassance et al., 2006) of the surrounding matrix material (Bonora, 1997). Upon further plastic deformation of the material the micro-voids tend to grow and possibly change shape by means of deviatoric and volumetric strain (Al-Rub and Voyiadjis, 2003; Mediavilla et al., 2006 and Lassance et al., 2006) which may result in the formation of micro-cracks as micro-voids start to combine.

Table 6.3: Summary of mechanical properties of EN8 subjected to heat treatment regime given in Table 5.1.

Mechanical property	Microstructure			
	A	B	C	D
Yield strength (MPa)	475.22	397.86	762.26	789.41
Ultimate strength (MPa)	694.68	492.59	762.57	789.41
% Elongation at fracture	13	16.9	11.8	9.4
% Reduction in area at fracture	34	31	27	24.4
Young's modulus (GPa)	208.96	150.21	280.177	332.33
Average grain size (μm)	123.46	156.25	46.3	39.6

Table shows 6.3 the results obtained in tensile tests. The reduction of the strength values observed in the steel B was attributed, among other factors, to course grains. The reduction in the yield strength and tensile strength values in specimen B was worsened by small volume fraction of the harder phase (martensite). Specimen B exhibited relatively lower strength and higher ductility as compared to specimen A.

This can be attributed to relatively large grains of specimen B as there is very little difference in the volume fraction of the fourth phase between specimens A and B (See Figure 6.17 and 6.18 and Table 6.1).

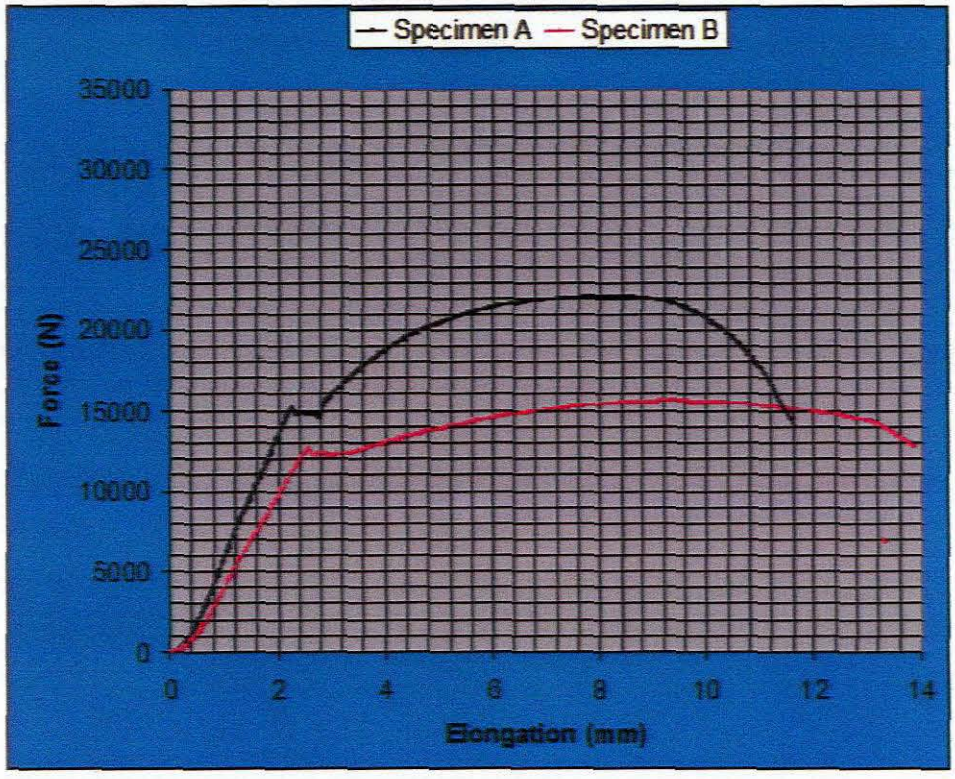

Figure 6.17: Force-extension curves for specimen A and B showing variation in yield force and extension.

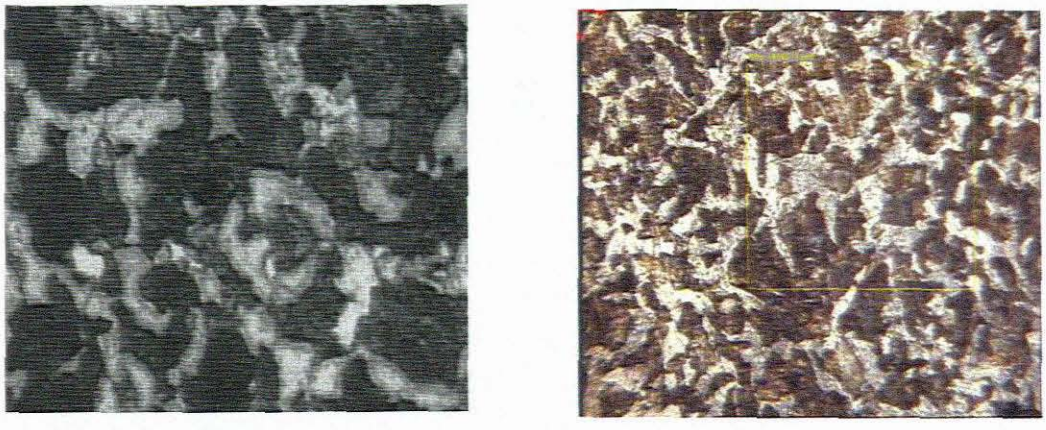

(a) (b)

Figure 6.18: Micrographs of EN8 showing variation in grain size

(a) Specimen B with larger grain sizes

(b) Specimen A with smaller grain sizes

Among the investigated specimens, the softest were specimens A and B, and also exhibited higher ductility and lower strength than the others. On the other hand, the highest tensile strength (σ_{uts}), the highest hardness (HV) and the lowest elongation at fracture (Ef) values were obtained from specimens C and D (See Figure 6.19).

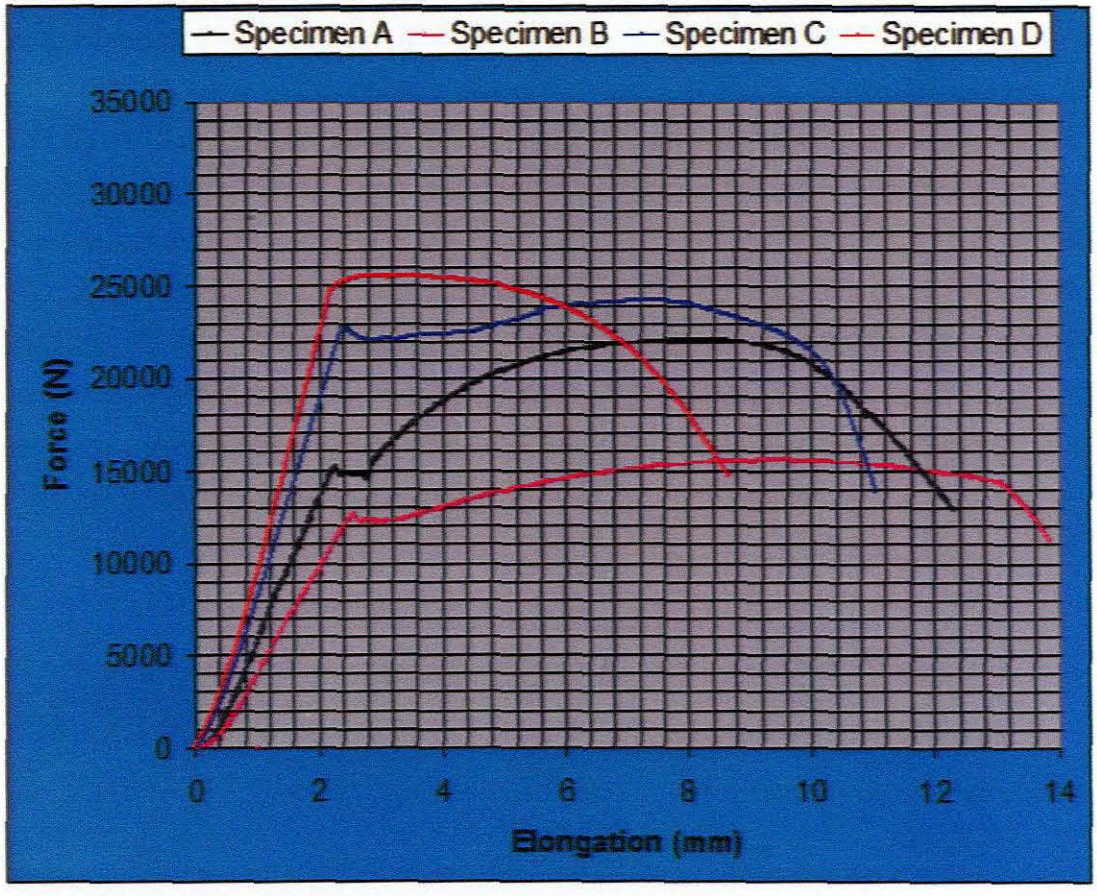

Figure 6.19: Showing the force-elongation response of the steel studied in this thesis

As shown in Figure 6.19, the yield strength, σ_y of the specimen B was measured to be (391 MPa), a significant decrease from that of specimen A (475 MPa). As the holding time was reduced, σ_y increased significantly whereas Ef, the elongation decreased (see Figure 6.19). Further decrease in the holding time at critical temperature temperatures resulted in increase in the yield strength, σ_y -values and reduction in Ef -values. The yield strength, σ_y of specimen D was (781MPa)

equivalent to over 8% enhancement compared with that of the specimen C. This is in agreement to the findings reported in Liu et al., (2006 (a)). They also report that a number of factors, amongst, heat treatment, alloying content and impurities affect the relationship between grain size and mechanical properties of steels. It is therefore imperative to control the heat treatment process and keep impurities in the steel to minimum acceptable levels. In this study the heat treatment regime was designed in such a way that formation of martensite and bainite phases was limited to a bare minimum (Qu et al., 2005). The annealing temperatures (within the intercritical range) and soaking times were carefully chosen using dilatometer data (see Figure 2.9) . This allowed the study to only consider the effect of heat treatment parameters on Hall-Petch relationship between grain size and mechanical properties. It was apparent that change in the grain size with varying cooling rate and holding time at critical temperature had resulted in the change of mechanical properties of the steel studied. The mechanical properties of the investigated steel (presented in Table 6.3 and Figure 6.19) are in good correlation with the Hall-Petch effect given by equation (4.1). From Table 6.3 and Figure 6.19, it was observed that the yield strength, σ_y and the ultimate tensile strength, σ_{uts} increased with decreasing grain size.

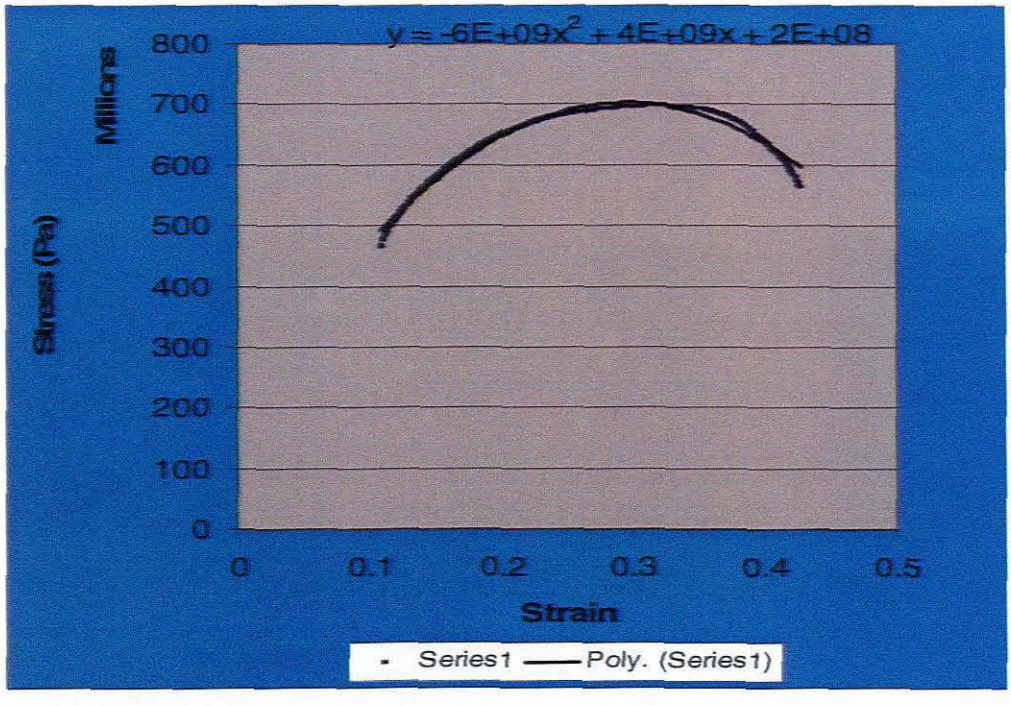

Figure 6.20: Stress-strain curve, rigid plastic material model used to fit the Hall-Petch relationship

A decrease in the grain size caused an increase in the flow stress (σ_o) and the variation was in accordance with the Hall-fetch relationship. The Hall-Petch intercept, σ_i increased linearly with strain and decreased monotonically with increase in holding time at annealing temperature. The experimentally measured stress-strain relations for the steel studied were fitted to the Hall-Petch equation as shown in Figure 6.20 above. These results were found to be in good agreement with the modified pile-up theory of grain boundary strengthening.

Figure 6.21 shows a graph of yield strength against the inverse square root of grain size. The graph was plotted to examine the possibility that the improved yield strength is primarily due to the Hall–Petch mechanism. The correlations between yield strength and and inverse square root of grain size was reasonably good, with correlation coefficients of 0.99, indicating that the improvement in strength in the steel with the heat treatment was largely due to the grain size refinement. This is in agreement with earlier studies (Liu et al., 2006 (a) and Morris, 2001 and) showing that both the yield and ultimate tensile strengths of steel increase with decreasing grain size due to reduction in the effective slip length.

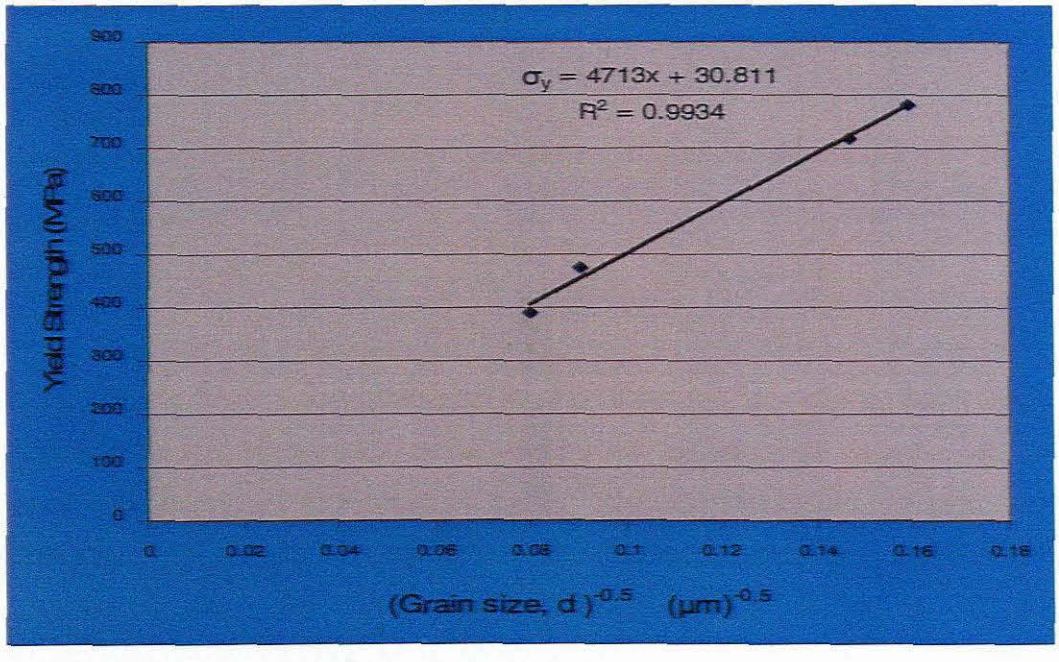

Figure 6.21: Showing variation of yield strength with inverse square root of the average grain size at room temperature.

6.3 Effects of Phase volume fraction on yield strength

It has been observed that the yield stress and work hardening of steel depend on individual phases present in the material (Park et al., 2000; Mahdi and Zhang, 2000; Liu, 2006 and Fromm, 2008). Considering the variation of yield strength with grain size (Sleboda et al., 2004 and Zhang et al., 1995) and phase volume fractions, the following material model (Mahdi and Zhang, 2000) was adapted:

$$\sigma_y = \left(\sigma_o + Kd^{-1/2}\right)\xi_f + \left(\sigma_o + Kd^{-1/2}\right)\xi_p \qquad (6.1)$$

where, ξ_f and ξ_p are phase volume fractions, σ_o^f and σ_o^p are yield strengths of ferrite and pearlite phases respectively.

By fitting equation (6.1) to the experimental data for yield stress for different phase volume fractions and grain sizes, optimum values for the constants were obtained and are given in table 6.4.

Parameter	Determined value
σ_o^f (Mpa)	0.878898
σ_o^p (Mpa)	-1.15903
K^f	56.41738
K^p	64.74823

No rigorous analysis was performed to determine the combined effect of varying phase volume fraction and grain size (Martin, 2004 and Akoy et al.,2004). However, results obtained reasonably agreed with the experimental results. Hence the mechanical properties of steel studied can be rationalized in terms of grain size and phase volume fractions. The following model was proposed for the steel studied:

$$\sigma_y = \left(0.879 + 56.417d^{-1/2}\right)\xi_f + \left(-1.159 + 64.748d^{-1/2}\right)\xi_p \qquad 6.2$$

6.4 Prediction of Formability

Based on the experimental results, the effects of microstructural features (such as grain size and phase volume fraction) and mechanical properties (Young's modulus, E the yield strength, σ_y the ultimate tensile strength, σ_{uts} and elongation at failure Ef) on the deformation behaviour of the steel studied can be predicted. Since any structural parameter that directly controls the yield strength, σ_y the ultimate tensile strength, σ_{uts} and elongation at failure, Ef should have some influence (direct or indirect) on the stress flow and formability of the material. The variations of the yield strength, σ_y with the grain size is given in Figure 6.20. Since the yield strength, σ_y increased linearly with decreasing grain size in conventional materials and and elongation at failure, Ef decrease with decreasing grain size, coarse grains (heat treatment B) would be beneficial for manufacturing processed that depend on material flow for example cold forming. Heat treatment C and D would be ideal for applications where high strength and high hardness values are requirements.

6.4 Prediction of Formability

Based on the experimental results, the effects of microstructural features (such as grain size and phase volume fraction) and mechanical properties (Young's modulus, E the yield strength, σ_y the ultimate tensile strength, σ_{uts} and elongation at failure Ef) on the deformation behaviour of the steel studied can be predicted. Since any structural parameter that directly controls the yield strength, σ_y the ultimate tensile strength, σ_{uts} and elongation at failure, Ef should have some influence (direct or indirect) on the stress flow and formability of the material. The variations of the yield strength, σ_y with the grain size is given in Figure 6.20. Since the yield strength, σ_y increased linearly with decreasing grain size in conventional materials and and elongation at failure, Ef decrease with decreasing grain size, coarse grains (heat treatment B) would be beneficial for manufacturing processed that depend on material flow for example cold forming. Heat treatment C and D would be ideal for applications where high strength and high hardness values are requirements.

CHAPTER SEVEN

7.1 Numerical simulations

In this chapter we discuss the numerical simulations of tensile test implemented in a public domain ANSYS code. As a crucial aspect of numerical simulations, we begin by giving a general overview of the numerical methods used, the Finite Element Methods. Since this work is not about Finite Element Methods (FEM), detailed discussions about its (FEM) mathematical formulations are not presented herein, however, in this regard we make reference to the works of (Kattan and Voyiadjis, 1990 and Belytschko et al., 2003).

7.2 The formulation of the Finite Element Method

7.2.1 General overview

Methods of the micromechanics of materials are based on solving continuum mechanics problems, which involve constitutive relations and conservation laws. The numerical solution can be obtained with the use of the Finite Element Method (FEM) among other numerical methods.

Finite element method (FEM) is now a powerful and fundamental indispensable technique in modelling and simulation of complex engineering physical problems (solid mechanics, heat transfer, fluid mechanics, acoustics, and so on) originally developed for numerical solution to stress analysis problems in structures. FEM has since then found many applications in different fields including medicine, transport, weather, communication, electronics and many others.

7.2.2 Governing equations

All equations governing advanced engineering physical systems are generally non-linear and cannot be solved analytically, thus, FEM is used to numerically analyse partial differential equations (PDE) as well as integral equations to determine the distribution of some field variables like the displacement in stress analysis, the temperature in thermal analysis, mole concentration in chemical analysis, and so on in the problem domain (Belytschko et al., 2003). All Finite Element codes endeavour to solve the differential equations governing the dynamics of engineering physical systems (continuous media). These equations are established through the application of balance laws (Makowski et al., 2006; Belytschko et al., 2003 and Davison et al., 1977) and compatibility equations (deformation of continuum body) as

discussed in chapter 2 and 4. According to (Belytschko et al., 2003) , this is achieved by either eliminating the differential equations completely (steady state problems), or rendering the PDE into an equivalent ordinary differential equations, which is then solved using three distinctive stream of numerical solution techniques (solution approaches):

- Finite difference method
- Finite element method
- Spectral method.

The main distinguishing features that separates the three solution approaches are associated with the way in which the field variables are approximated and the with discretisation processes. A continuous function of an unknown field variable is approximated using piecewise linear functions in each sub-domain, called and element, as shown in Figures 7.1 and 7.3. The discritization can be either Eulerian or Lagrangian spatial discretisation. Both descriptions have shortfalls and selection should be based on the required accuracy and time integration. Detailed work can be found in the work of Belytschko et al., 2003.

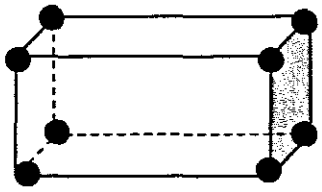

Figure 7.1: 8 node brick element

The use of numerical methods in solving partial differential problems presents with challenges. The primary challenge is to create a numerical solution algorithm that approximates the equation under study, which is numerically convergent, consistent and stable. Convergence is the mathematic concept that describes the property of the numerical method to give a solution which approaches the exact solution as the element size is reduced to zero. A numerical scheme is said be consistent if it produces a system of algebraic equations which can be demonstrated to be equivalent to the original governing equation as the grid spacing tends to zero. In a stable numerical system, errors in the input data and intermediate calculations do not accumulate and cause the resulting solution to be meaningless. There are a number

of methods of ensuring that a numerical solution algorithm is stable, consistent and convergent, however these are not discussed in the present thesis.

7.3 Structural Model

In this section we present the simulation of the structural model for tensile test. It is possible for a component such as the one shown in Figure 7.2 to have six components of stress when subjected to arbitrary three-dimensional loadings. When referenced to a Cartesian coordinate system these components of stress may be given as:

Normal Stresses: σ_x , σ_y , and σ_z;

and

Shear stresses: τ_x, τ_y, and τ_z.

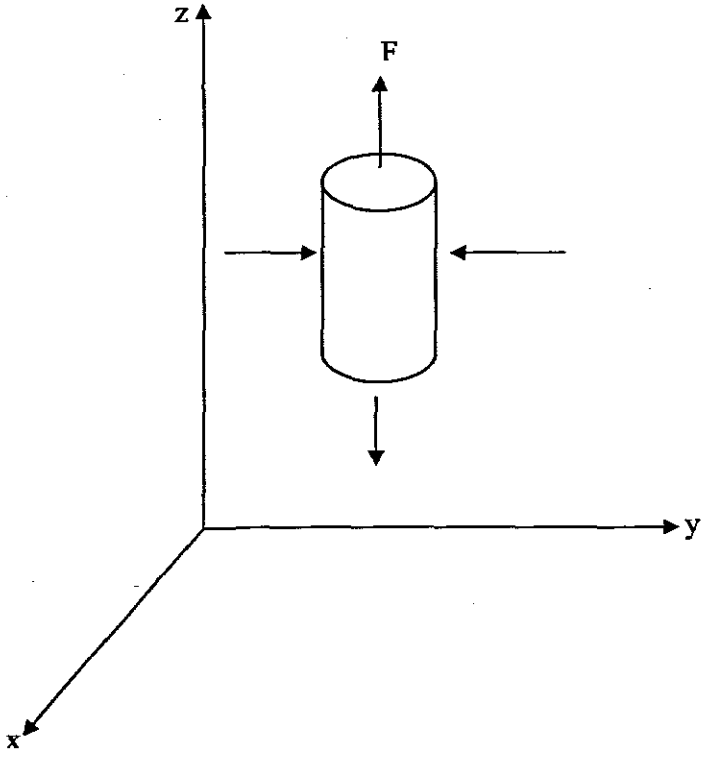

Figure 7.2: Schematic diagram showing multiaxial stresses in a tensile test piece

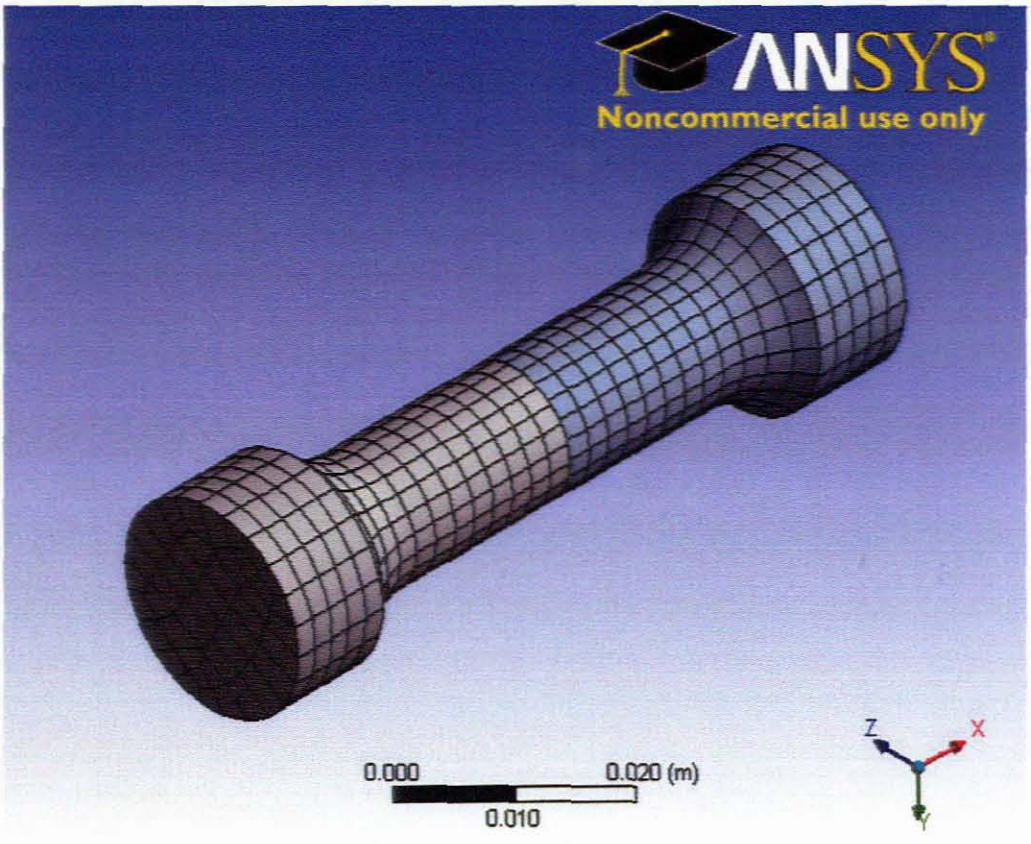

Figure 7.3: Three dimensional meshed model.

7.4 Analysis software

ANSYS is a commercial finite element code used to solve a wide variety of real world engineering problems. It can model many different phenomena including heat transfer, linear and nonlinear structural analysis, buckling, modal analysis, full harmonic response, transient dynamic response, electro-magnetic and fluid flow problems. One of the members of the family of the ANSYS products is ANSYS Structural. ANSYS Structural supports both 2-D and 3-D analyses and provides for a variety of studies including rigid or flexible dynamics, from steady state thermal analyses to coupled thermo-mechanical transient

7.5 Material Model

ANSYS Structural is fully complemented by nonlinear elements, nonlinear and linear material constitutive laws, and plastic material models. It allows simulation of many different types of structures, from the most intricate of structures to the complicated

assemblies, by using nonlinear contact functionality. ANSYS Structural has a number of metallic and non-metallic material models and uses wide range of element types.

In this study, the tensile specimens were modelled as a bilinear isotropic elastic-plastic material with isotropic hardening. The material model uses the von Mises yield criterion with associative flow rule (Figure7.4).

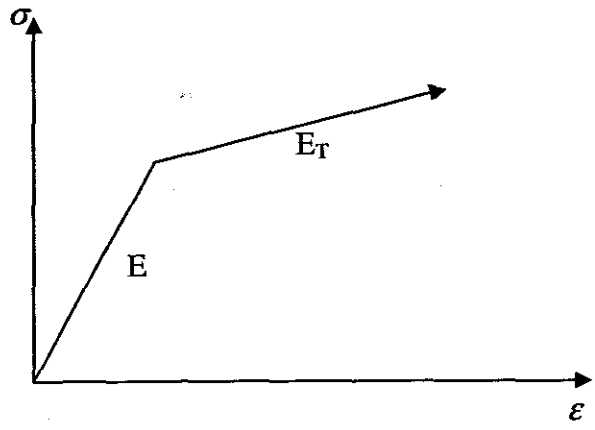

Figure 7.4: Schematic figure of a bilinear elastic-plastic material

7.6 Numerical Results

Microstructure studies have shown that, in the welding or heat treatment of low carbon steel and low alloy steel, it is possible to obtain a multiphase structure with different grain sizes and morphology as discussed above. In order to understand the effect of microstructural features on mechanical properties of EN8 steel component subject to loading, it is necessary to know the distribution of von Mises stress and equivalent plastic strain in a structure. For this aim, virtual composite tensile specimens with two different ferrite and pearlite grain sizes and phases produced by different heat treatments were created as shown in Figure 7.5. The simulations were used to investigate the microstructural aspects of the deformation. Specifically, the von Mises strain and equivalent plastic across the specimen length were explored.

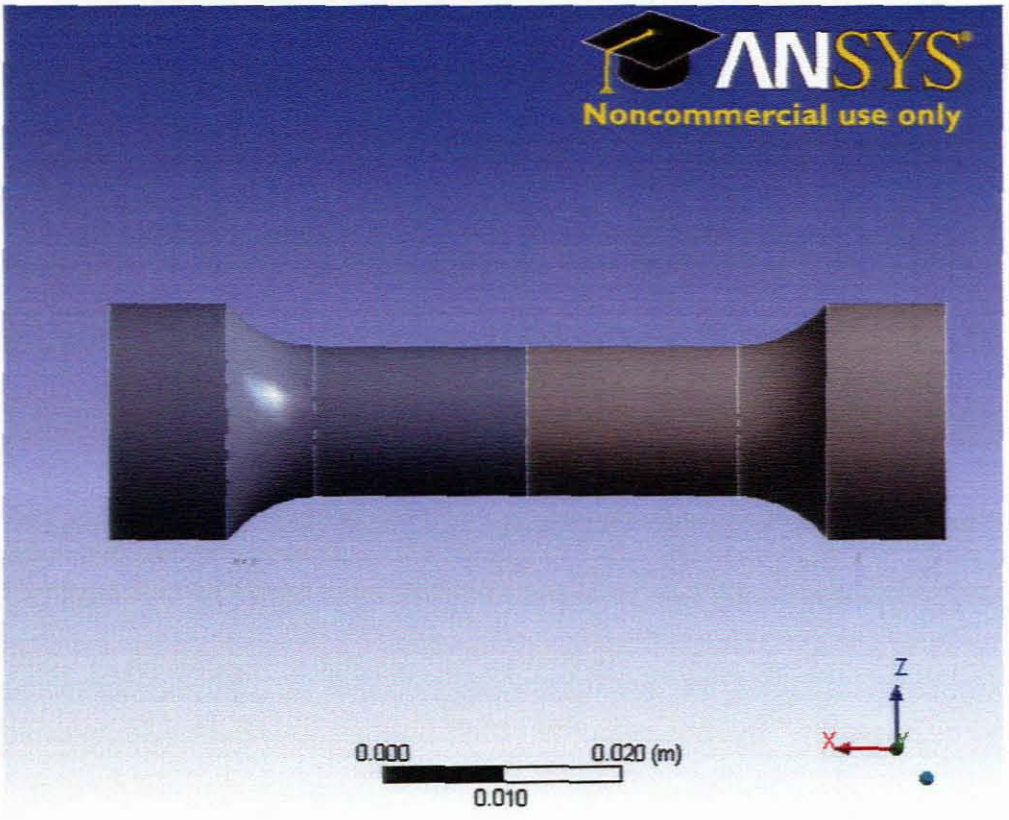

Figure 7.5 Virtual Composite Tensile Specimen

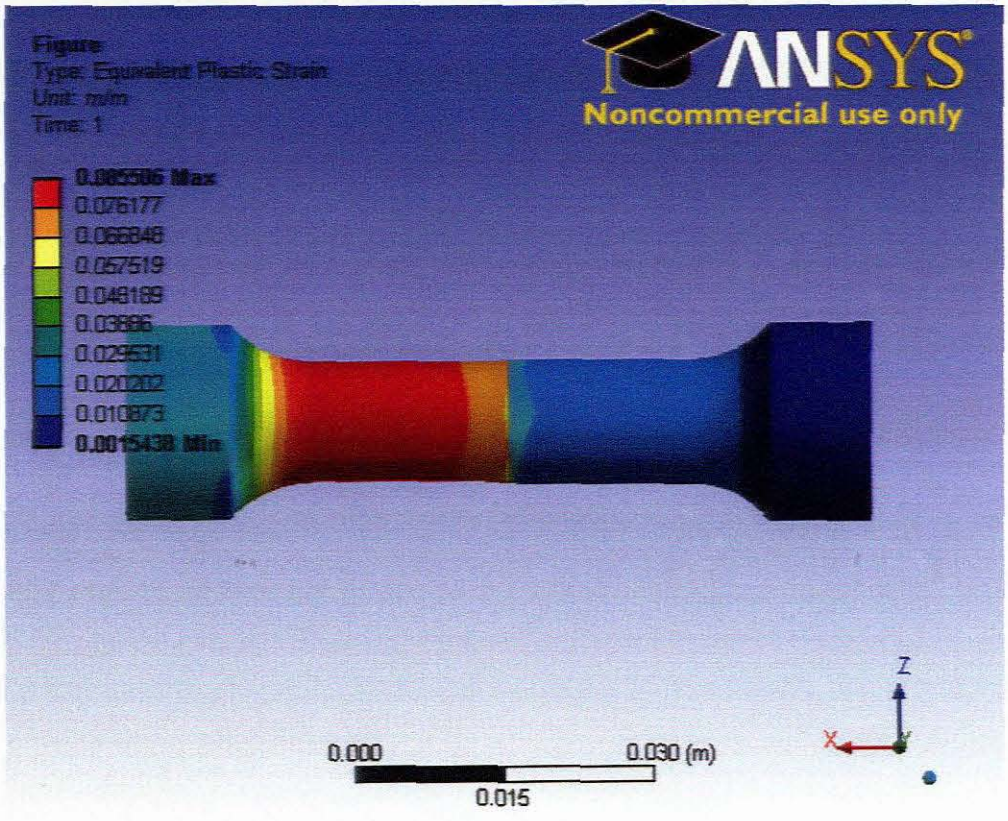

Figure 7.6: Showing Equivalent Plastic Strains for a virtue tensile test obtained by combining microstructures obtained in heat treatments A and B

The tensile specimens in Figures 7.6 and 7.7 were created by combining heat treatments and A and B. Microstructure formed by heat treatment B represents a larger volume fraction of Pearlite and coarser grains than those obtained in heat treatment A. As shown in Figure 7.6, maximum plastic deformation occurred in microstructure obtained by heat treatment B away from the virtual phase/grain boundary. This might suggest that in a multiphase structure, the weakest point may lie within the weaker phase and not on the phase/grain boundary.

The analysis of Figure 7.7 showed that the von Mises stress was higher in the microstructure obtained heat treatment A than the one obtained in heat treatment B. This did not come as a surprise. As one would expect, microstructure obtained by heat treatment A with smaller grain sizes and equal volume fractions of Pearlite and Ferrite would be able to sustain more stress than heat treatment B. But what is of particular note is the location and distribution of the plastic strain in microstructure B. As explained above, the maximum plastic strain occurred in the weaker phase away from the point of maximum stress.

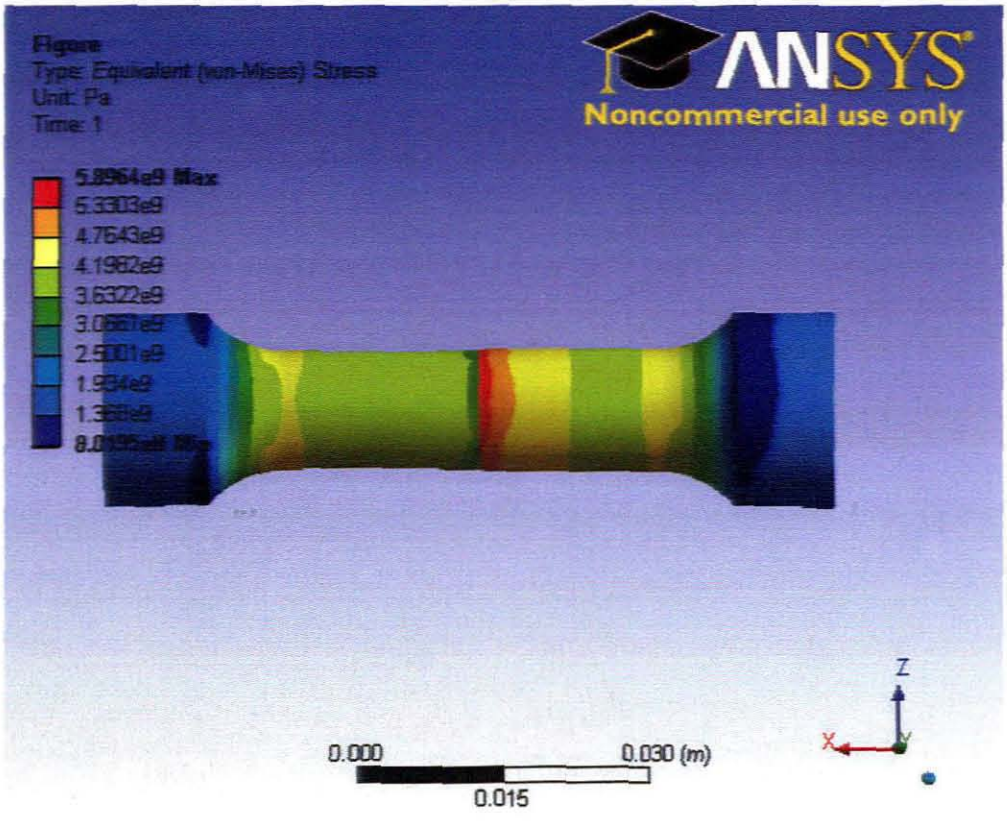

Figure 7.8: Showing Equivalent Stress for a virtue tensile test obtained by combining microstructures obtained in heat treatments A and B

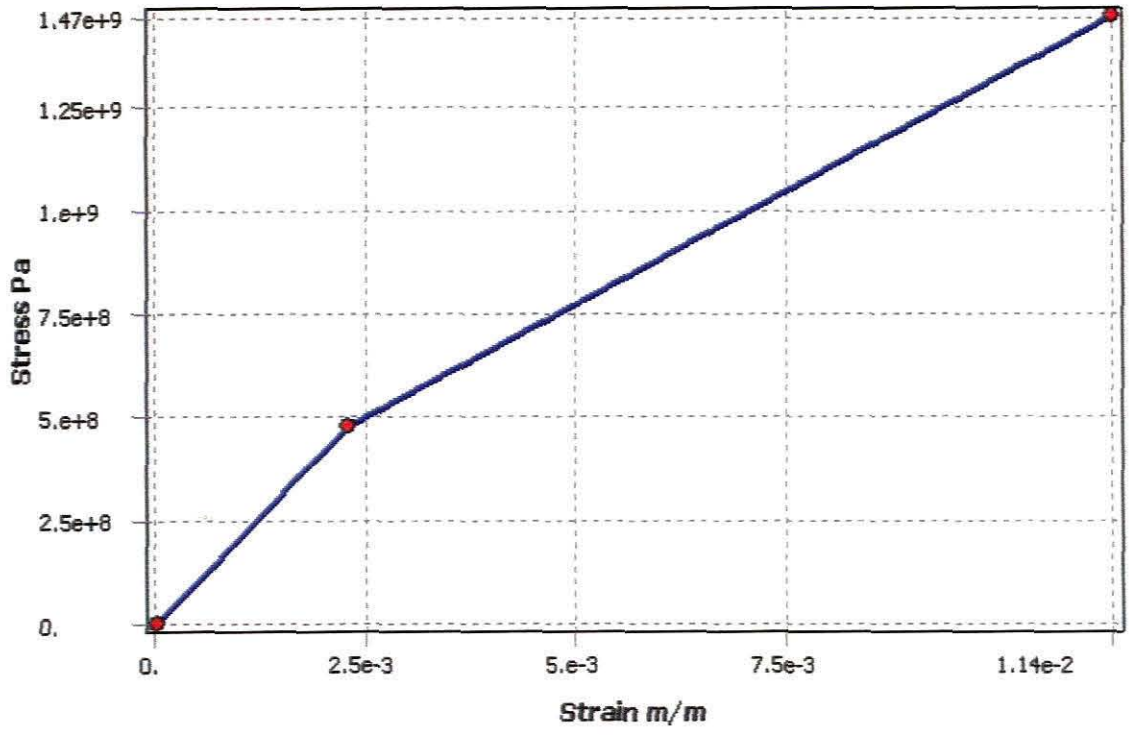

Figure 7.9: Showing bilinear model for microstructure obtained in heat treatment A

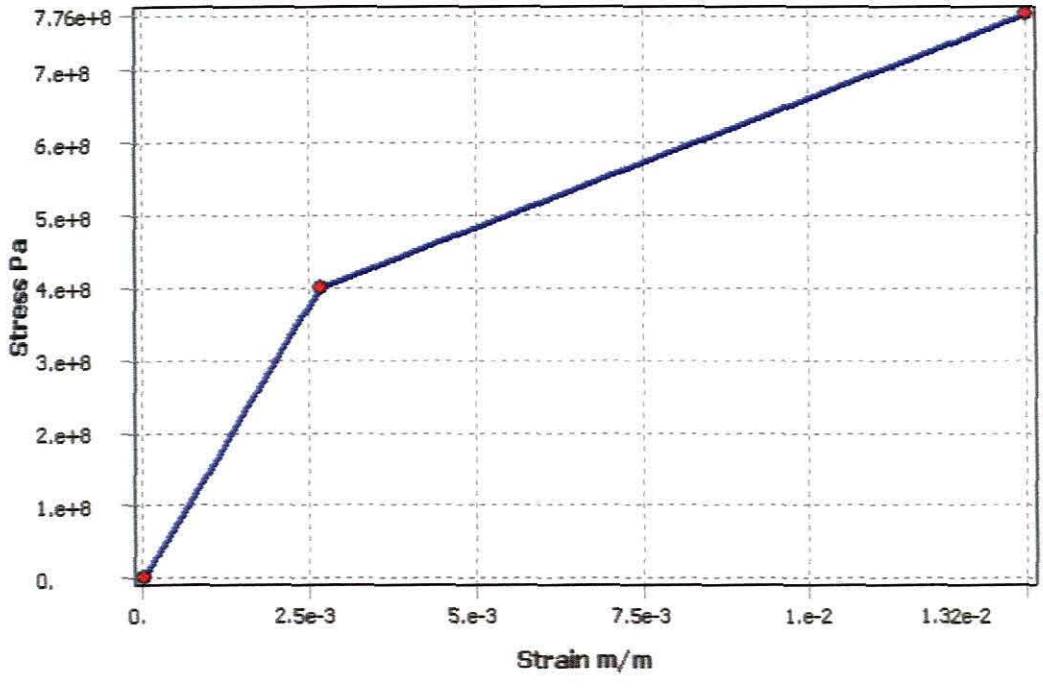

Figure 7.10: Showing bilinear model for microstructure obtained in heat treatment B

The tensile specimens in Figures 7.11 and 7.12 were created by combining heat treatments and C and D. Microstructure D was formed by heat treatment appropriate for the production of smaller grain sizes than that obtained in heat treatment C. However, both heat treatments favoured the formation of Martensite. From the volume fractions given in Table 6.1, microstructure D had slightly higher Martensite volume fraction.

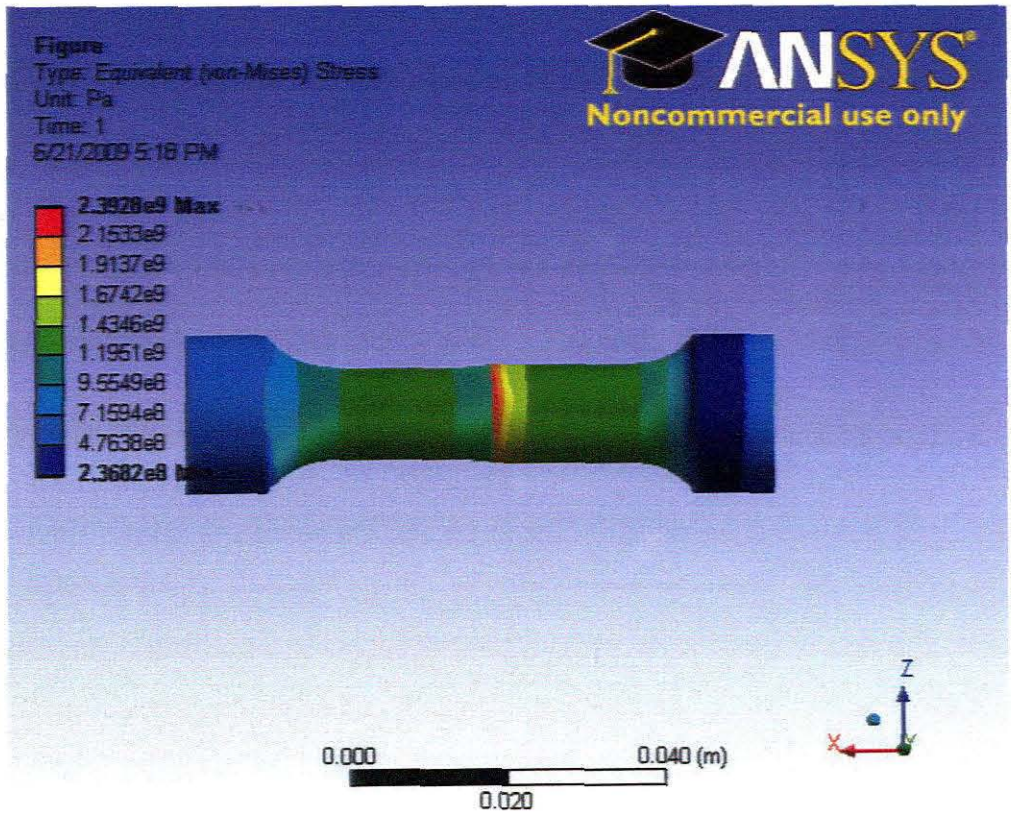

Figure 7.11: Showing Equivalent Stress for a virtue tensile test obtained by combining microstructures obtained in heat treatments C and D

The distribution of the von Mises stress (Figure 7.11) didn't show any significant difference across the specimen except for the portion near the "phase/grain" boundary. This is because microstructures C and D have relatively similar properties (see Figure 6.19 and Table 6.3). It was important to observe the stress raiser at the "phase/grain" boundary. Looking at Figure at Figure 7.12, we saw similar results obtained in Figures 7.5 and 7.6 above. The maximum plastic strain occurred in the weaker phase away from the "phase/grain" boundary and the von Mises stress was higher in the "stronger" phase. It was observed that the weaker phase yielded while the stronger phase did not. This ability to show high plastic flow in microstructure C

was attributed to relatively smaller Martensite volume fraction as compared to that in microstructure D. The yielding observed in the "weaker" phase and the higher von Mises stress observed in the "stronger" were consistent with experiment observation. Also considering that the slopes of the hardening curves for all the microstructures were not the same, one would expect, the "weaker" phases to show all the yielding and plastic deformation as observed.

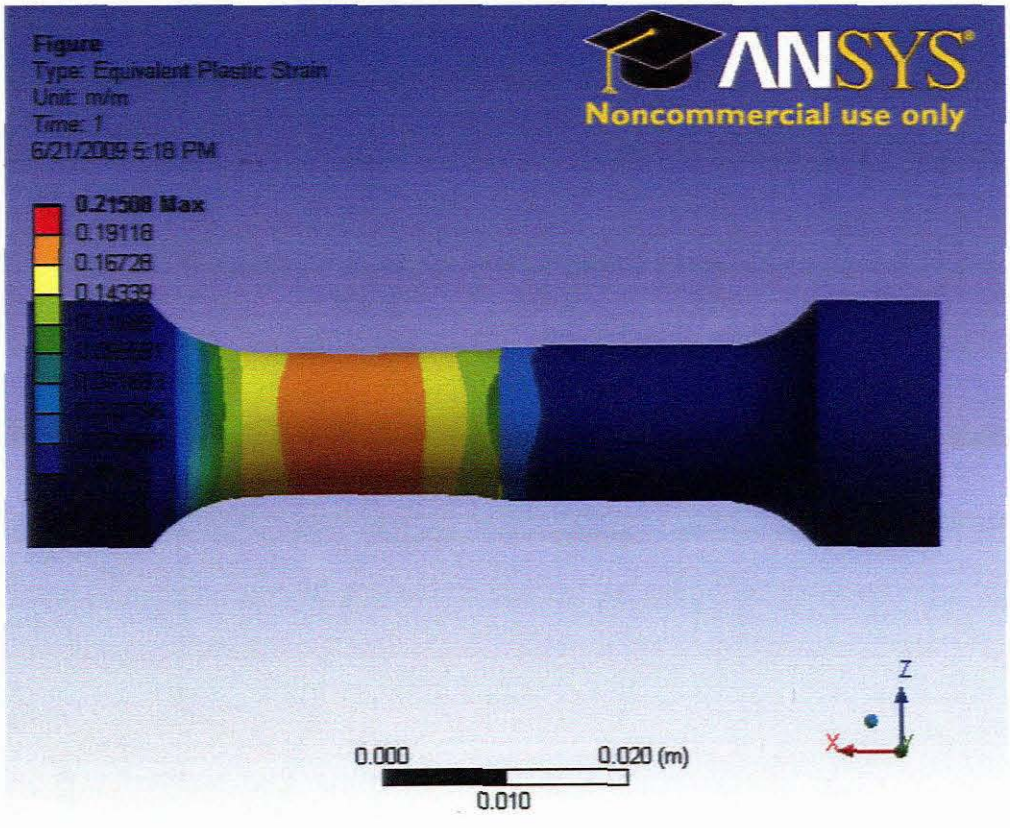

Figure 7.12: Showing Equivalent Plastic Strain for a virtue tensile test obtained by combining microstructures obtained in heat treatments C and D

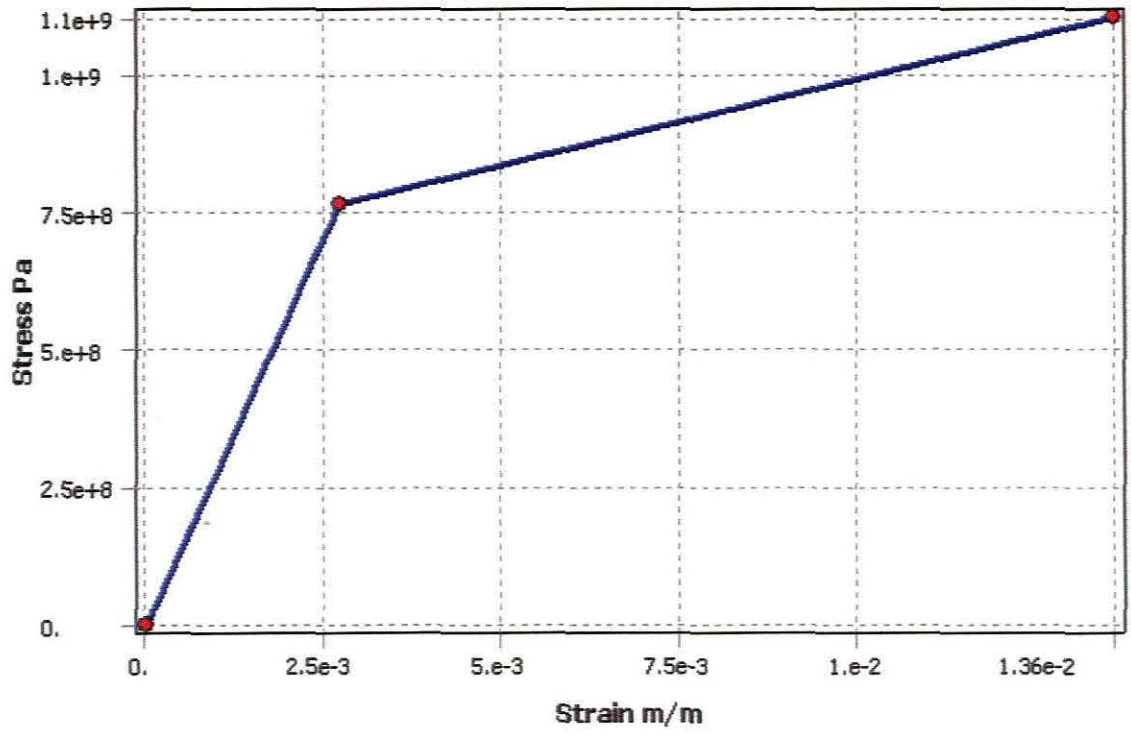

Figure 7.13: Showing bilinear model for microstructure obtained in heat treatment C

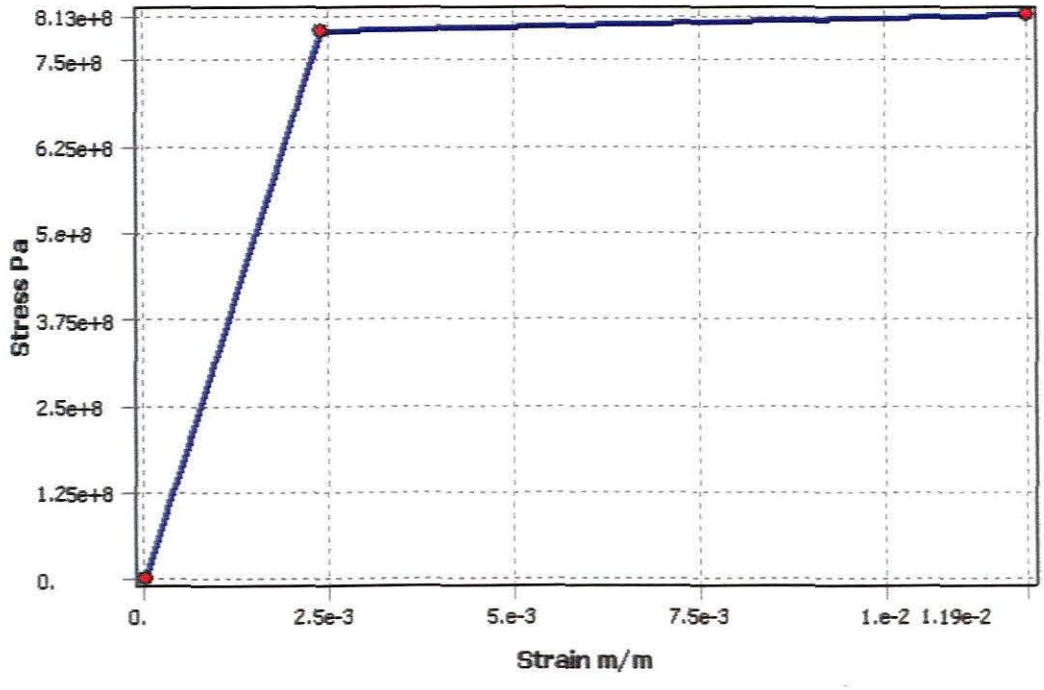

Figure 7.14: Showing bilinear model for microstructure obtained in heat treatment D

CHAPTER EIGHT

8.0 Conclusions

The goal of this work has been to study and analyse the influence of microstructure on mechanical behaviour of EN8. The plastic deformation behavior has been studied and experimental methods used to quantify grain size and mechanical properties were described and the following conclusions and observations can be drawn from this study:

- Grain size and its distribution have a significant impact on the yielding characteristics of steel. It was observed that when a structure is composed of multiphase with different grain size distribution, the maximum plastic deformation will occur within the "weaker" phase. While the "stronger" phase will experience higher von Mises stress. This is typical in welded or heat treated structures with large cross sectional areas. Due to temperature gradients within the component; the outer layer (exposed to faster cooling rates) will contain finer grain structure with higher Martensite volume fraction while the inner section (subjected to slow cooling rates) will have coarser grained structure with significantly reduced Martensite volume fraction.
- The annealing temperature and holding time have great influence on the grain size and phase distribution. The increase in annealing temperature and soaking time promotes the coarsening of grains and even an increase in formation of second phases (bainite and martensite) upon cooling.
- The study of grain size effects on the mechanical properties of steel should be done in conjunction with the effects of other microstructural features (such as phase, grain orientation etc.) in order to obtain the more accurate results.
- From numerical simulations the maximum stresses were obtained at the mid section of the specimen which is usually true due to the design of tensile specimens but in this instance we also had the effect of the sudden grain size and/or phase transition acting as a stress concentrator and to a much lesser extent the effect of finite element mesh discontinuity (bonded contact).
- In physical specimens we would expect a more gradual transition related to the temperature gradient through the material. Nevertheless the numerical tests highlight problems one generally experiences in for instance welded specimens if the materials used can transform their microstructure to cause such a transition. Such welded specimens are more likely to fail due to the

higher stresses in the transition zone making the material susceptible to fracture.

8.1 Future work

Understanding the combined effects of phase volume fractions and grain size on deformation behaviour in metals is crucial in the development of advanced and new materials with better thermo-mechanical properties. A systematic analysis of different mechanisms and how they depend on external variables like strain rate and temperature combined with numerical methods on the evolution of plastic deformation and damage at various working conditions would be a worthwhile undertaking in the future. To fully understand the distribution of the plastic strains and von Mises stresses in welded or heat treated structures it is suggested that a component with a large cross section in conjunction with careful selection of cooling rates be used to produce a structure with multiphase and different grain size. Then tensile specimens made from such a structure could be analysed. It would also be necessary to create a model that would have grain size and phase distribution as inputs in numerical software. We could also then develop phenomenological models to combine the properties of materials measured with specific phases for ones with distributed phases. This would help to determine the critical combination of grain size and phase distribution that would give the optimum or desired material properties and the ability to better design welding procedures and heat treatment processes.

REFERENCES

Abu Al-Rub, R.K. and Voyiadjis, G., (2003) On the coupling of anisotropic damage and plasticity models for ductile materials, International Journal of Solids and Structures, Vol. 40, Issue 11, pp. 2611-2643, Elsevier Science Ltd.

Akoy, M. A., Kayali, E. S. and Cimenoglu, H., (2004) The Influence of Microstructural Features and Mechanical Properties on the Cold Formability of Ferritic Steel Sheets, ISIJ International, Vol. 44, No. 2, pp. 422–428

Ashby, M. F., (1970) The deformation of plastically non-homogenous materials, Phil. Mag. 21(399-424).

ASM International, (2006) Fundamentals of Heat Treating of Steel, Practical Heat Treating, Second edition, www.asminternational.org, 10 July 2007.

Barlat, F., Aretz, H., Yoon, J.W., Karabin, M.E., Brem, J.C., and Dick, R.E., (2005) Linear transfomation-based anisotropic yield functions, International Journal of Plasticity 21, pp. 1009–1039, 2004 Elsevier Ltd.

Belytschko, T., Liu, W.K., and Moran, B., (2003) Nonlinear Finite Element for Continua and Structures, John Wiley & Sons Ltd, England.

Bhadeshia, H. K. D. H., (1997) Models for the Elementary Mechanical Properties of Steel Welds, Mathematical Modelling of Weld Phenomena III, Institute of Materials, London, 1997, pp. 229–284

Bonora, N., (1997) A nonlinear CDM model for ductile failure, Engineering Fracture mechanics, Vol. 58, No.1\2, pp 11-28, Elsevier science, Great Britain.

Brunig, M., (2003) An anisotropic ductile damage model based on irreversible thermodynamics, International Journal of Plasticity, Vol. 19, pp. 1679-1713, Elsevier science Ltd.

Cailletaud, G., Diard, O., Feyel, F. and Forest, S., (2003) Computational Crystal Plasticity : From Single Crystal to Homogenized Polycrystals, Technische Mechanik, Band 23, Heft 2-4, (2003), 130– 145 Manuskripteingang

Chen, S. Y. and Gan, D., (1986) Effects of Grain Boundary Carbides on the Tensile and Impact Properties of Type 316 Stainless Steel, Materials Science and Engineering, 84, pp. 65-76, Elsevier Sequoia, The Netherlands

Choi, S., (2003) Model for estimation of transformation kinetics from the dilatation data during a cooling of hypoeutectoid steel, Materials Science and Engineering A 363, pp. 72-80, 2003 Elsevier B.V.

Chunlei, L., (2006) Dislocation-Based Crystal Plasticity Finite Element Modelling of Polycrystalline Material Deformation, PhD Thesis University of California Los Angeles

Clarke, K.D. and Van Tyne, C.J. (2005) Effect of Prior Microstructure and Heating Rate on Austenite Formation Kinetics in Three Steels for Induction Hardened Components (Progress Report - December 1, 2005), Department of Metallurgical and Materials Engineering, Colorado School of Mines, Golden, CO 80401 USA

Coret, M. and Combescure, A., (2002) A mesomodel for the numerical simulation of the multiphasic behavior of materials under anisothermal loading (application to two low-carbon steels), International Journal of Mechanical Sciences 44, pp. 1947–1963, Elsevier Science Ltd.

Davison, L., Stevens, A.L., and Kipp, M.E., (1997) Theory of Spall Damage Accumulation in Ductile Metals, Journal Mech. Phys. Solids, Vol. 25, pp. 11-28, Pergamon Press, Great Britain.

Dingley, D. J. and McLean, D., (1967) Components of the Flow Stress of Iron, Acta Met. Vol.15, pp. 885-901.

EIS Group, The Virtual Try-Out Company, 2004 Predictive Simulation of Welding and Heat Treatment with SYSWELD,

Ferguson, B.L., Li, B.L. and Freborg, A.M., (2005) Modelling heat treatment of steel parts, Computational Materials Science, Vol. 34. pp. 274 –281, Elsevier B.V.

Finel, A., Maziere, D. and Veron (2002) Thermodynamics, Microstructures and Plasticity, Proceedings of NATO Advanced Study Institute on , Microstructures and Plasticity, Vol. 108, pp. 253-262 and 439-464, Kluwer Academic Publishers, Netherlands.

Fromm, B.S., (2008) Incorporating Grain Size Effects In Taylor Crystal Plasticity, Masters Thesis, Department of Mechanical Engineering Brigham Young University

Greger, M., Kocich, R., Kander, L. and Dorociáková, G., (2006) Strength enhancement possibilities of low carbon steels, Journal of Achievements in Materials and Manufacturing Engineering 18, Issue 1-2

Guduru, R. K., (2006) A dissertation submitted to the Graduate Faculty of North Carolina State University in partial fulfillment of the requirements for the Degree of Doctor of Philosophy Materials Science And Engineering Raleigh, NC, USA. 2006

Gupta, C., Dey, G.K., Chakravartty, J.K., Srivastav, D. and Banerjee, S., (2005) A study of bainite transformation in a new CrMoV steel under continuous conditions, Scripta Materialia 53, pp. 559-564, Elsevier Ltd.

Kallerova, P. and Wald, F., (2007) Mechanical properties of steel at elevated temperatures, Centre for Integrated Design of advanced Structures, Czech Technical University in Prague, www.cideas.cz

Kanasaki, H., Umehara, R., Mizuta, H. and Sayama, T., (1997) Effects of strain rate and temperature change on the fatigue life of stainless steel in PWR primary water, Transactions of the 14th International Conference on Structural Mechanics in Reactor Technology (SMiRT 14), Lyon, France, August 17-22, D07/2

Kattan, P.I. and Voyiadjis, G.Z. (1990), A coupled Theory of Damage Mechanics and Finite Strain Elasto-Plasticity—1 Damage and Elastic Deformations, Int. J. Engng Sci. Vol. 28, No. 5, pp 421-435, Pentagon Press plc, Great Britain

Keehan, E., (2004) Effect of Microstructure on Mechanical Properties of High Strength Steel Weld Metals, Department of Experimental Physics, Chalmers university of technology and Göteborg university, Göteborg, Sweden

Kumar, S.R.S. and Kumar, A.R.S., Metallargy of Steel http://nptel.iitm.ac.in/courses/IIT-MADRAS/Design_Steel_Structures_I, 10 July 2008

Hall, E.O., (1951) The Deformation and Ageing of Mild Steel: III Discussion of Results, Proceedings of the Physical Society of London, Vol. B64, pp. 747-753.

Han, H.N., Lee, C.G., Suh, D.W. and Kim, S.J., (2007) A microstructure-based analysis for transformation induced plasticity and mechanically induced martensitic transformation, Materials Science and Engineering A xxx (2007) xxx–xxx, 2007 Elsevier B.V.

Henrik, S.,(2006) Fracture toughness properties of duplex stainless steels, Masters Thesis, Department of Materials Science and Engineering, Royal Institute of Technology SE-100 44 Stockholm, Sweden, ISBN 91-7178-354-7, ISRN KTH/MSE--06/38--SE+MAT/AVH , Stockholm 2006

Hirth, J. P. (1972) The Influence of Grain Boundaries on Mechanical Properties, Met.Trans 3: 3047-3067.

Jiang, M., (1995) A damaged evolution model for strain fatigue of ductile metals, Journal of Engineering Fracture Mechanics, Vol. 52, No. 6, pp. 971-975, Elsevier Science Ltd, Great Britain.

Ju, D.Y., Zhang, W.M. and Zhang, Y., (2006) Modelling and experimental verification of martensitic transformation plastic behavior in carbon steel for quenching process, Materials Science and Engineering A, 2006 Elsevier B.V.

Lassance, D., Scheyvaerts, F. and Pardoen, T., (2006) Growth and coalescence of penny-shaped voids in metallic alloys Engineering Fracture Mechanics 73, pp. 1009–1034, Elsevier Ltd

Lei, G., (2007) Modelling of Microstructure in TRIP-Assisted steels, Master thesis Department of Ferrous Technology, Graduate Institute of Ferrous Technology, Pohang University of Science and Technology

Lim, H. K., Kim, D. H., Lee, J.Y., Kim, W.T. and Kim, D.H., (2007) Effect of grain size on the tensile deformation of wrought Mg–MM–Al–Zn–Sn alloy, Materials Letters xx (2007) xxx–xxx, Elsevier B.V.

Liu, K., Shan, Y., Yang, Z., Liang, J., Lu, L., and Yang, K., (2006, a) Effect of Heat Treatment on Prior Grain Size and Mechanical Property of a Maraging Stainless Steel, Journal of Material. Science and Technology, Vol.22, No.6

Liu, P., Wanga, Y.Y., Lia, J., Lua, C., Quekb, K.P., and Liuc, G.R., (2003) Parametric study of a sprocket system during heat-treatment process, Finite Elements in Analysis and Design 40, pp. 25–40, 2002 Elsevier B.V.

Liu, Y.C, Sommer, F., and Mittemeijer, E.J., (2006, b) The austenite–ferrite transformation of ultralow-carbon Fe–C alloy transition from diffusion- to interface-controlled growth, Acta Materialia 54, pp. 3383–3393, Elsevier Ltd.

Liu, C., (2006) Dislocation-Based Crystal Plasticity Finite Element Modelling Of Polycrystalline Material Deformation, Doctoral Thesis, University Of California Los Angeles

Lubarda, A.V., (1999) Deformation Theory of Plasticity Revised, The Montenegrin Academy of Science and Arts, Vol. 13, UDK 539.319

Mahdi, L. and Zhang, L., (2000) A Numerical Algorithm for the full coupling of mechanical deformation and phase transformation in surface grinding, Computational Mechnaics 26, pp. 148-156, Springer-Verlag

Makowski, J., Stumpf, H. and Hackl, K., (2006) The fundamental role of nonlocal and local balance laws of material forces in finite elastoplasticity and damage mechanics, International Journal of Solids and Structures 43, pp. 3940–3959, 2005 Elsevier Ltd.

Manesh, H.D. and Taheri, A.K., (2003) The effect of annealing treatment on mechanical properties of aluminum clad steel sheet, Materials and Design 24, pp. 617–622, 2003 Elsevier Ltd.

Mashayekhi, M., Ziaei-Rad, S., Parvizian, J., Nikbin, K. and Hadavinia, H., (2005) Numerical Analysis of Damage Evolution in Ductile Solids, SID, vol.1, no.1, pp.67-82, 2005 Tech Science Press

Martin, S.R., (2004) Experimental Characterization Of The Effect Of Microstructure On Dynamic Behavior Of Sic, Masters Thesis, Georgia Institute of Technology,

Maugin, G.A., (1992) The thermodynamics of plasticity and fracture, Cambridge University Press, England.

Mediavilla, J., Peerlings, R.h.J., and Geers, M.G.D.,(2006) A nonlocal triaiality-dependent ductile damage model for finite strain plasticity, Computer Methods in Applied Mechanics and Engineering Vol. 195, Issues 33-36, pp. 4617-4634, Science Direct

Miokovic, T., Schulze, V., Vohringer, O. and Lohe, D., (2006) Prediction of phase transformation during laser surface hardening of AISI 4140 including the effects of inhomogeneous austenite formation, Material Science and Engineering A 435-436, pp. 547-555, Elsevier B.V.

Morris, J.W. Jr., (2001) The Influence of Grain Size on the Mechanical Properties of Steel, Lawrence Berkeley National Laboratory, University of California, Paper LBNL-47875, eScholarship Repository

Muszka, K., Majta, J., and Bienias, L., (2006) Effects of Grain Refinement on Mechanical Properties of Microalloyed Steel, Metallurgical and Foundary Engineering, Vol. 32, No. 2.

Tsuji, N., Ueji, R., Minamino, Y. and Saito, Y., (2002) A new and simple process to obtain nano-structured bulk low-carbon steel with superior mechanical property Scripta Materialia 46, pp, 305–310

Panov, V., (2006) Modelling of Behaviour of Metals at High Strain Rates, Cranfield University School of Engineering, Phd. Thesis Academic,

Park, J., Kim, J. and Chung, Y., (2004) Grain refinement of steel plate by continuous equal-channel angular process, Scripta Materialia 5, pp. 181–184, Published by Elsevier Ltd.

Park, K., Kim, Y., Lee, J.G. and Shin, D.H., (2000) Thermal stability and mechanical properties of ultrafine grained low carbon steel, Materials Science and Engineering A293, pp.165–172.

Petch, N.J., (1953) The Cleavage Strength of Polycrystals, Journal of the Iron and Steel Institute, vol. 174, pp. 25-28.

Phillips, W. L. and Armstrong R. W., (1969) The influence of specimen size, polycrystal grain size, and yield point behaviour on the fatigue strength of low-carbon steel, J. Mech. Phys. Solids, vol. 17, pp. 265- 270. Pergamon press, Great Britain.

Pirondi, A., Bonora, N., Steglich, D., Brocks, W., and Hellmann, D., (2006) Simulation of failure under cyclic plastic loading by damage models, International Journal of Plasticity 22, pp. 2146–2170, Elsevier Ltd.

Qu, J., Dabboussi, W., Hassani, F., Nemes, J. and Yue, S., (2005) Effects of Microstructure on Static and Dynamic Mechanical Properties of a Dual Phase Steel Studied by Shear Punch Testing, ISIJ International, Vol. 45, No. 11, pp. 1741-1746

Ueji, R., Tsuji, N., Minamino, Y. and Koizumi, Y., (2002) Ultra grain refinement of plain low carbon steel by cold rolling and annealing of martensite, Acta Materialia 50, pp 4177–4189

Rack, H. J., (1978) Age Hardening-Grain Size Relationships in 18Ni Maraging Steels, Materials Science and Engineering, Vol. 34, pp. 263 – 270, Elsevier Sequoia S.A., Lausanne – Printed in the Netherlands

Rocha, A. da S. and Hirsch, T., (2005) Fast in situ X-ray diffraction phase and stress analysis during complete heat treatment cycles of steel, Materials Science and Engineering A 395, pp. 195–207

Seifert, T., (2003) Identification of material parameters using instrumented indentation test data, Masters thesis, Fraunhofer Institute for Mechanics of Materials (IWM) Freiburg and Institute of Applied Mechanics, University of Stuttgart

Sen, I., Tamirisakandala, S., Miracle, B.D. and Ramamurty, U., (2007) Microstructural effects on the mechanical behaviour of B-modified Ti–6Al–4V alloys, *Acta Materialia 55, pp. 4983–4993*

Serajzadeh, S., (2004, b) A mathematical model for prediction of austenite phase transformation, Materials Letters 58, pp.1597– 1601, Elsevier B.V

Serajzadeh, S., (2004, a) Modelling of temperature history and phase transformations during cooling of steel, Journal of materials processing technology 146, pp. 311-317, Elsevier B.V

Shen, W.,Peng, L.H., and Tang, C.Y., (2005) An anisotropic damage-based plastic yield criterion and its application to analysis of metal forming process, International Journal of Mechanical Sciences, Vol. 47, pp. 1897–1922, Elsevier Ltd

Schiotz, J., (2001) Simulation of nanocrystalline metals at the atomic scale, What can we do? What can we trust?, Proceedings of the 22nd Riso International Symposium on Materials Science: Science of Metastable and Nanocrystalline Alloys, Properties and Modelling, Rios National Laboratory, Roskilde, Denmark.

Shin, D.H., Pak, J., Kim, J.K., Kim, Y.S. and Park, K.T., (2002) Effect of pressing temperature on microstructure and tensile behavior of low carbon steels processed by equal channel angular pressing, Materials Science and Engineering A323, pp. 409–415, Elsevier Science B.V

Shulkosky, R.A., Rosburg, D.L., Chapman, J.D. and Barnes, K.R., (2003) A Microstructure Evolution Model Used For Hot Strip Rolling, Materials Science & Technology Conference, ISS and TMS

Singh, A. P., Sengupta, D., Jha, S., Yallasiri, M.P. and Mishra, N.S., (2004) Predicting microstructural evolution and yield strength of microalloyed hot rolled steel, Materials Science and Technology, pp. 1317, ProQuest Science Journals

Sleboda, T., Kane, J., Wright, R.N., Stoloff, N.S. and Duquette, D.J., (2004) The effect of thermomechanical processing on the properties of Fe–40 at.%Al alloy, Materials Science and Engineering A368, pp. 332–336, 2003 Elsevier B.V

Storojeva, L., Ponge, D., Kaspar, R. and Raabe, D., (2004) Development of microstructure and texture of medium carbon steel during heavy warm deformation, Acta Materialia 52, pp. 2209–2220, Published by Elsevier Ltd

Tamehiro, H., and Nakasugi, H., (1985) Austenite Grain Size of Titanium-microalloyed, Continuously Cast Steel Slabs, Research Article (311), Transactions ISIJ, Vol. 25

Tai, W.H., and Yang, B.X., (1987) A damage criterion for ductile fracture and its modification applied to sheet metal forming, Journal of Mechanical working Technology, Vol. 15, pp. 319-333, Elsevier Science Publisher B.V., The Netherlands

Tkalcec, I., (2004) Mechanical Properties and Microstructure of A High Carbon Steel, Thèse No 3089 (2004) École Polytechnique Fédérale De Lausanne Présentée À La Faculté Sciences De Base Institut De Physique De La Matière Complexe Section De Physique Pour L'obtention Du Grade De Docteur Ès Sciences

Tsuji, N. Ueji, R., Minamino, Y. and Saito, Y., (2002) A new and simple process to obtain nano-structured bulk low-carbon steel with superior mechanical property, Scripta Materialia 46, pp.305–310, Published by Elsevier Science Ltd

Ueji, R., N. Tsuji, N., Minamino, Y. and Koizumi, Y., (2002) Ultragrain refinement of plain low carbon steel by coldrolling and annealing of martensite, Acta Materialia Inc. Published by Elsevier Science Ltd

Voyiadjis, G.Z. and Abed, F.H.,(2006) A coupled temperature and strain rate dependent yield function for dynamic deformations of bcc metals, International Journal of Plasticity, Vol. 22, pp. 1398–1431, Elsevier Ltd

Wang, T., (1993) Thermal and mechanical load induced damage behaviour of a low alloy steel: Mechanism and modelling, Engineering Fracture Mechanics, Vol. 44, No. 6, pp. 971-980, Pregamon Press Ltd, Great Britain

Wei, Z.G., and Batra, R.C., (2007) Damage model for anisotropic materials, and its application to analysis of stability and spallation, International Journal of Impact Engineering, 2006 Elsevier Ltd

Yeh, W.C and Lin, H.Y., (2006) An endochronic model of yield surface accounting for deformation induced anisotropy, International Journal of Plasticity 22, pp.16–38, 2005 Elsevier Ltd.

Zhang, H. Y., Hu, Z. Q. and Lu, K. (1995) Hall-Petch relationship in the nanocrystalline selenium prepared by crystallization from the amorphous state, American Institute of Physics

Zhao, M. Hanamura, T., Qiu, H., Nagai, K. and Yang, K., (2006) Grain growth and Hall–Petch relation in dual-sized ferrite/cementite steel with nano-sized cementite particles in a heterogeneous and dense distribution, Scripta Materialia 54, pp.1193–1197

Zhu, Y.Y., and Cescotto, S., (1995) A fully coupled elasto-visco-plastic damage theory for anisotropic, International Journal of Solids Structures, Vol. 32, No. 11, pp 1607-1641, Elsevier Science Ltd, Great Britain

Zmika, J., Kvackaja, T., Sripinproachb, D. and Sricharoenchai, P., (2003) Influence of plastic deformation conditions on structure evolution in Nb–Ti microalloyed steel, Journal of Materials Processing Technology 133, pp. 236–242, Elsevier Science B.V

C:\EDS\USR\Cullen\virgin X2K.spc

Label:virgin X2K

kV:25.0 Tilt:0.0 Take-off:39.4 Det Type:SUTW+ Res:156 Amp.T:100.0

FS : 7499 Lsec : 100 11-Dec-2007 11:26:45

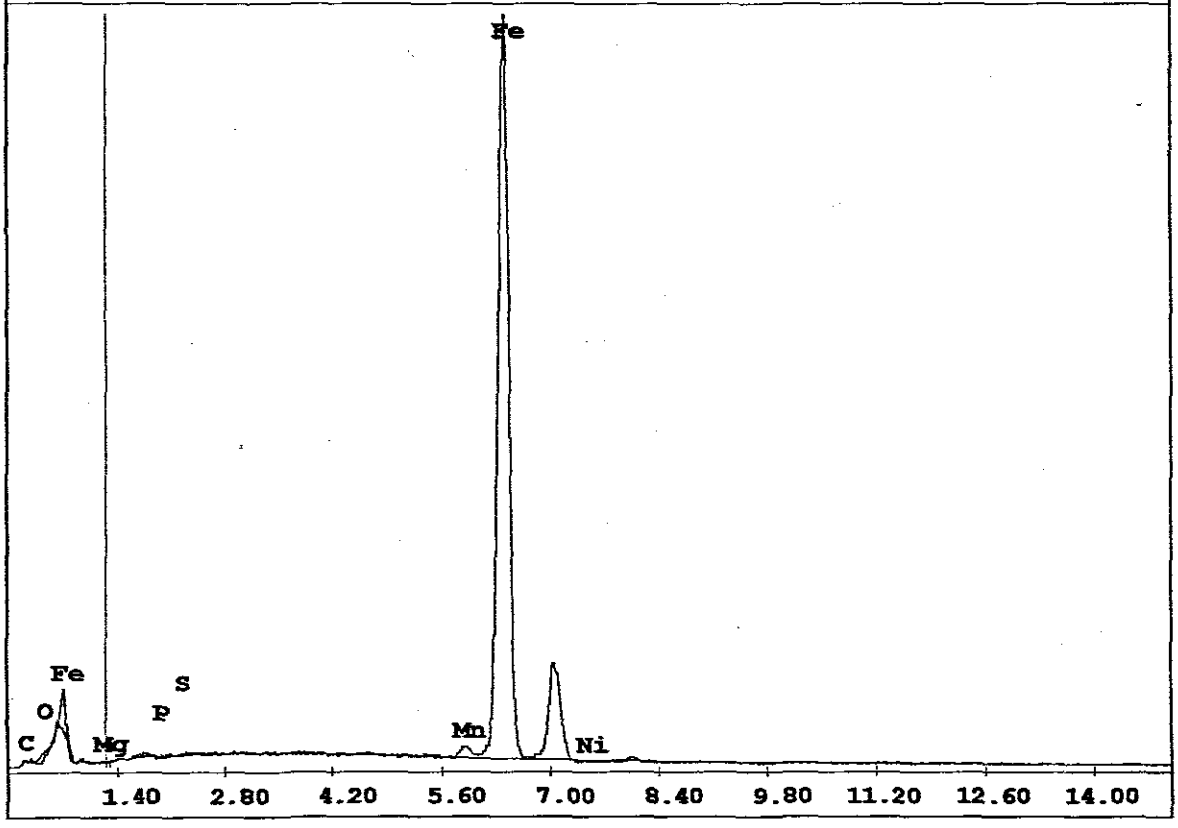

Element	Wt %	At %	K-Ratio	Z	A	F
C K	0.60	2.73	0.0012	1.1716	0.1686	1.0007
O K	0.00	0.00	0.0000	1.1534	0.3667	1.0062
MgK	0.00	0.00	0.0000	1.1084	0.1758	1.0000
P K	0.05	0.10	0.0003	1.0712	0.4684	1.0038
S K	0.11	0.18	0.0007	1.0990	0.5842	1.0070
MnK	1.44	1.43	0.0140	0.9787	0.9940	1.0000
FeK	97.80	95.57	0.9771	0.9988	1.0002	1.0000
NiK	0.00	0.00	0.0000	1.0179	0.8362	1.0000
Total	100.00	100.00				

Element	Net Inte.	Bkgd Inte.	Inte. Error	P/B
C K	0.76	2.97	34.06	0.26
O K	0.00	11.18	0.00	0.00
MgK	0.00	3.48	0.00	0.00
P K	0.35	7.19	109.66	0.05
S K	0.86	8.44	48.98	0.10
MnK	7.98	7.50	6.01	1.06
FeK	491.28	6.79	0.46	72.35
NiK	0.00	5.48	0.00	0.00